# MASTERARBEIT

Titel der Masterarbeit

## „The Tectonic Evolution of the Upper Austrian Molasse Foreland Basin and its Mesozoic Basement Based on 3D Seismic Fault Attributes"

Verfasser

## Manfred Retzl, BSc

angestrebter akademischer Grad

## Master of Science (MSc)

Wien, 2014

# TABLE OF CONTENTS

# ABSTRACT

The primary aim of this thesis is the development of a tectonic concept describing the evolution of Mesozoic to Neogene faults in the Molasse foreland basin and its Mesozoic basement in Upper Austria. The novel concept should contribute to a better understanding of known reservoirs, enable a de-risking of future exploration projects, and support the extrapolation of fault patterns to the sub-thrust areas below the Flysch and Calcareous Alps. Fault analysis was accomplished by using the software Petrel 2012 for processing a seismic volume provided by the Rohöl-Aufsuchungs AG Austria. Seismic fault mapping covered an area of around 1800 km² located between the rivers Inn and Enns. Faults were interpreted from 3D seismic data in two-way-time (TWT) depth.

The second task was the development of a special 3D seismic processing routine for displaying all fault structures in the study area, using Petrel 2012. Therefore, a workflow provided by the RAG Austria was modified and adapted for the given issue. Various algorithms included in the software for extracting seismic attributes were tested on small representative cropped volumes to enable faster testing loops and then applied on the whole seismic volume.  The resulting fault attribute cube shows faults as high-contrast features and allows a very fast tectonic overview. This is particularly useful when starting with the interpretation of a large seismic volume. Moreover, if tuned very accurate, it enables automated fault extraction. The workflow can be highly recommended for cases where no precise interpretation is required and the task is to get an impression of the tectonic setting. In principle it is also possible to extract very subtle fault features. This, however, has to be done very carefully because wrong tuning may result in nicely looking, but tectonically meaningless seismic attribute features.

The fault interpretation supported by the fault attribute volume yields the following results. Paleozoic NNW-SSE to NW-SE, respectively NE-SW striking fault systems of the Bohemian Massif were repeatedly reactivated during the Upper Cretaceous to Oligocene, when the Penninic Ocean became subducted and the Alpine orogenic wedge was thrust towards and over the Helvetic Shelf. Growth strata and the upward termination of faults allow distinguishing between distinct periods of fault reactivation.
Pre-existing fault systems might have also served as weakness zones for the formation of normal and conjugated normal faults, which strike subparallel to the Alpine trust front and mainly dip towards the Alps. Their age was determined to range from the Kiscellian (Oligocene) up to the Eggenburgian (Lower Miocene), due to upward fault terminations and growth strata. Normal faulting resulted from extensional deformation due to flexural bending of the European crust during the northward movement of the Alpine thrust wedge and the formation of the Molasse foreland basin.

# ZUSAMMENFASSUNG

Wesentliches Ziel dieser Arbeit war die Erstellung eines tektonischen Konzeptes für die einzelnen Störungsgenerationen der Molasse und des mesozoischen Untergrundes im Vorlandbecken Oberösterreichs. Dieses soll einerseits helfen bereits bekannte Lagerstätten besser zu verstehen und deren Produktionsverhalten besser zu bewerten, als auch das Risiko zukünftiger Bohrprojekte verringern und eine Extrapolation in den überschobenen Bereich unter Flysch und Kalkalpen ermöglichen. Für die Bearbeitung und Interpretation des von der Rohöl AG Austria zur Verfügung gestellten und vom Inn bis zur Enns reichenden 3D Seismik Volumens wurde die Software Petrel 2012 verwendet. Die Störungskartierung umfasst in etwa 1800 km² des Volumens, dessen Tiefe in Zeit gegeben ist (TWT).

Zusätzlich sollte ein neues 3D Seismik Volumen mit Petrel 2012 erstellt werden, welches alle Störungsstrukturen in dem Volumen darstellt. Ein Beispiel der dafür zu verwendenden Algorithmen und Bearbeitungsschritte wurde von der RAG Austria bereitgestellt. Nach längeren Testphasen an kleineren Ausschnitten des Volumens, was eine enorme Verkürzung der Rechenzeit zur Folge hatte, wurden die modifizierten Arbeitsschritte an der kompletten Seismik angewandt. Störungen sind nunmehr als stark kontrastierte Bereiche zu erkennen und ermöglichen somit einen schnellen tektonischen Überblick. Dies kann sich speziell dann als sehr nützlich erweisen, wenn begonnen wird an einer großen Seismik zu arbeiten. Darüber hinaus dient das Störungsvolumen, sofern alle Parameter passend eingestellt wurden, als Basis für die in Petrel enthaltene automatische Störungskartierung. Dessen Resultate erscheinen auf den ersten Blick oft sehr nützlich, weil es unter anderem möglich ist Details zu extrahieren, die in der unbearbeiteten Seismik sonst nicht erkennbar sind. Um eine genaue Interpretation zu erhalten erweist es sich jedoch als sinnvoller die Störungen händisch zu kartieren, da bei genauerer Betrachtung vieles tektonisch nicht der Realität entsprechen kann. Das neu erstellte Volumen wurde daher nur als Unterstützung bei der Interpretation der Störungen verwendet. Diese ergab dass NNW-SSO bis NW-SO, und NO-SW streichende paläozoische Störungen der Böhmischen Masse von der Oberkreide bis ins Oligozän mehrmals reaktiviert wurden. Dies ist auf die Subduktion des Penninischen Ozeans und die Überschiebung des alpinen Orogenkeils auf den Helvetischen Schelf zurückzuführen. Die verschieden Aktivitätsphasen lassen sich anhand der Störungsenden und Growth Strata bestimmen.

Zusätzlich dürfte das paläozoische Störungssystem als strukturelle Schwächezone für die Bildung von Abschiebungssystemen vom Kiscellium (Oligozän) bis Eggenburgium (Unteres Miozän) gedient haben. Das Streichen dieser Abschiebungen verläuft subparallel zum Streichen der Orogenfront, in dessen Richtung auch der Großteil der Störungen einfällt. Die Ursache für die Bildung der Störungen ist extensionelle Deformation aufgrund einer Flexur der europäischen Kruste, während der Nordbewegung des alpinen Orogenkeils und der Bildung des Molasse Vorlandbeckens.

# 1   INTRODUCTION

The project aims at a comprehensive mapping of all major fault structures in the Upper Austrian Alpine Foreland Molasse Basin and its Mesozoic basement, as well as the development of a tectonic concept for specific fault generations. This should be reached by developing a special 3D seismic processing routine in cooperation with the E&P National Team of the RAG Austria (Rohöl - Aufsuchungs Aktiengesellschaft).

The Northern Alpine foreland is characterized by an east-west trending sedimentary foreland basin, commonly known as the Molasse Basin, which originated from the flexural bending of the crust, caused by the weight of the northward advancing Alpine orogenic wedge. Since the basin was target for oil and gas exploration over decades, a huge amount of geological data has been accumulated, including hundreds of exploration and development wells. The high availability of seismic, well and stratigraphic data provides an ideal basis for a regional tectonic analysis of the basin. The novel fault maps and their tectonic interpretation, in turn, is important input data for future exploration and field development.

Through applying different processing algorithms on the RAG Austria's 3D seismic data cube by using the software Petrel 2012, seismic attribute volumes have been created which are helpful in displaying the information needed for stratigraphic or tectonic interpretation. During the course of this project, a workflow with optimized processing steps was developed, which provides the basis for the creation of a new seismic fault attribute volume. In the latter, faults appear as high-contrast features, meaning more or less as black lines on a white background. Therefore they are very easy to track just by sliding planes through the 3D volume (e.g. Inlines, Crosslines or time slices), or by creating a three dimensional model. The method proved very useful when dealing with a large seismic dataset, for getting a fast overview of the regional fault patterns.

The initial seismic processing opens several options depending on the required accuracy of the mapped fault surfaces. It is either possible to automatically or manually track fault planes. The latter turned out to be far better for reaching a reliable understanding of the fault geometries, kinematics, and deformation ages as it allows exploring important details.

Over 350 different faults have been manually tracked over an area of more than 1800 km², using the newly generated seismic fault attribute volume as help. The main benefit for RAG Austria is a regional dataset of 3D fault surfaces, along with some detailed mappings and interpretations of key fault structures, leading to a good understanding of fault kinematics and fault ages. This data may be

important for discoveries of smaller trap structures in the well explored Alpine foreland, and a better understanding of the production behavior in already known reservoirs.

Another application is the extrapolation of the fault model into the sub-thrust area below the Flysch Units and Calcareous Alps. Additionally the assessment of risks, and uncertainties associated with them, can be enhanced.

# 2  DATA

The seismic volumes as well as all mapped horizons were provided by RAG Austria (Rohöl-Aufsuchungs Aktiengesellschaft) and cover over 3000 km² of Upper Austria extending to a small area in Germany (seismic cube T_PrSTM5_AT_OOE; Figure 1, Figure 2). Seismic data are pre-stack time migrated (PrSTM), indicating that data is displayed in terms of two-way-time (TWT), which is the time interval a sound wave needs to travel from the surface to a reflector and back again. Migration relocates reflectors, creating a more accurate image of the subsurface. These datasets were used for further processing and creating relevant models, such as surfaces, faults and attribute volumes.
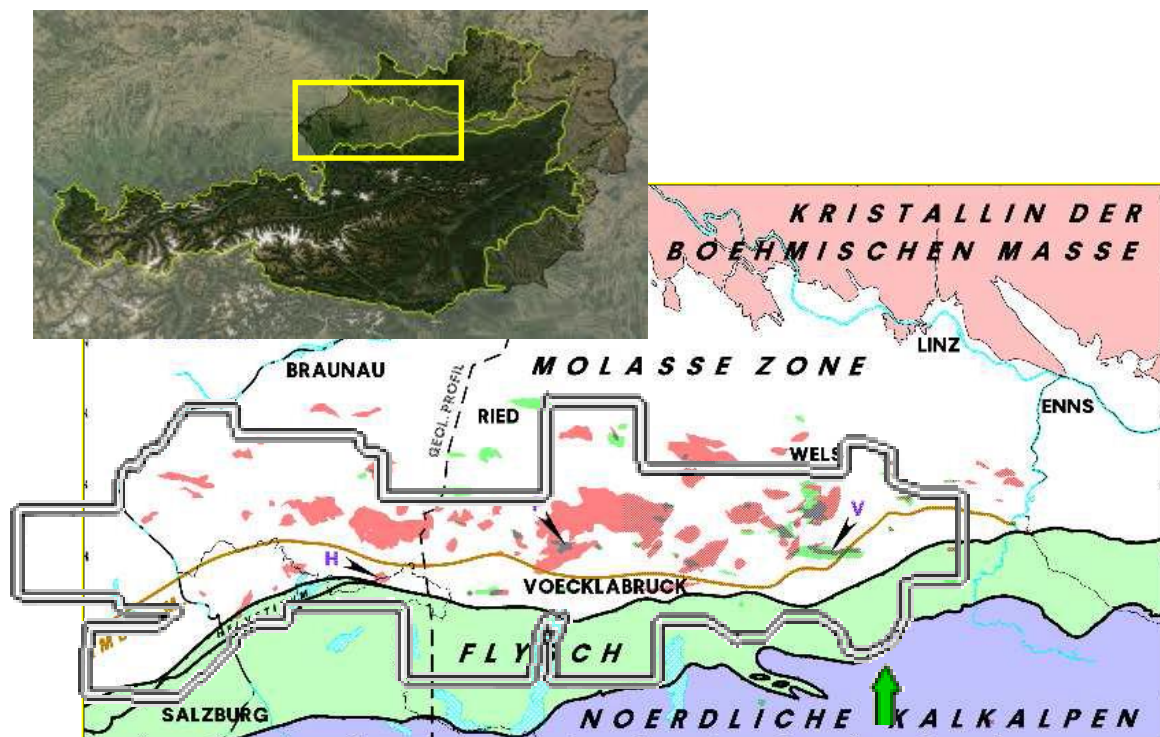


**Figure 1: Geological overview and approximate coverage of seismic volume (modified from Nachtmann, 2003); Satellite image (modified after NASA)**
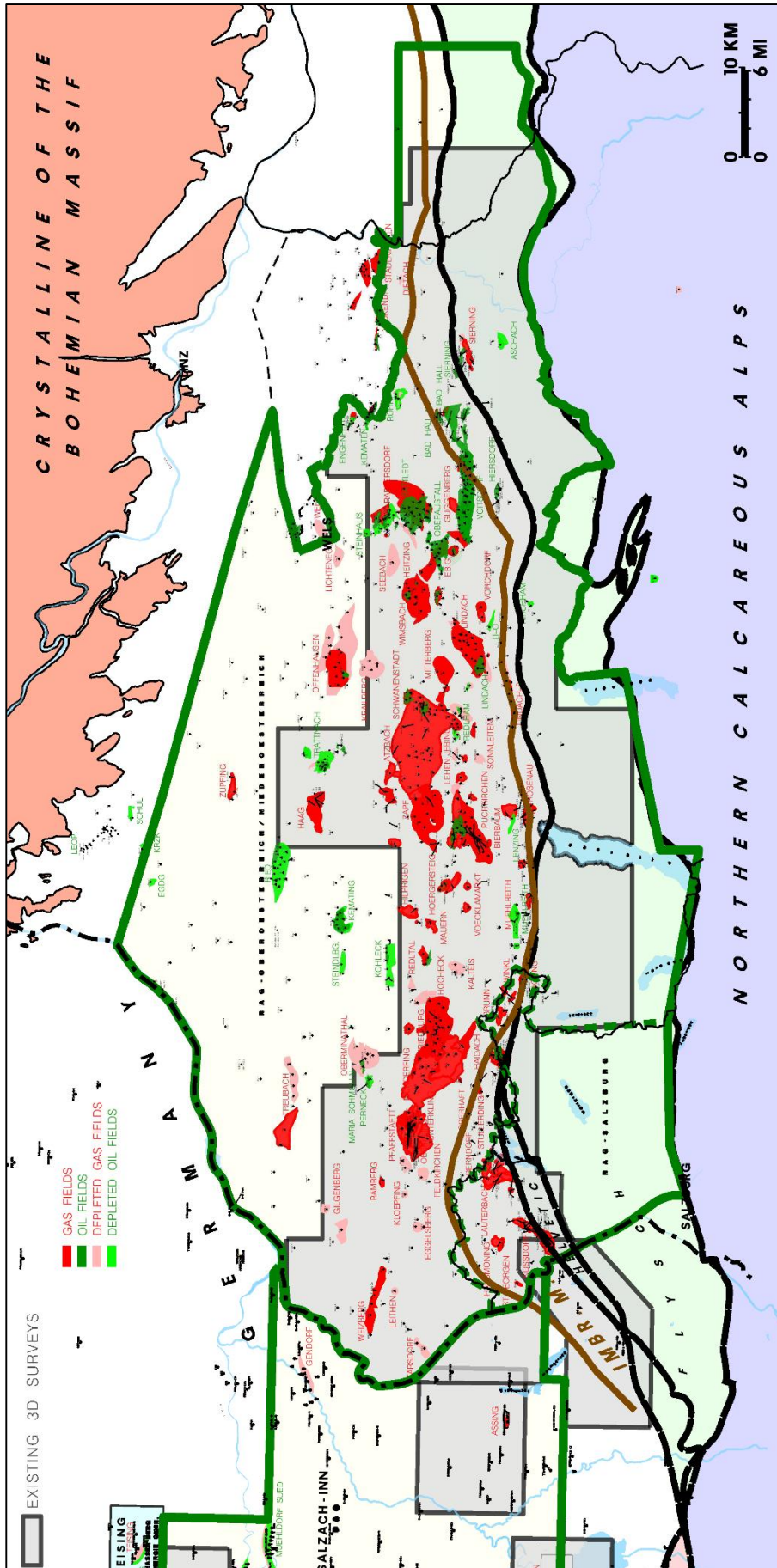
**Figure 2: Geological overview with approximate coverage of the seismic volume (grey) as well as known oil and gas fields (map by RAG Austria).**

## 2.1 Table of Mapped Faults

Faults were mapped throughout the entire area of the autochthonous Molasse covered by the seismic cube T_PrSTM5_AT_OOE (Figure 1). Mapping covered an approximate area of 1800 km², extending about 140 km along the strike of the Molasse basin between the rivers Inn and Enns. A table of mapped faults and a regional map showing these fault surfaces is included in the Attachments at the end of the thesis.

# 3   METHODOLOGY

The main idea and the guidelines for the steps described in the following came from the RAG Austria and were modified and adapted in the course of the master's thesis.

## 3.1 Seismic Attribute Extraction

For the 3D seismic processing and interpretation the software Petrel 2012 was used.

The first step in generating an appropriate processing sequence was to create two smaller cropped volumes, which should be representative for the whole 3D seismic data, with respect to the structural features above the crystalline basement. This turned out to be a challenging task because of the huge area covered by the seismic. Tectonic structures and faults occur in different depths, resolution and size all over the seismic block, making it difficult to reach a good compromise in selecting representative volumes. Those two cropped volumes were further used to test numerous workflows and processing steps. Reducing the data amount resulted in an enormous reduction of the time required for computing the various algorithms.

A long period of try and error resulted in learning and understanding of the applied software tools and their effects on the seismic attribute volume. This understanding was necessary to produce data showing faults as high-contrast features while avoiding to create processing artifacts. The huge number of possible combinations of algorithms with various settings and even more options for displaying the outcome resulted in hundreds of test runs using the representative volumes.

Good results were finally obtained from optimizing the consecutive processing steps, fine-tuning the settings for each individual step, and combining them into a single fault attribute volume.

When the algorithms giving the best results for the cropped volumes had been chosen, the attributes were created for the whole seismic volume. At this stage it turned out that there was still some more tuning required, as the testing on a small percentage of the volume could not account for all local characteristics of the whole seismic.

Finally two major attribute volumes, a horizontal and a vertical one according to the extracted features, have been generated through combining attributes in a sequential workflow.
The combination of both volumes using a formula provided by RAG Austria yields in a 3D seismic dataset that is specialized for identifying fault structures, the Final Fault Attribute Volume. This data constitutes the basis for the fault extraction, fault interpretation and models of fault systems developed afterwards.

The next points of Chapter 3 explain the processing workflow in more detail. The description of the workflow refers to the software documentation of Petrel as well as own expertise, experience, and graphics.

## 3.2 Horizontal Volume Attribute

(PETREL HELP, 2012)

### 3.2.1 Relative Acoustic Impedance

The attribute highlights apparent acoustic contrast and indicates sequence boundaries, unconformity surfaces and discontinuities (Figure 3).

### 3.2.2 RMS Amplitude

RMS amplitude computes the Root Mean Squares on instantaneous trace samples over a window of a specified size. The best results were obtained for a window size of 9 (Figure 3).

### 3.2.3 Instantaneous Phase

The Instantaneous Phase is a good indicator of continuities, faults, pinch-outs, bed interfaces, sequence boundaries, and regions of onlap patterns. The cosine of instantaneous phase is generally used due to the amplitude invariant nature of the attribute. Long windows are used for high accuracy and therefore the maximum size of 100 was chosen (Figure 3).

Figure 3 shows the effects of the different algorithms. All pictures show the same portion of a selected Inline after applying the different sequential attributes.
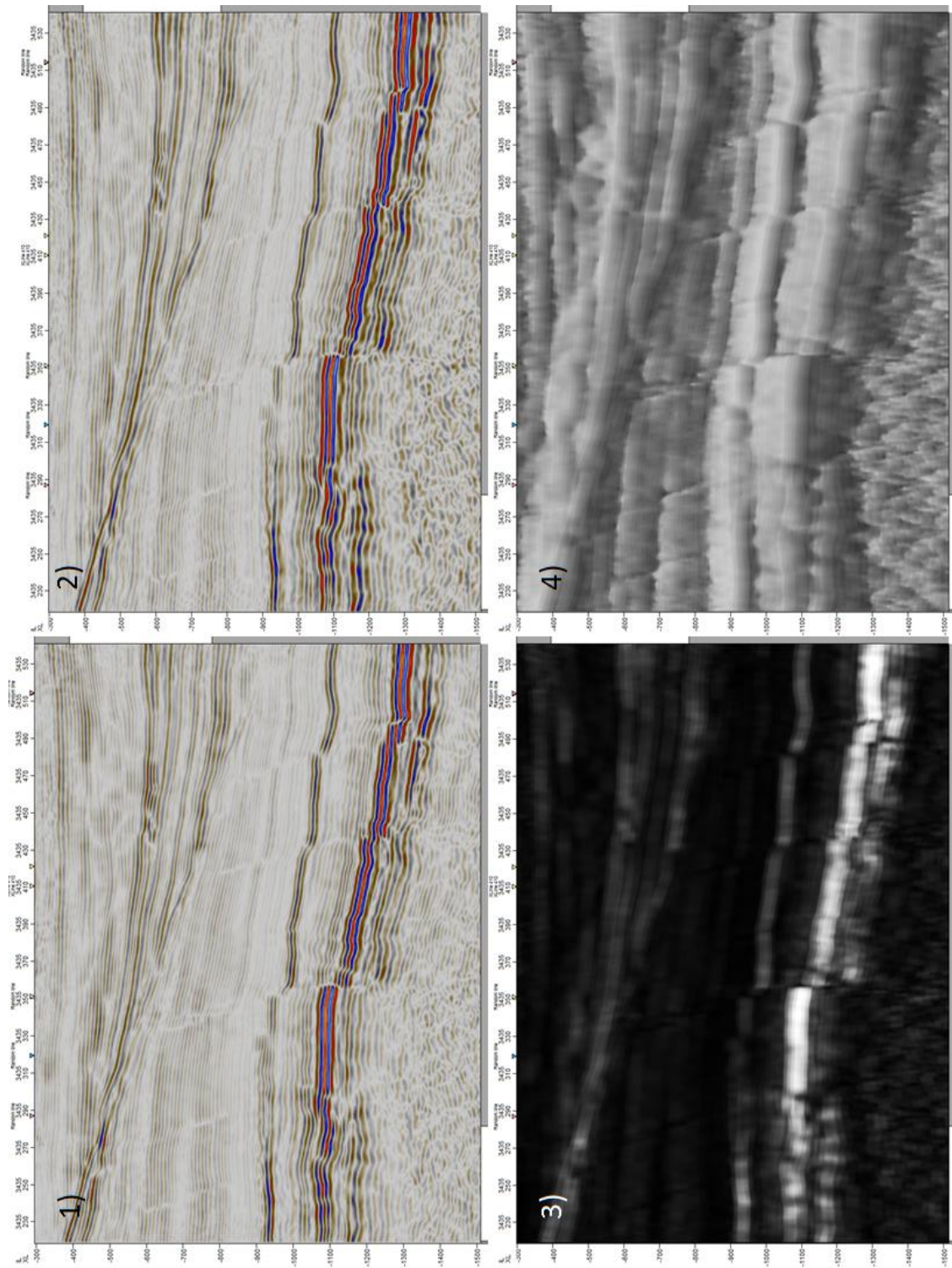
**Figure 3: Inline 3435 of the 3D volume T_PrSTM5_AT_OOE in TWT, showing the horizontal volume attributes as described in Figure 13; 1) Original seismic, 2) Relative Acoustic Impedance showing the apparent acoustic contrast, 3) RMS Amplitude smoothing over fine reflectors, 4) Instantaneous Phase is a good indicator of continuities, faults, pinch-outs, bed interfaces, sequence boundaries, and regions of onlap patterns.**

# 3.3 Vertical Volume Attribute

(**PETREL HELP,** 2012)

In Figure 4 some of the processing steps for treating the seismic data to highlight structural elements are shown. The best applicable workflow for the given issue was chosen after hundreds of try-and-error loops (Figure 4, red arrows). The modified process was applied on the overall seismic data as described below.
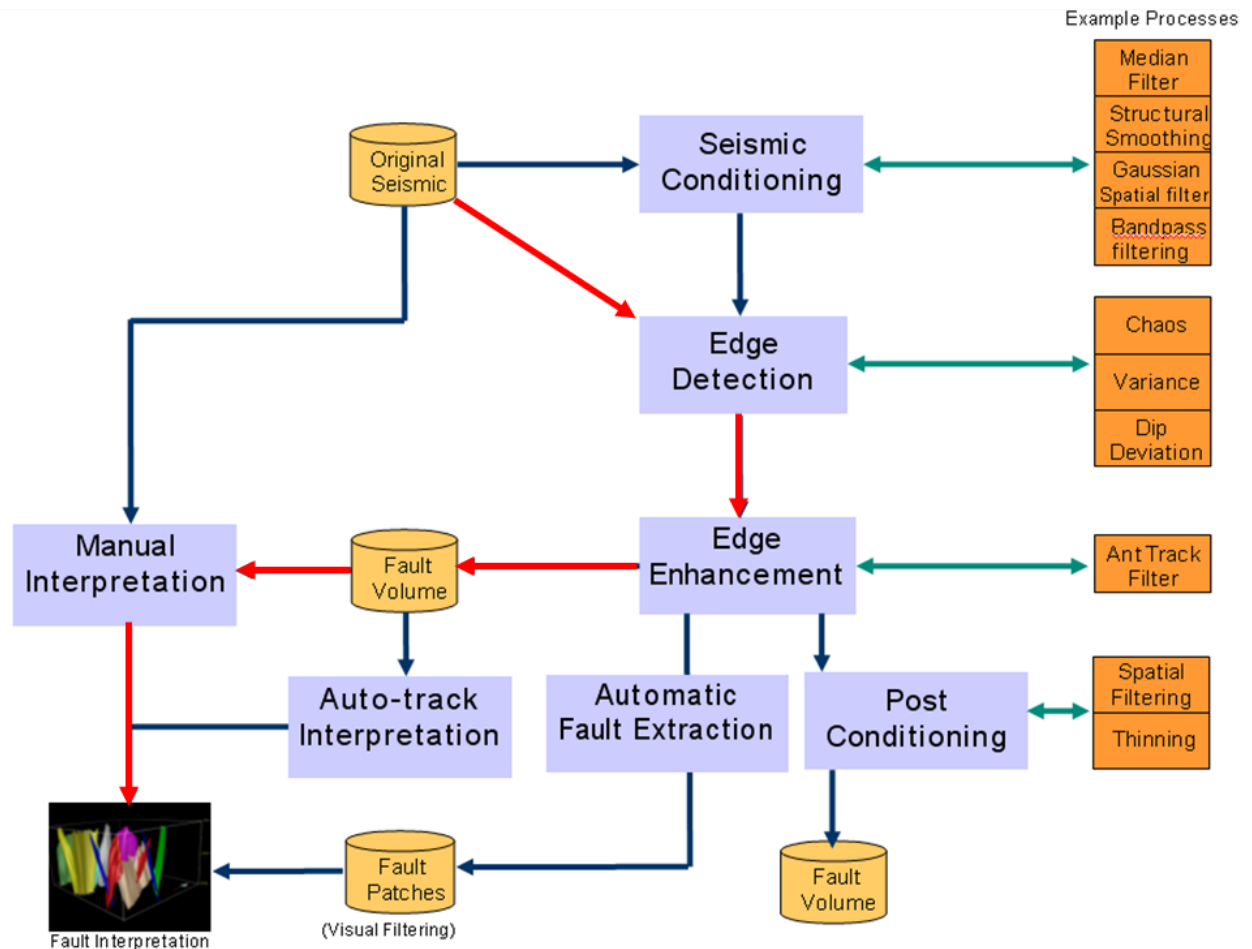


Figure 4: Possible workflows for treating the seismic data with the aim to isolate tectonic elements. The red arrows show the finally selected path, yielding the best results compared to all the other tested workflows. The Seismic Conditioning was abandoned because structural smoothing extinguished subtle features. For edge detection the process Variance gave the best results. Automated fault extraction was not satisfactory either and therefore manual interpretation was decided (modified from Petrel Help, 2012).

## 3.3.1 Structural Smoothing

Smoothing of the input signal increases the continuity of seismic reflectors (Figure 5). It highlights the major discontinuities on costs of the smaller ones, which tend to disappear. It was ultimately decided to skip this step as important small-scale features were lost by the process.

### 3.3.2  Variance (Edge Method)

The Variance attribute can be used to isolate edges from the input data set (Figure 5, Figure 12). Edges are defined by discontinuities in the horizontal continuity of amplitude. Dip guided variance is useful for accentuating structural features like faults.
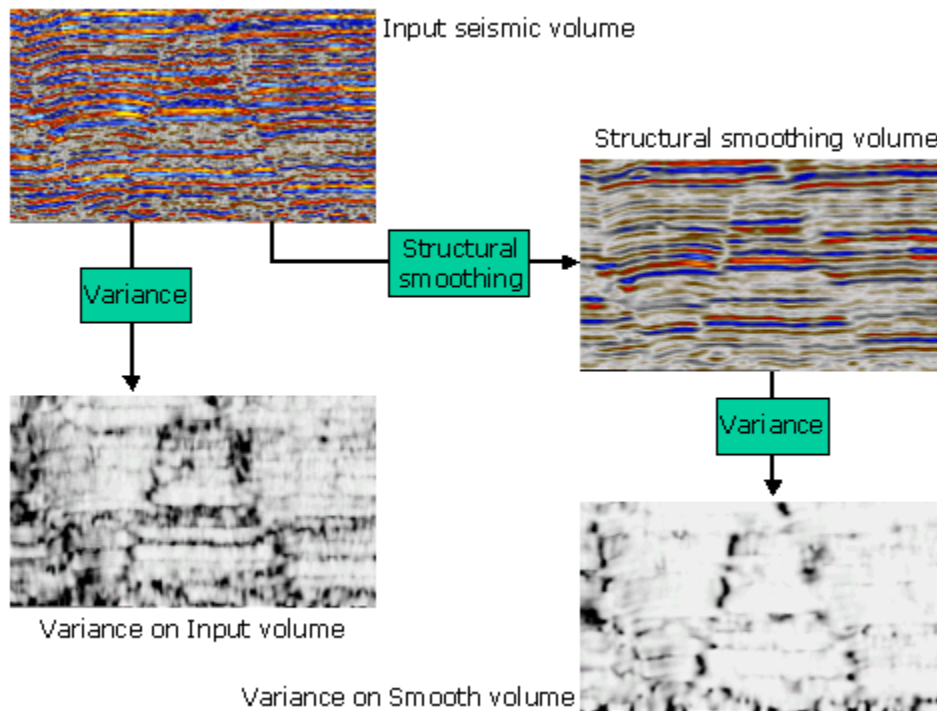


**Figure 5: Example of the Variance attribute with and without applying Structural Smoothing (Petrel Help, 2012). Structural smoothing was not applied in the current work as it tends to obliterate or delete small discontinuities, which, however, depict important fault structures.**

### 3.3.3  Ant Tracking

This workflow is used to extract fault information from the pre-processed variance attribute volume (Figure 12). The algorithm extracts surfaces appearing like trends in very noisy data, according to the principles from ant colony systems. Intelligent software agents, the ants, extract features that are expected to correspond to the behavior of faults. This implies that if these expectations are fulfilled it should be true fault information being extracted by many ants, whereas noise and artifacts of reflectors should not be extracted or only by single ants (in this case they will be deleted). The algorithm takes advantage of three dimensional information in the surrounding voxels and makes the derivation of detailed information from the attribute possible. The extracted surfaces define a dataset referred to as an ant track cube, which contains only what is likely to be true fault information (**PETREL HELP,** 2012).

Iterating Ant Tracking, from aggressive tracking mode to more passive ones, can be used for harder constraints and noise reduction. The following subchapters explain the various parameters included in the algorithm and used for fine tuning.

**Ant mode**

The aggressive tracking mode gives more detailed information than the passive one, which should extract only major regional fault zones. Thus it captures subtle fault zones in the data too.

**Initial ant boundary**

Ant boundaries are defined by a radius in voxels for the distribution of the ants. If the agent is unable to identify a local maximum or make an orientation estimate within its radius, the agent will be exterminated (Figure 6).
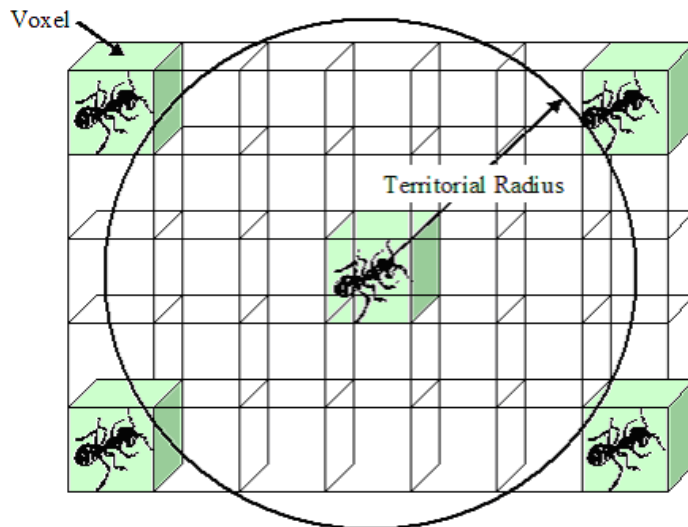


**Figure 6: Initial ant boundary (Petrel Help, 2012). The agent searches for new maxima in a given radius. Finding none will exterminate it.**

**Ant track deviation**

This parameter controls the maximum allowed deviation from a local maximum while tracking. The agents assume a planar shape, and can only deviate 15 degrees from the initial orientation. The method allows the agent to accept one voxel on either side of the predicted position as legal. If the maximum is outside the ant track step range, the track deviation parameter comes into play. If local maxima deviate much from a plane, the agents are not able to track them for long. This parameter allows the agents to deviate from local maxima and therefore follow the structure longer (Figure 7).

A value of 1 would allow the agent to deviate by one voxel in either direction from the legal positions to search for a local
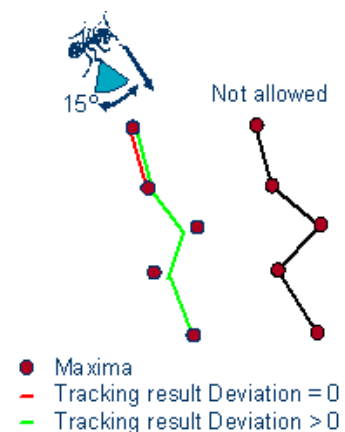


**Figure 7: Ant track deviation (Petrel Help, 2012). Controls the maximum allowed deviation of the agent from new local maxima and therefore follow the structure longer.**

maximum. If a maximum is not found, this would be recorded as an illegal step. If a maximum is found, the legal position closest to this maximum would be used as the legal step.

## Ant step size

Sets the number of voxels the ants are allowed to advance in a single searching step. Increasing this value will allow an agent to search further, but it will lower the resolution of the result (Figure 8).
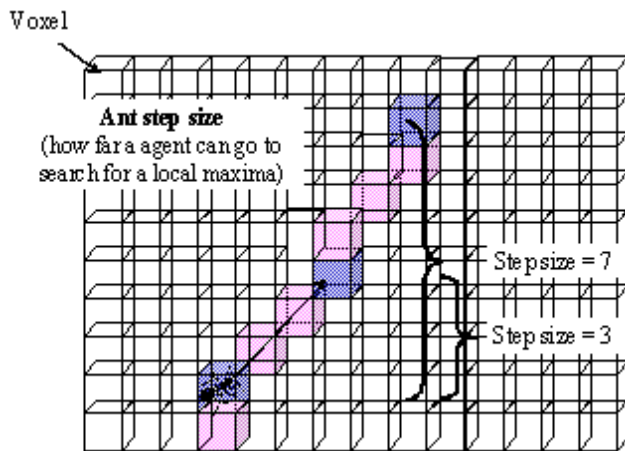


**Figure 8: Ant step size (Petrel Help, 2012). Controls how many voxels the agent is allowed to search for new maxima.**

## Illegal steps allowed

Defines how many steps an agent is allowed to go without finding a local maximum (Figure 9).

## Legal steps required

Defines the number of steps that must contain a valid value for the agent to continue and hence controls how connected a detected edge must be to help distinguish an edge from un-oriented noise (Figure 10).
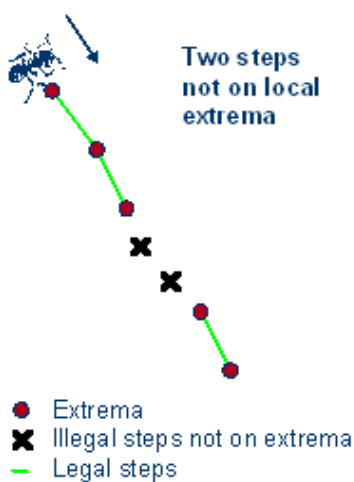


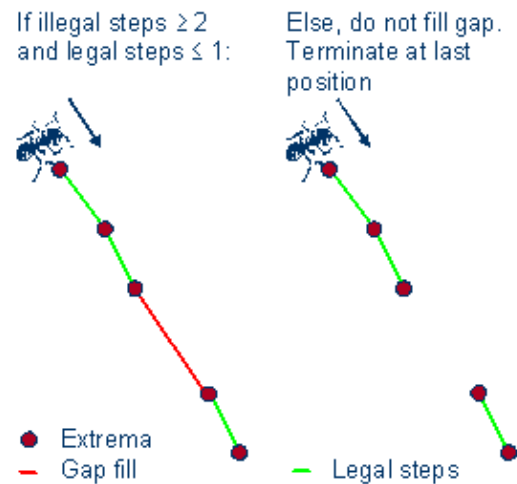**Figure 9: Illegal steps allowed (Petrel Help, 2012); Steps without maxima.**

**Figure 10: Legal steps required (Petrel Help, 2012); Steps with maxima required to continue.**

**Stop criteria**

This attribute parameter terminates the track if the number of illegal steps in an ant's path exceeds the allowed percentage. This ensures that it is legitimate fault geometry being tracked (Figure 11).
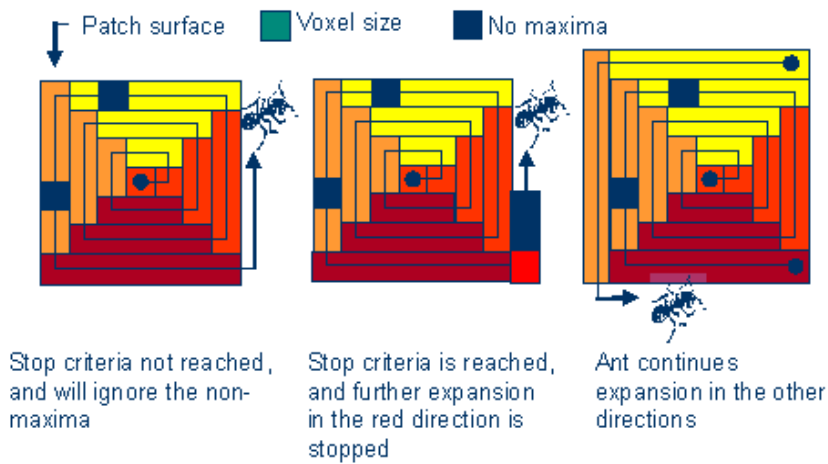


**Figure 11: Stop criteria (Petrel Help, 2012). If the number of illegal steps exceeds the set percentage tracking in one direction is stopped and continued in another direction if possible.**
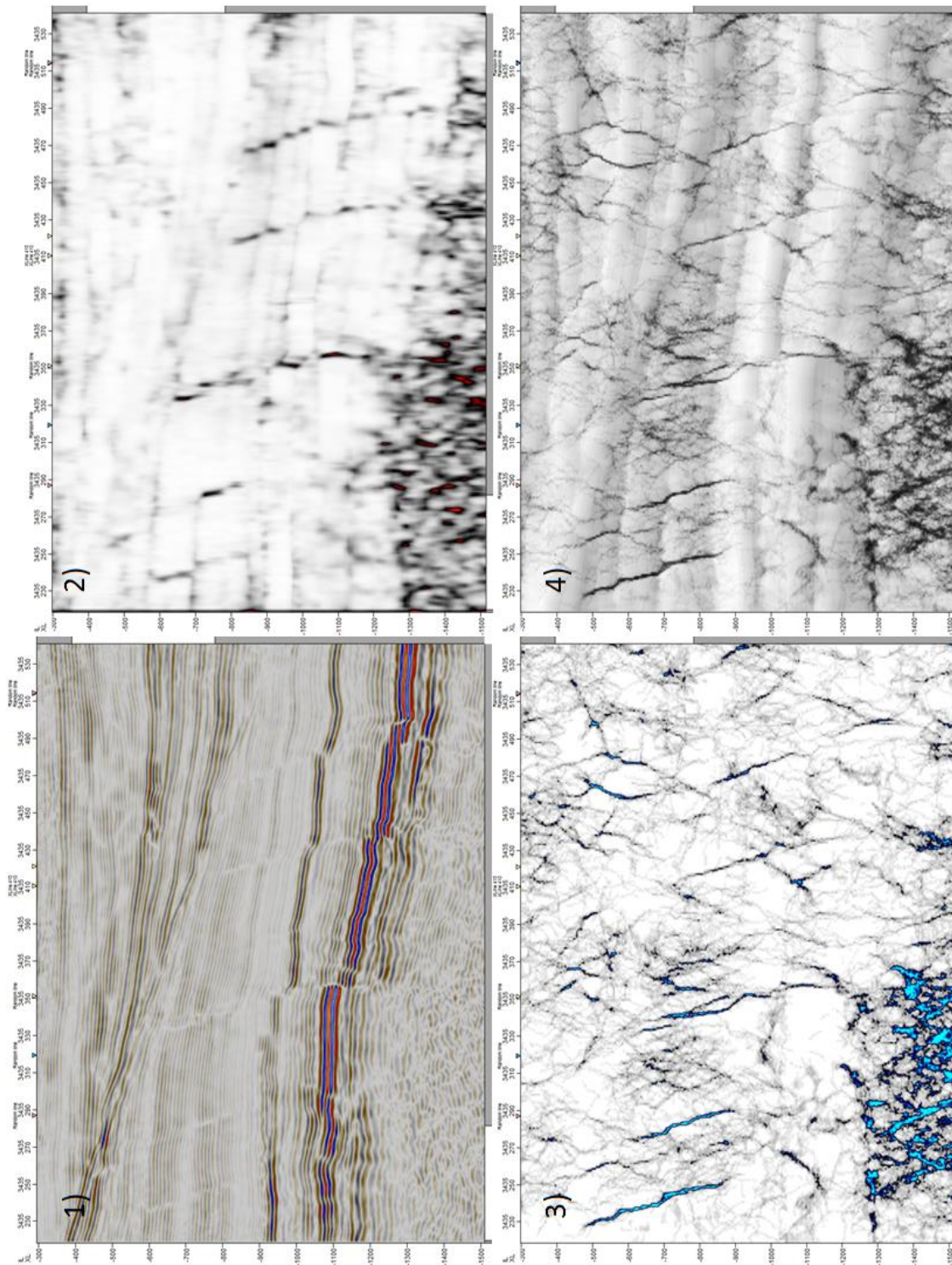
**Figure 12: Inline 3435 of the 3D volume T_PrSTM5_AT_OOE in TWT, showing the vertical volume attributes and the Final Fault Attribute Volume as described in Figure 13; 1) Original seismic data, 2) Variance attribute: highlights horizontal discontinuities, 3) Ant Tracking: connects the discontinuities from the variance attribute 4) Final Fault Attribute Volume: combines the Vertical and the Horizontal Attribute Volume in a way that faults are depicted sharply as high-contrast features. Details which are not or hardly seen in the original data become visible. The pattern is credible suggesting existence of conjugate faults in the shown example (detailed interpretation in the chapters below). The attribute, however, has to be used very carefully as in some cases the result highlights data artifacts rather than tectonic structures.**

# 3.4 Final Fault Attribute Volume (FFAV)

Two major volumes were created with the workflow and a sequence of consecutive steps described above, which include the Horizontal and the Vertical Volume Attribute. Finally the vertical and horizontal attribute information was combined in one and the same volume by the workflow shown in Figure 13.

**Original 3D seismic volume**
T_PrSTM5_AT_OOE

**Horizontal Volume Attribute**

Relative Acoustic Impedance
Input: T_PrSTM5_AT_OOE
No parameters
Output: T_PrSTM5_AT_OOE_-_RAI

RMS Amplitude
Input: T_PrSTM5_AT_OOE_-_RAI
Window: 9
Output: T_PrSTM5_AT_OOE_-_RAI_RMS

Instantaneous Phase
Input: T_PrSTM5_AT_OOE_-_RAI_RMS
Window: 100
Output: T_PrSTM5_AT_OOE_-_RAI_RMS_IPH

**Vertical Volume Attribute**

Variance (Edge Method)
Input: T_PrSTM5_AT_OOE
Inline range: 3
Crossline range: 3
Vertical smoothing: 15
Dip correction: On
Inline scale: 1.0
Crossline scale: 1.0
Vertical scale: 1.5
Plane confidence threshold: 0.0
Dip guided smoothing: Off
Output: T_PrSTM5_AT_OOE [Var] [Realized] 1

Ant Tracking
Input: T_PrSTM5_AT_OOE [Var] [Realized] 1
Ant mode: Custom
Initial ant boundary: 5
Ant track deviation: 2
Ant step size: 3
Illegal steps allowed: 2
Legal steps required: 2
Stop criteria (%): 10
Output: T_PrSTM5_AT_OOE [Var] [AntTrack] [Realized] 1

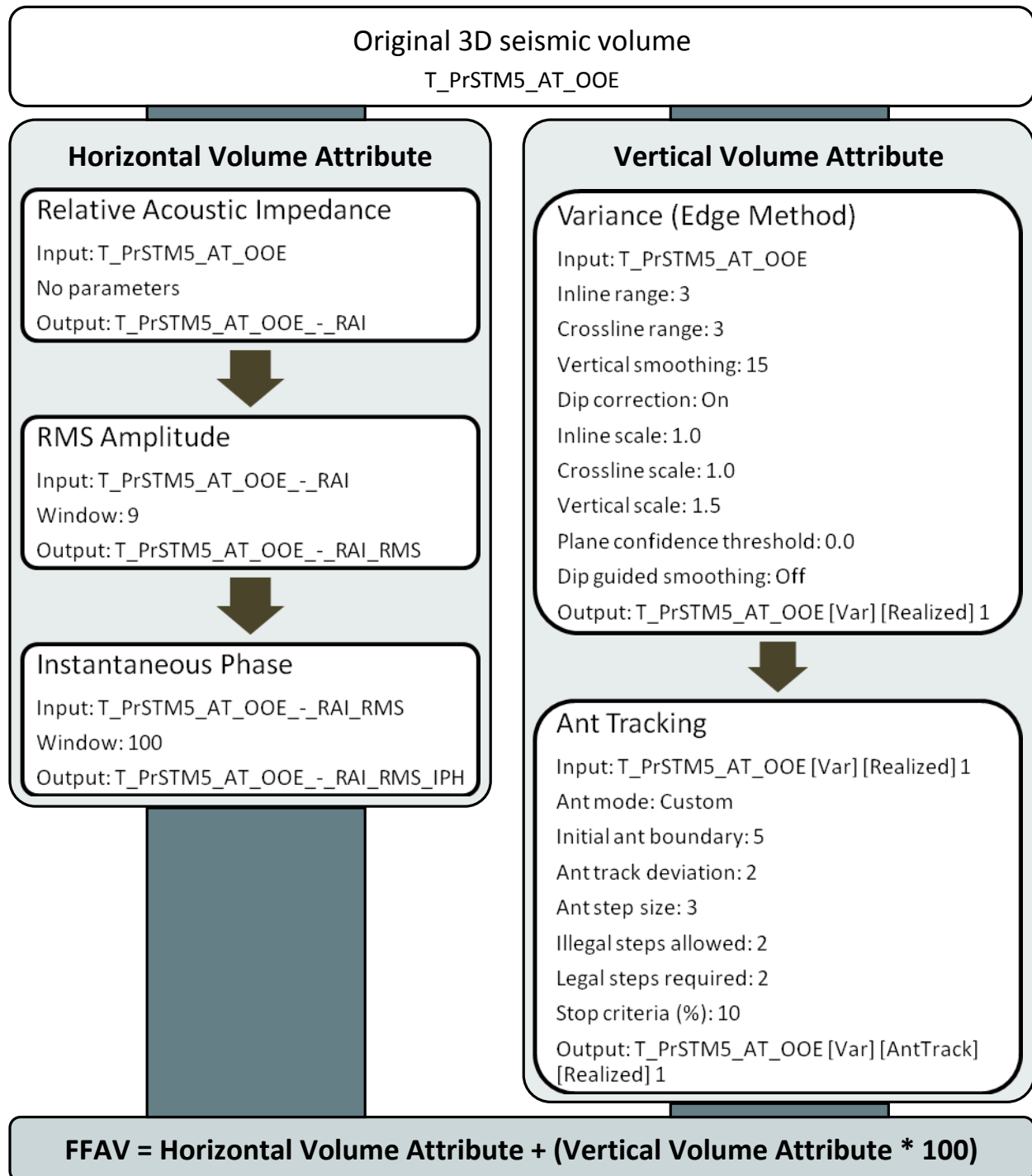**FFAV = Horizontal Volume Attribute + (Vertical Volume Attribute * 100)**

**Figure 13: Parameters used for creating the Horizontal, the Vertical and ultimately the Final Fault Attribute Volume (FFAV). Algorithms, settings and parameters used for creating the horizontal and vertical volume attributes are listed in the white boxes. The FFAV is obtained from the combination of both volume attributes.**

The Final Fault Attribute Volume is optimal data for easily detecting, tracing and interpreting structures. Interpretation, however, needs to be handled with care, because sometimes it may not be true fault information being tracked. Examples for a possible application are shown in Figure 14 and Figure 15.
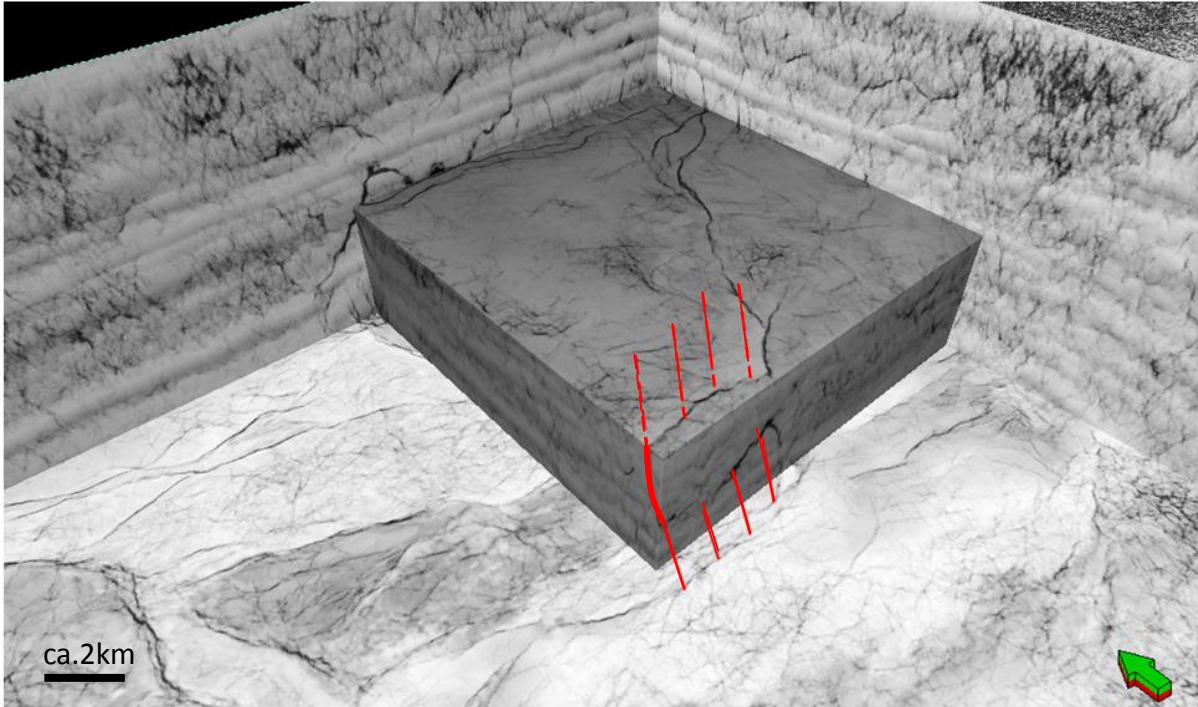


**Figure 14: Inline, X-line, time slice and Geobody cube in TWT displaying the Final Fault Attribute Volume. High-contrast features should be faults, except in the uppermost parts of the seismic and in the crystalline basement due to the lower quality of the original seismic data in these parts of the volume. The red lines indicate a possible interpretation of fault sticks connecting the black lines in the different sections of the Geobody cube.**
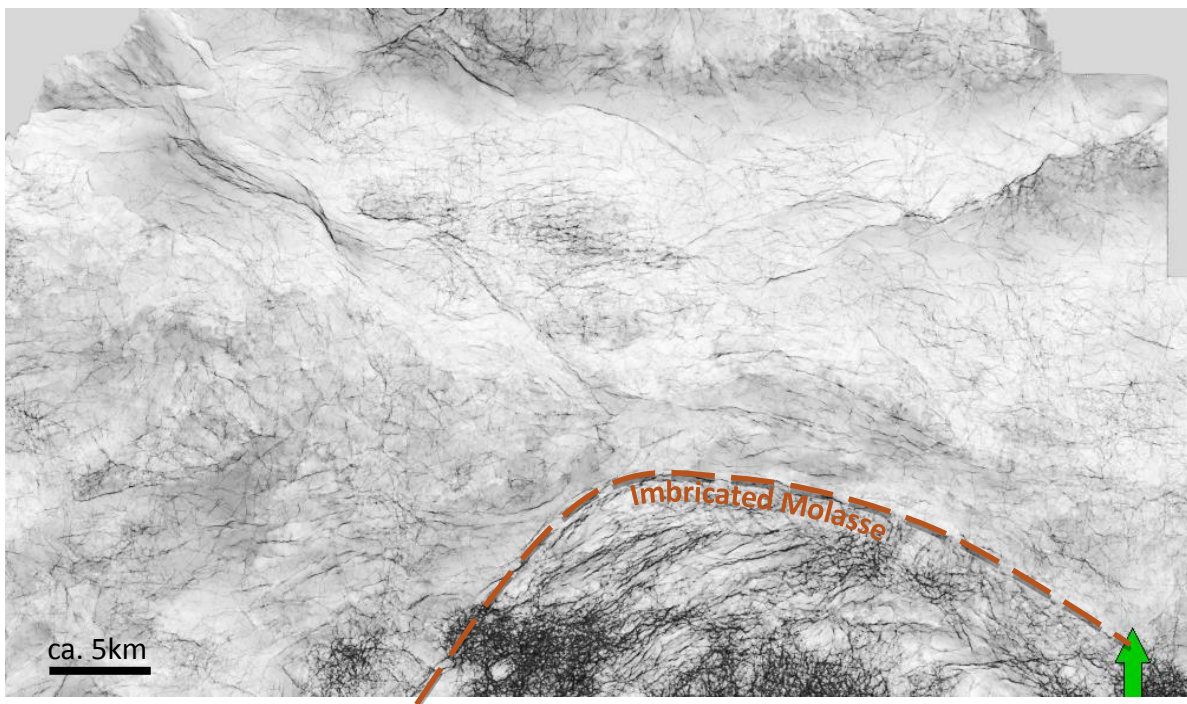


**Figure 15: Time slice displaying the Final Fault Attribute Volume, showing the autochthonous Molasse of Upper Austria and also parts of the Imbricated Molasse in the south of the dotted line.**

## 3.5 Fault Extraction

### 3.5.1 Automatic Fault Extraction

At the very first the major aim was to pre-process the whole seismic in a way that automated fault extraction delivers a reasonable result, so that a lot of time could be saved compared to manually picking or interpreting the fault data. The process is used to generate fault patches in the selected volume based on the set parameters. These patches can then be sorted by different filtering methods, like size, direction and many others.

Trying to reach this aim included many hours of try and error to evaluate the program's automated capability and to compare results to manual fault picks.

Since Automatic Fault Extraction would have been the last step in processing, if it worked, all the previous steps had to be well tuned. Unfortunately the tuning encountered as a problem and led to overthinking of the whole processing. Mistakes were revealed and tried to be overhauled, but ultimately all the time spent in trying to fix everything and recreating the volumes still yielded no satisfying result.

### 3.5.2 Seeded 3D Fault Auto-Tracking Tool

To overcome the drawbacks of fully automated fault picking, a partly automated process was tested by using the seeded 3D fault auto-tracking. This tool allows to auto-track single faults, which are displayed in a 3D window in the Final Fault Attribute Volume, just by clicking on parts of their traces (Figure 16). If the tracking result doesn't cover the whole fault, further seed points can be set. In the end the fault polygons can be merged and smoothed to get clean results without peaks.
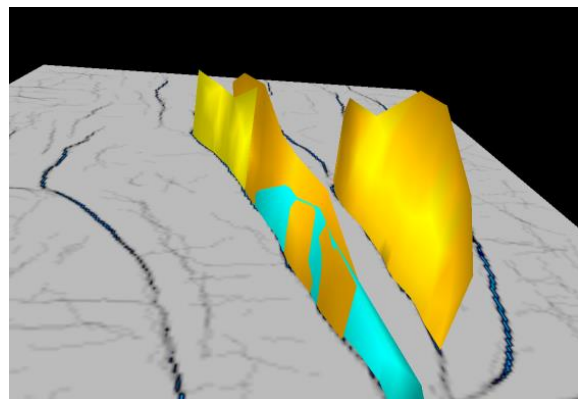


**Figure 16: Example for automated fault extraction and tracking (Petrel Help, 2012)**

The method still didn't turn out to be very reliable and so the faults were manually picked with the Fault Interpretation tool, by "drawing" the fault planes line by line. This process may become very complicated, tricky and time consuming, particularly in tectonically complicated areas. In fact more than 350 faults of different sizes were picked by switching through In-, Cross- and Random Lines and creating fault sticks.

# 3.6 Further Helpful Processing and Displaying

Creating surfaces from interpreted stratigraphic horizons (provided by RAG Austria) in two-way-time (TWT) gives a first continuous regional model (Figure 17). These surfaces allow identifying edges with vertical offset as well as tilting directions.
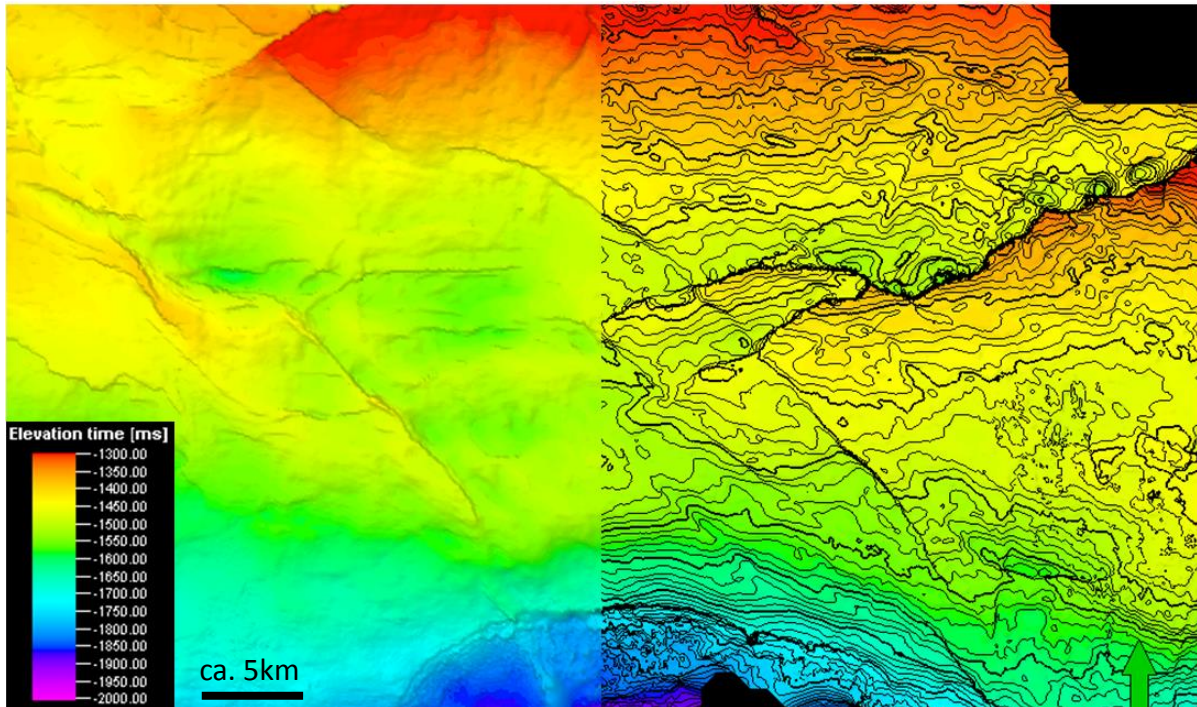


**Figure 17: Top Eocene surface in TWT showing the northwestern part of the seismic area; right with and left without contour lines. Faults are highlighted by marked steps in the relief of the surface.**

**Extract Value** generates attribute information on surfaces, which means that every point on the surface gets attributed with the attribute volumes' data at the corresponding coordinates (Figure 18).

Another application on the surfaces, called **Edge Detection**, attributes these with gradient information (Figure 19). If point sets and appropriate filters for these are created, areas with higher dip angles of the horizon can be isolated. Synoptic displays of multiple datasets allow assessing differences in thickness and offsets of horizons, or their continuity to detect and trace faults (Figure 20).

Additionally the "**Fault Detect**" surface operation is also a good possibility for extracting fault data. It computes the absolute difference between the original and the smoothed surface. The tool proved very useful to highlight the major faults in a volume. When adjusting the opacity, so that only fault relevant values are shown, it provides a similar result as the image shown in Figure 20.

**Figure 18: Top Eocene in TWT attributed with FFAV data, showing the northwestern part of the seismic area. The visualization allows checking if the fault attribute fits to the offsets shown by the surface and therefore shows true fault information. Furthermore very subtle lines can be seen, which often seem to occur randomly but nevertheless sometimes show apparent fault trends. The quality of the image is depending on the fine tuning of the FFAV.**
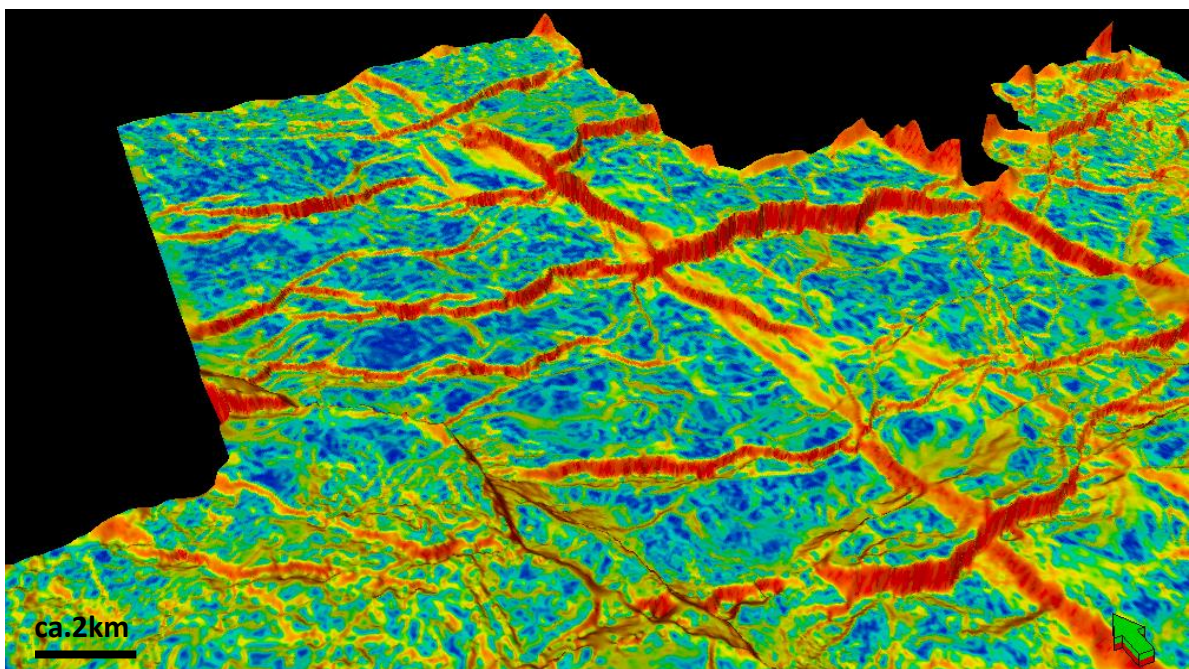


**Figure 19: Top Jurassic in TWT attributed with Edge Detection data showing the central area of the seismic. Faults respectively offsets in the Jurassic horizon are illustrated by red/orange color.**
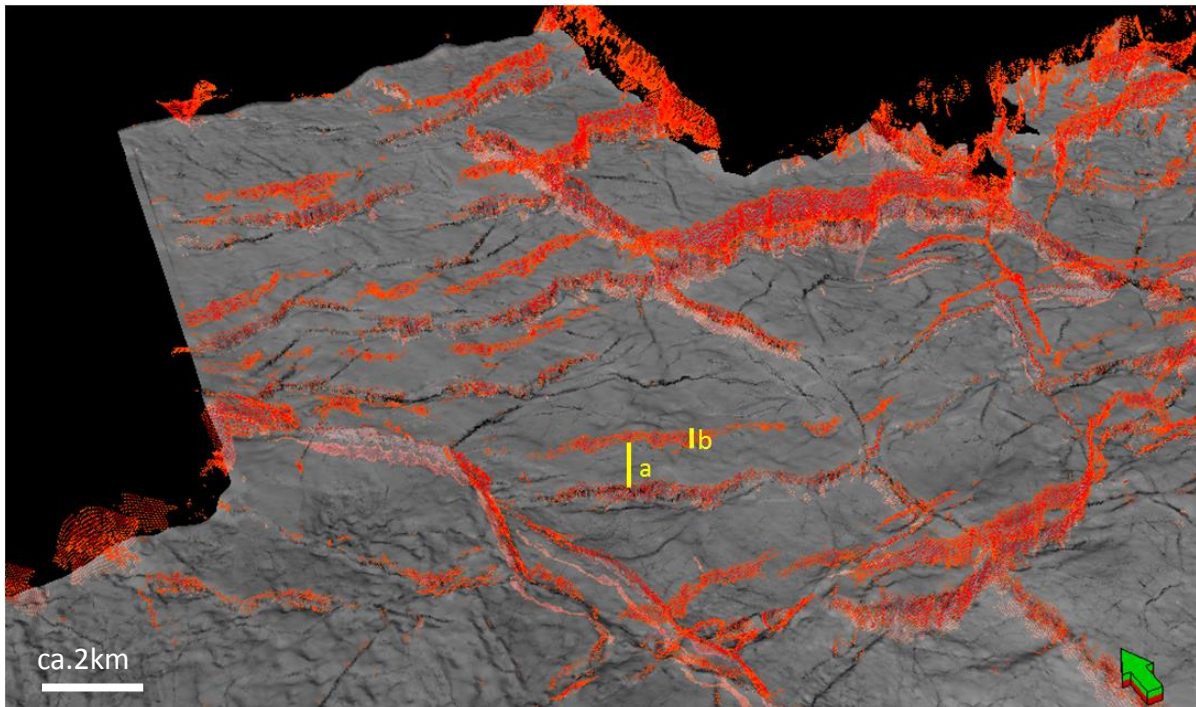
**Figure 20: Top Jurassic in TWT attributed with FFAV data, showing the central area of the seismic and filtered point sets from Edge Detection surfaces. Data illustrates offsets of the different horizons except Base Hall and therefore gives information of the continuity and dip of faults, as well as thicknesses; a) thickness, b) offset.**

# 4   REGIONAL OVERVIEW

The study area is located in the Upper Austrian Foreland Basin between the rivers Inn and Enns (Figure 21). The regional cross section gives a first quick insight into some major sedimentary cycles and formations dealt with (Figure 22).

The following chapter provides an overview of the geological evolution of the Molasse Zone, the Bohemian Massif and the Eastern Alps in order to account for the complex and polyphase tectonic evolution of the area.  This is important for a better understanding of the processes and the key to a reasonable tectonic interpretation, as many of the mapped faults appear to be Variscian and Mesozoic structures, which were reactivated during the Alpine orogeny.

The overview starts with the paleogeographical location of the area in the Precambrian, followed by the northward drift and the Variscian orogeny, the Mesozoic formation of the passive continental margin in the south of the Bohemian Massif and the opening of the Penninic Ocean, the subduction of the Penninic units whilst the Alpine orogeny, thrusting of the Alpine orogenic wedge over the European foreland, and the formation of the Molasse Foreland Basin.
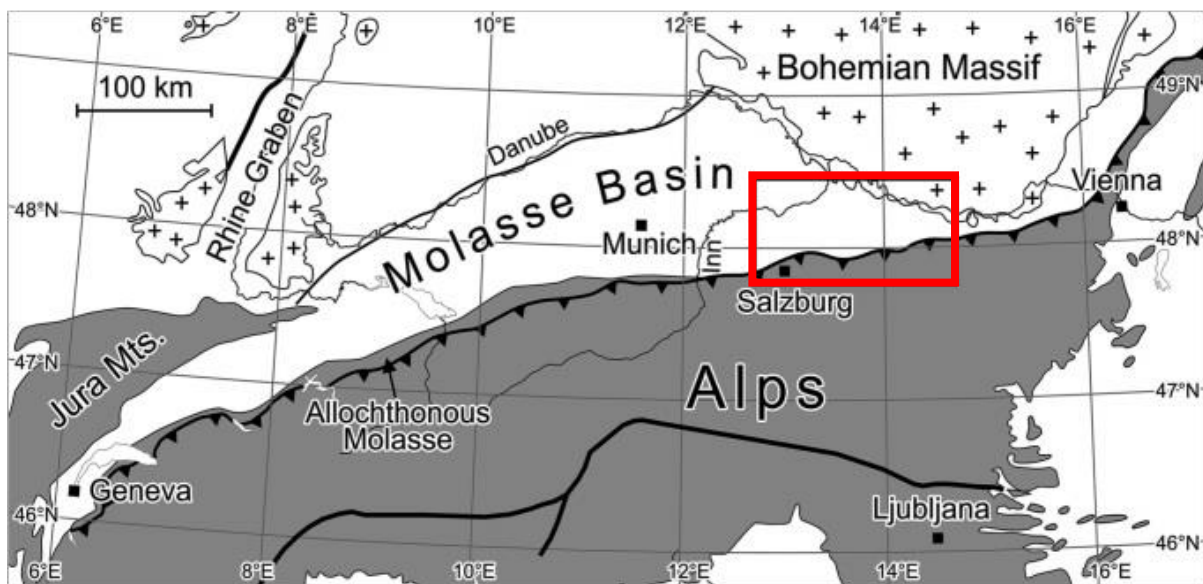
Figure 21: Geological overview. The red rectangle shows the approximate outline of the area of interest in the Upper Austrian Molasse Basin (modified after Sachsenhofer et al., 2010).
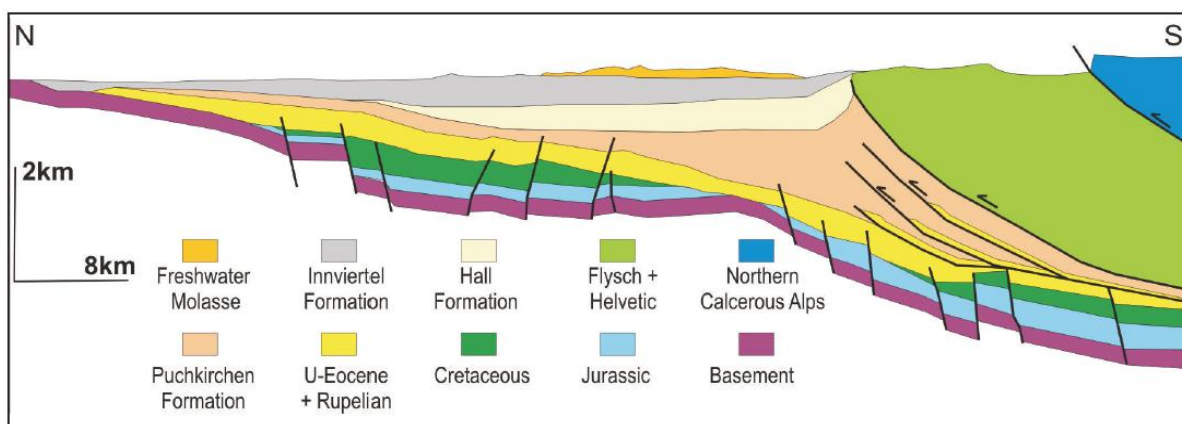


Figure 22: Simplified geological cross-section through the Upper Austrian Foreland Basin showing the crystalline basement, the autochthonous Mesozoic sediments (Cretaceous, Jurassic), the Molasse succession (Eocene, Rupel, Puchkirchen Fm., Hall Fm., Innviertel Fm. and Freshwater Molasse) as well as the Alpine orogenic wedge (Flysch and Helvetic Units, and Northern Calcareous Alps) (after Hinsch, 2008; Wagner, 1996).

# 4.1 The Crystalline Basement

(SCHUSTER et al., 2011; LINNER et al., 2011)

About **650 my ago** the crustal parts of today's Bohemian Massif and the Alps were located on the northern edge of Gondwana, thus in higher latitudes on the southern hemisphere.

Until and during the **Devonian** (416-359 Ma) the continent drifted continually northwards and entered a tropical environment with more favorable conditions for carbonate producing marine organisms. During the **Upper Devonian** a new supercontinent, called Pangaea, began to form by the collision of the continents Gondwana and Laurussia. This induced the Variscian orogeny, which also affected parts of nowadays Bohemian Massif and Alps.

Underlying a continuous convergence and intensive magmatism, lower parts of the crust have been exhumed and a NE-SW and NW-SE striking conjugated fault system developed during the **Upper Carboniferous**. The southern part of today's Bohemian Massif is dominated by these dextral NW-SE ("Pfahl and Danube Fault") and sinistral NE-SW ("Rodl and Diendorf Fault") striking fault systems that formed in the Carboniferous (359-299 Ma) and have been reactivated during the lower Permian (Figure 23; BRANDMAYR et al., 1995; MATTERN, 2001). From now on massive erosion shaped the Variscian relief further.
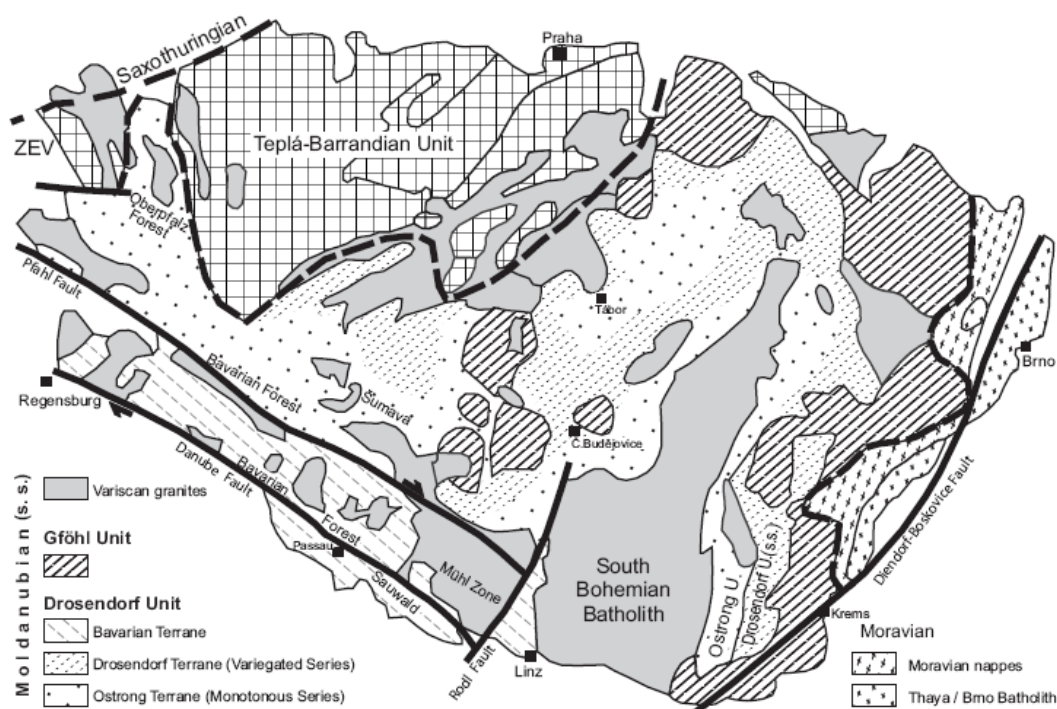


**Figure 23: Map of the tectonic units and major faults in central and southern Bohemia (Finger et al., 2007).**

The basement topography shows swell areas, such as the NW-SE trending Central Swell Zone, which is a major structural feature of the basement and the continuation of the Landshut-Neuötting High of Eastern Bavaria (NACHTMANN, 1987; MALZER et al., 1993). These basement highs are supposed to be repeatedly reactivated during the Mesozoic and Paleogene (NACHTMANN, 1987).

## 4.2 Mesozoic Passive Continental Margin

(SCHUSTER et al., 2011; RUPP, 2011)

During the **Triassic** (251-200 Ma) the area of today's Bohemian Massif still remained an island in the shelf sea throughout the whole period (Figure 24).
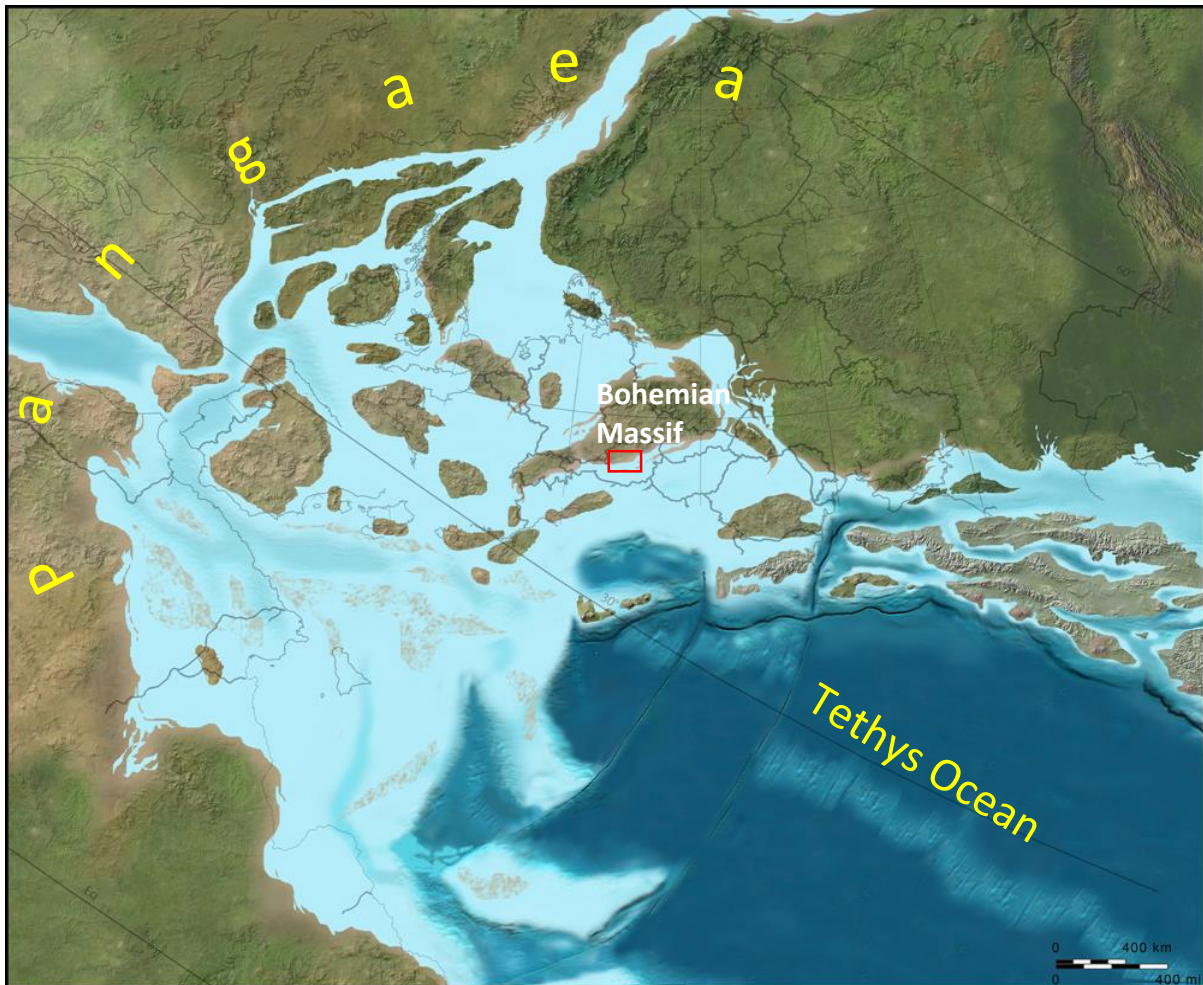
**Figure 24: Paleogeographic sketch map for the period around 200 my ago (Triassic/Jurassic). The red rectangle shows the approximate location of the study area (modified after Blakey, 2011); the area of the Bohemian Massif remains an island in the shelf sea. The Permo-Triassic rifting had no remarkable influence on the area of interest.**

The **Middle Jurassic** (174-163 Ma) was the time when the supercontinent Pangaea began to split and the central Atlantic Ocean started to open up between nowadays western Africa and southern North America. The new middle oceanic ridge advanced along huge transform faults far to the east. There the Penninic Ocean opened up between nowadays European continent with its Helvetic Shelf in the west and Africa with the Adriatic shelf in the east (Figure 25; FRISCH, 1979; HANDY et al., 2010). Uplifts of the Helvetic Shelf formed islands and the Permotriassic deposits were completely eroded. When the shelf subsided and the area was flooded again, the sedimentation of the first major cycle started. Sediments include carbonates and siliciclastic deposits. This first sedimentation cycle lasted until the Lower Cretaceous. Subsequent regional erosion removed some of the material again and karstified the remaining carbonates. The sediments of this cycle constitute the lower part of the Autochthonous Mesozoic and the lowest significant depositional succession above the crystalline of the Bohemian Massif. Figure 27 gives more detailed information about the lithostratigraphy of the Mesozoic succession and an overview of depositional and erosional phases.

The crystalline basement to the south and southeast of the Bohemian Massif evolved into a passive continental margin during the Jurassic and Lower Cretaceous. Sediments of the distal margin are incorporated into the allochthonous Gresten Unit, which contains a typical passive margin succession with Lower Jurassic clastic sediments, Middle Jurassic shelf deposits, and Upper Jurassic to Lower Cretaceous deep-marine sediments (FAUPL, 1975; see review by WESSELY, 2006).



**Figure 25: Paleogeographic sketch map for the period around 150 my ago (Jurassic). The red rectangle shows the approximate location of the study area (modified after Blakey, 2011); The Penninic Ocean opens up between Laurussia and Gondwana, while the area of interest is located on the Helvetic Shelf where the first cycle of sediments (Autochthonous Mesozoic) with carbonates and siliciclastic sediments is deposited (Figure 27).**

In the **Upper Cretaceous** (100-65 Ma) a further transgression, referred to as the second major sedimentary cycle, took place starting in the Cenomanian (Figure 26). It induced the sedimentation of sands and clay, which represent the main deposits for this period. Large parts of those were to be eroded again during the Paleogene regression (FREUDENBERGER & SCHWERD, 1996; WAGNER, 1998; KRÖLL et al., 2006b), when all the Mesozoic sediments along the Central Swell Zone were removed from its crystalline basement (Figure 28; MALZER, 1993; WAGNER, 1998; KRÖLL et al., 2006b).
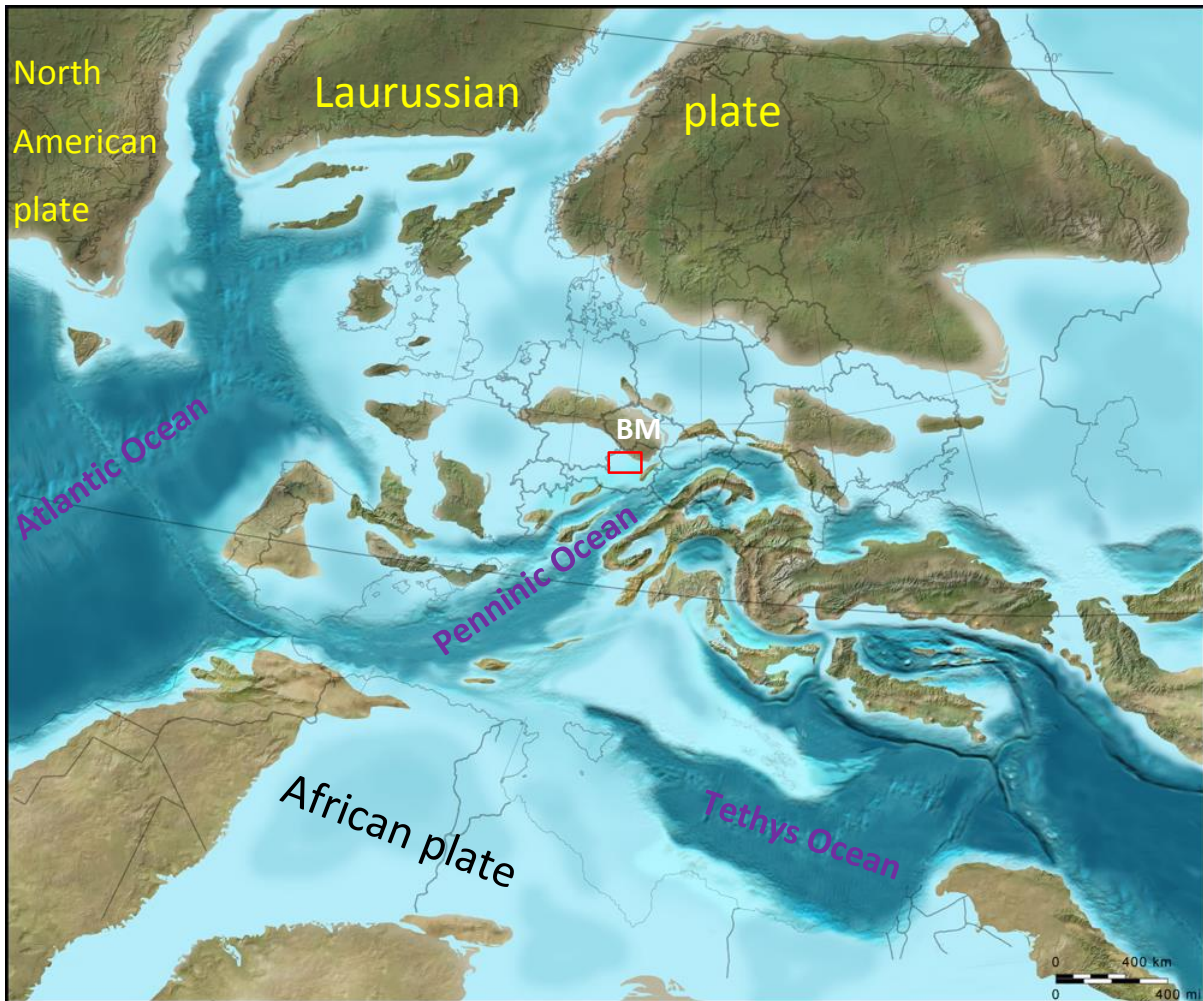
**Figure 26: Paleogeographic sketch map for the period around 75 my ago (Upper Cretaceous). The red rectangle shows the approximate location of the study area (modified after Blakey, 2011); The Penninic Ocean is being subducted below the Austroalpine. On the Bohemian Massif sedimentation of the second major cycle takes place after a long period of erosion in the Lower Cretaceous. Mainly sands and clays were deposited. BM= Bohemian Massif.**
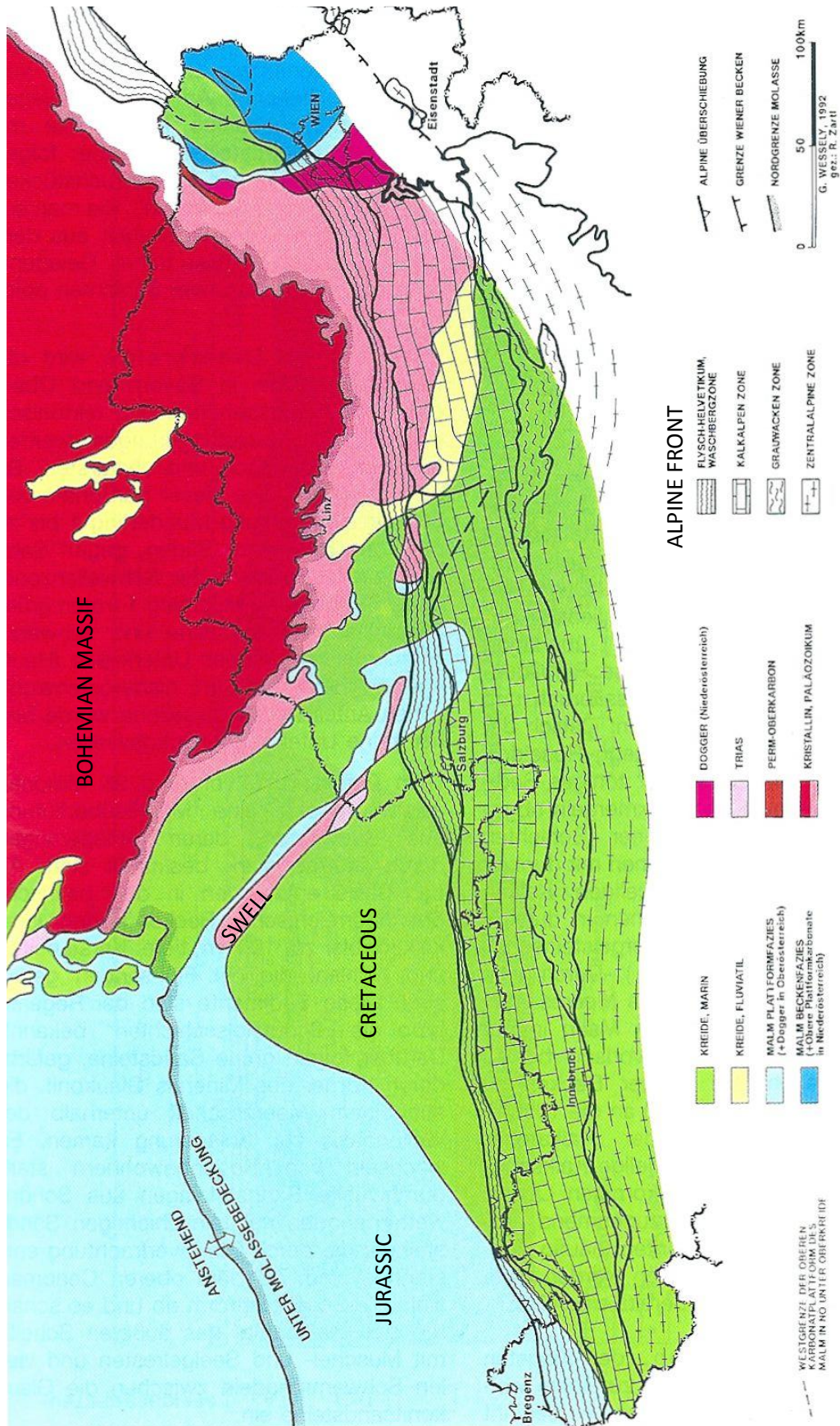
**Figure 27: Stratigraphic chart of the Molasse basement from the Salzach/Inn to the Bad Hall Basin showing the two depositional phases of the Autochthonous Mesozoic. First sedimentary cycle: blue; second sedimentary cycle: green (modified after Malzer et al., 1993).**

**Figure 28: Distribution of the autochthonous Mesozoic sediments on the crystalline of the Bohemian Massif (modified Malzer, 1993; Wessely, 1992). Green: Cretaceous, marine; yellow: Cretaceous, fluviatile; light blue: Malmian platform carbonates; red: crystalline Bohemian Massif; rose: Triassic.**

# 4.3 Alpine Shortening and formation of the Foreland Basin

(SCHUSTER et al., 2011; RUPP, 2011)
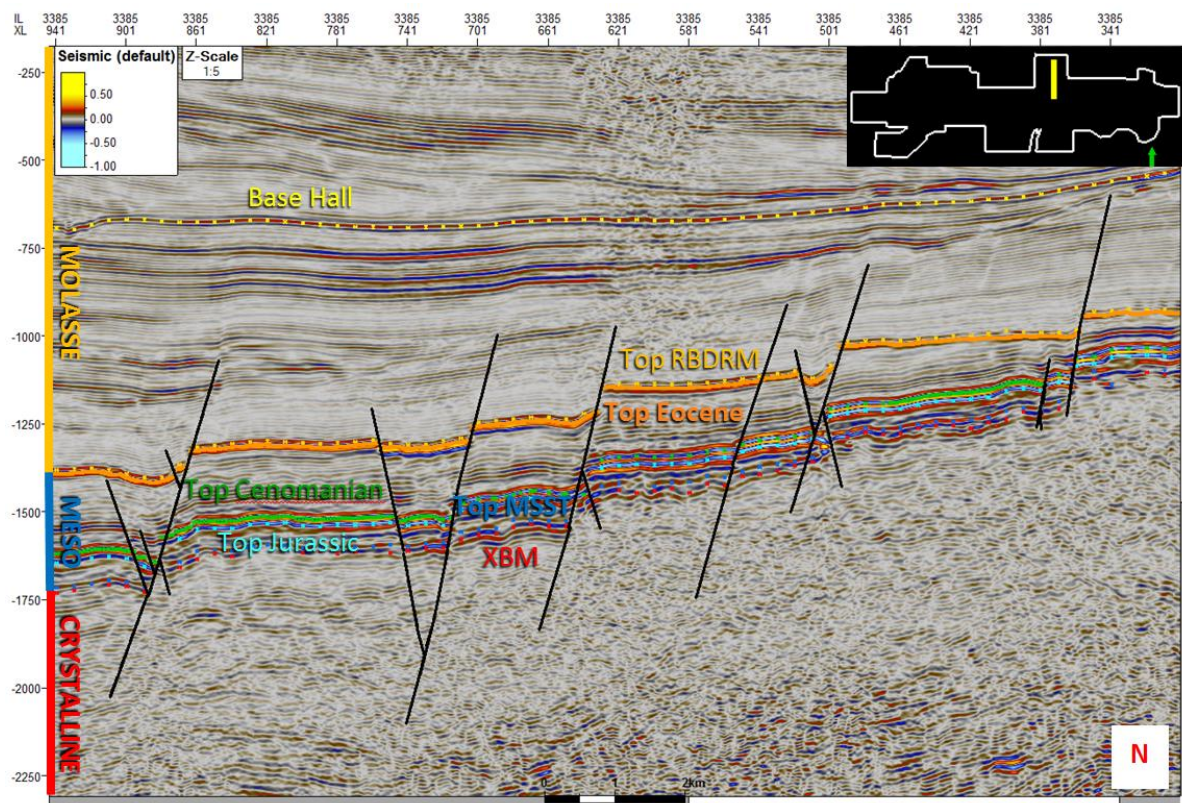


**Figure 29: Inline 3385 in TWT showing the central part of the seismic area; the intersection illustrates the three major depositional cycles and the typical foreland basin pattern very well. Above the crystalline basement the Autochthonous Mesozoic can be clearly identified. The first Jurassic cycle is shown in light blue, the second Upper Cretaceous cycle in green. The Mesozoic successions are overlain by the Molasse sediments.**

## 4.3.1 Paleogene (65-23 Ma)

About 50 my ago, in the early **Eocene** the Penninic Ocean had nearly closed (Figure 30). The Alpine orogenic wedge was thrusting on the Helvetic Shelf and sheared off parts of the autochthonous sediments, which formed the Helvetic and Ultrahelvetic thrust units (WESSELY, 2006; RUPP et al., 2011). Continental lithosphere of the Helvetic shelf entered the subduction zone and forced shortenings in the orogenic wedge.

By time, the for over hundred million years subducted lithospheric mantle slab broke off (BLANKENBURG & DAVIS, 1996; BLANKENBURG et al., 1998) and caused intense isostatic compensational movements, which led to a further rising of the central Alps (FRISCH et al., 1998).
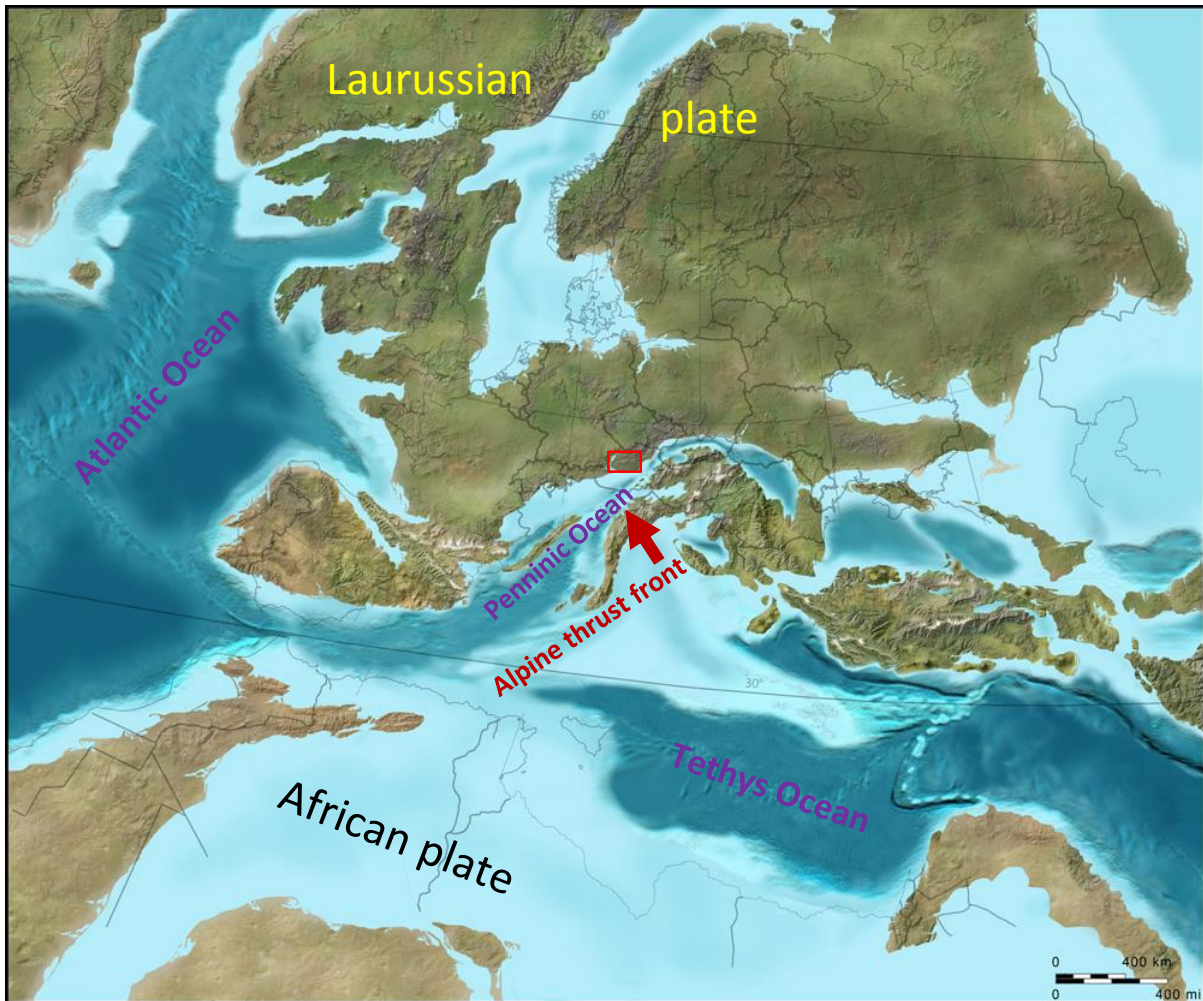
**Figure 30: Paleogeographic sketch map for the period around 50 my ago (Eocene). The red rectangle shows the approximate location of the study area (modified after Blakey, 2011). The Penninic Ocean is nearly closed and the Alpine orogenic wedge was thrusting on the Helvetic Shelf and sheared off parts of the autochthonous sediments, incorporating these. The basin is getting filled with the Molasse sediments.**

Thrusting of the Alpine thrust wedge over the European foreland and the southern part of the Molasse Basin started in the Late Eocene (37 Ma) and continued throughout the Oligocene (DECKER & PERESSON, 1987; HINSCH, 2013).

At the turn from the Eocene to the **Oligocene** (35 Ma), northward thrusting of the Alpine thrust wedge on the European plate and the weight of the overthrust units induced the downward flexure and subsidence of the Alpine foreland (Figure 29). A new marine Molasse foreland basin originated, which was part of the Paratethys (Figure 31; RÖGL, 1999; STEININGER & WESSELY, 2000). Sedimentation in the Molasse Basin followed after a long erosional phase in the lower Paleogene and is referred to as the third major cycle of the crystalline basements sedimentary covers (WAGNER, 1998).

**Figure 31: Paleogeographic sketch map for the period around 25 Ma ago (Oligocene). The red rectangle shows the approximate location of the study area (modified after Blakey, 2011). The load of the north moving Alpine wedge induces flexural bending of the crust below. Parts of the Molasse become sheared off from their basement and incorporated into the wedge during the Late Oligocene and Early Miocene (Allochthonous or Imbricated Molasse).**

In the Molasse Basin of Upper Austria a northern lagoon was divided from the open sea by the Central Swell Zone (Figure 28). The Perwang Group was deposited, including from north to south the limnic Voitsdorf Formation, overlain by the brackish Cerithien Layers and the shallow marine Ampfinger Sandstone, the Lithothamnien (Rhodophyta-) Limestone on the swell, followed by Nummulite Sandstone and Discocycline Marls (Eocene; Figure 33).

Through further subsidence of isolated parts of the basin anoxic deep water environments developed where sediments with a high organic content were deposited, like the Schöneck Formation (Kiscellian). This anoxic succession (also called Latdorf-Fischschiefer, MALZER, 1993) is one of the most important source rocks in Upper Austria.

Isolation of the basin and lowering of the salinity through a rising freshwater input led to the deposition of the Dynow Formation (Kiscellian), consisting to a large part of euryhaline nannoplankton skeletons (SCHULZ et al., 2004). After lowering of the freshwater influx the salinity normalized again and the Eggerding Formation (Kiscellian), which is a synonym for the Rupelian

28

banded marl (MALZER, 1993), was deposited. The Zupfing Formation (Kiscellian) was deposited at the time when the connection to the open ocean came into existence again.

The worldwide lowering of the sea level, which occurred in the latest Kiscellian (around 26 my ago), caused a regression from the part of the Molasse basin west of Munich (REISER, 1987; KUHLEMANN & KEMPF, 2002; BIEG, 2005), whereas subsidence in the part to the east of today's Inn river continued and the deep marine Puchkirchen Formation was deposited (Egerium; Figure 33; WAGNER, 1998). These sediments consist of detritus derived from the western part of the Molasse Basin and the rising Alps, whereas rivers transported material from the Bohemian Massif into the shallow northern part of the basin and formed marine sand deposits. The basin floor is dominated by a huge deep marine channel with basin floor fans (HINSCH, 2007). The sedimentation of the Puchkirchen Formation lasted until the Lower Miocene, Eggenburgian (RÖGL & RUPP, 1996).

## 4.3.2 Neogene (23-2.6 Ma)

At the beginning of the Neogene the Eastern Alps experienced a change in their tectonic evolution, which resulted in the shift of the tectonic style from mainly north-directed thrusting (Paleogene) to **Miocene** eastward extrusion towards the Pannonian Basin (late Oligocene-Miocene; LINZER et al., 1995; PERESSON & DECKER, 1997). During that period WSW-ENE striking sinistral strike-slip faults including the Salzach-Ennstal-Mariazell-Puchberg Fault (LINZER et al., 1990), the Innsbruck-Salzburg-Amstetten Fault (EGGER, 1997) and the Königssee-Lammertal-Traunsee Fault (DECKER et al., 1994) formed in the northern Eastern Alps.

Shortening of the Molasse Basin continued and parts of the successions were accreted into the orogenic wedge (Imbricated or Allochthonous Molasse; HINSCH, 2013). The youngest deep marine deposits are represented by the Hall Formation, consisting of clay marls and sandstone layers. Above the Hall Formation only shallow marine successions followed by brackish and limnic/fluviatile sediments were deposited.

Since the Upper Eggenburgian (ABERER, 1958) respectively Ottnangian (RUPP, 2011) the ancient Salzach river's proximal fan-delta transported sediments into the shallow Paratethys sea. In the upper Ottnangian the Paratethys split into several smaller basins and the Oncophora Formation was deposited while desalinization continued (PAPP et al., 1973). Due to the change in marine circulation, as a consequence of changing seaways, the final regression of the Paratethys Sea from the Molasse Basin in Upper Austria occurred about 17 my ago  (Ottnangium-Karpatium; Figure 33; RUPP, 2011; PILLER et al., 2004). From that time on only limnic/fluviatile sediments, gravels, sands, clay, and coals of the Upper Freshwater Molasse were to be deposited (Figure 32; RUPP, 2011; PILLER et al., 2004).
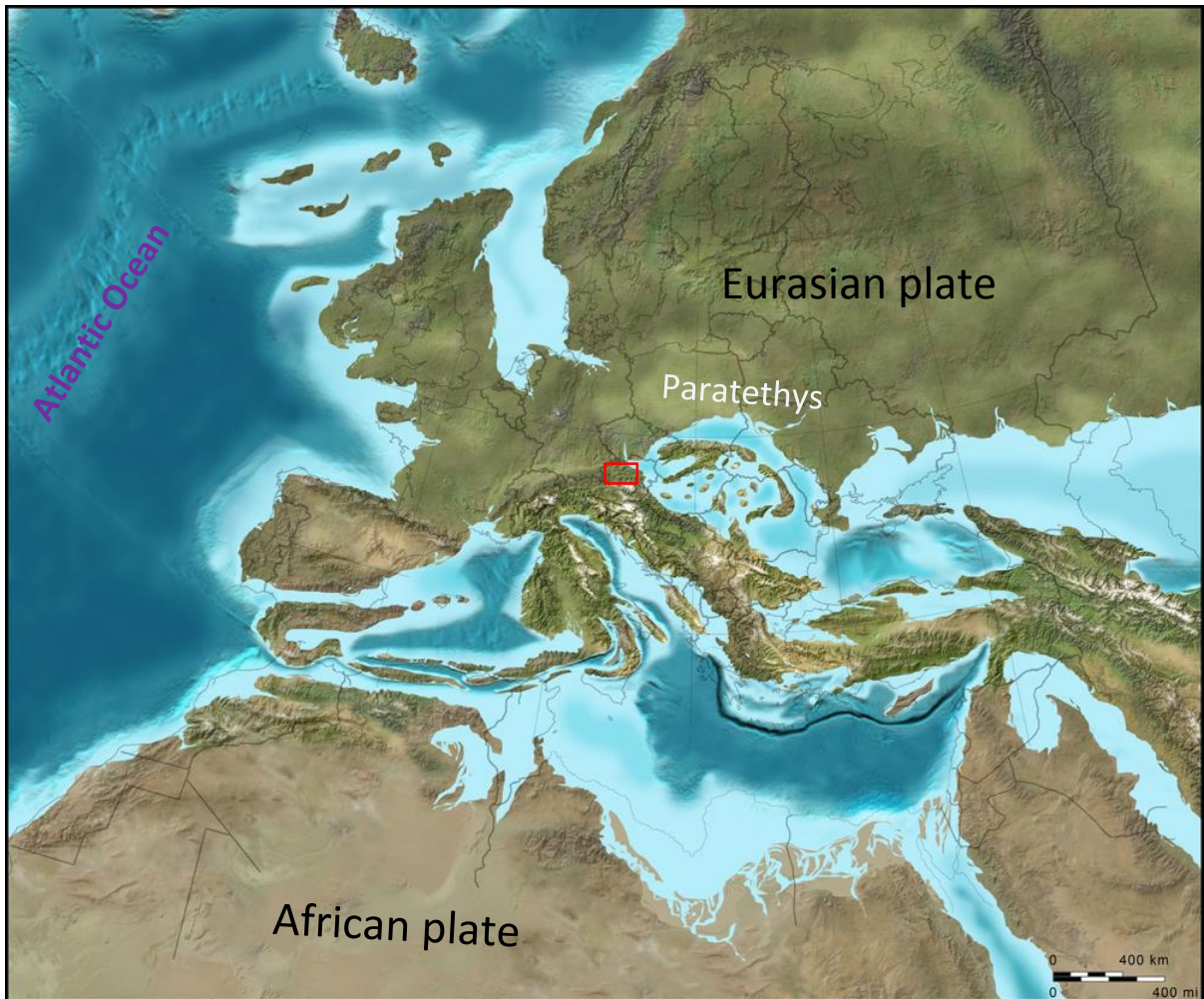
**Figure 32: Paleogeographic sketch map for the period around 13 my ago (middle Miocene, Badenian). The red rectangle shows the approximate location of the study area (modified after Blakey, 2011); The Paratethys regressed from the study area and only limnic and fluviatile sediments are deposited in the Molasse Basin of Upper Austria.**
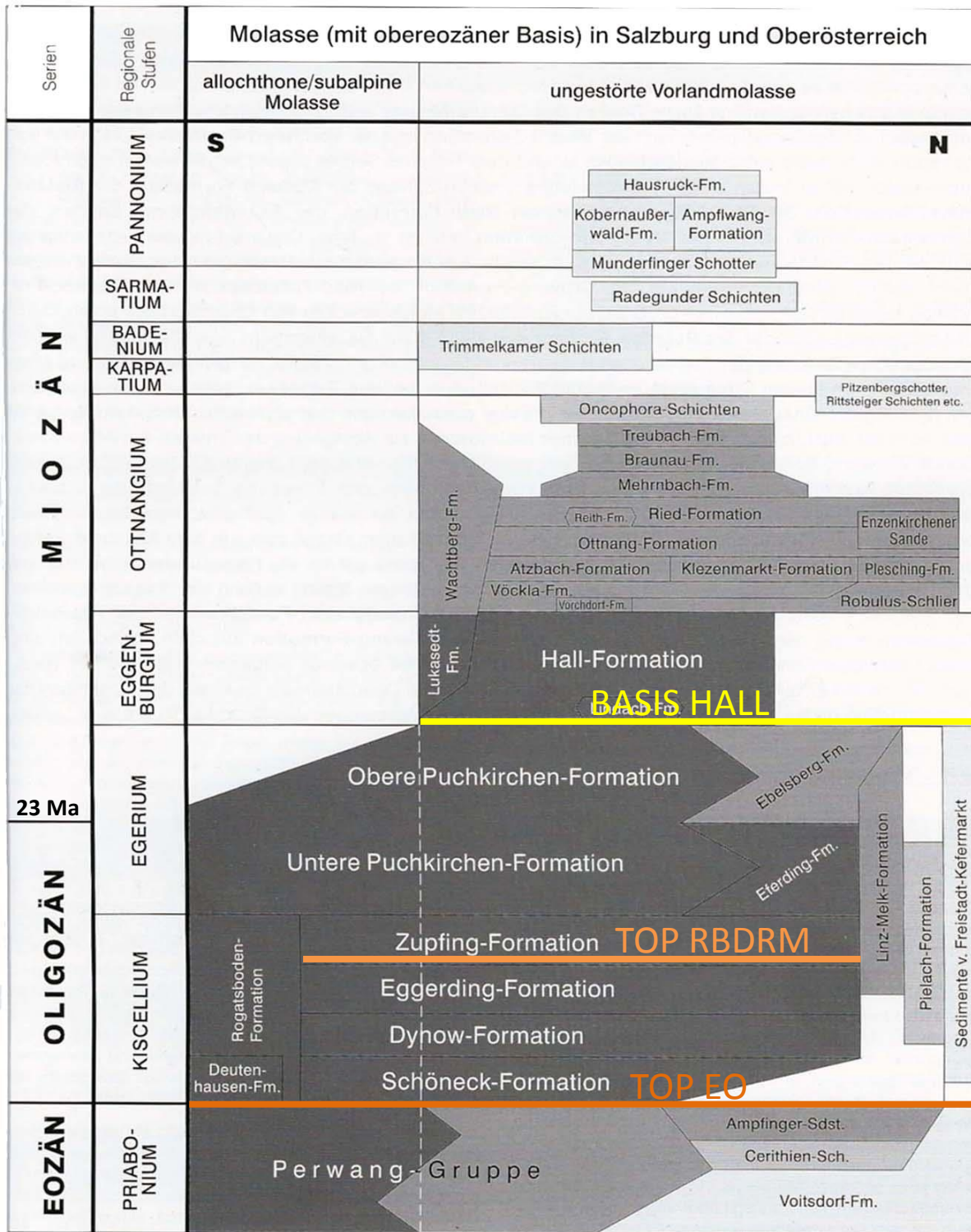
Figure 33: Stratigraphic chart of the Molasse sediments from Salzburg to Upper Austria; colored lines show horizons mapped in the seismic data by RAG Austria, which are used in this thesis (modified from Rupp, 2011; Wagner, 1998).

# 5 MAPPED FAULTS

**Fault Mapping**

The relevant area for fault interpretation of Upper Austria's autochthonous Molasse and its Mesozoic basement is shown in Figure 34 and reaches from the river Salzach/Inn to the Enns. The whole area includes about 3000 km² of Pre-Stack Time Migrated (PrSTM) 3D seismic.

For the given issue more than 350 faults of different sizes have been manually tracked with the software Petrel 2012 to define structures, find trends and describe the tectonic evolution. Manual tracking means that fault polygons were created by drawing piles (fault sticks) for each 10th Inline, Crossline or Random Line, depending on and preferably perpendicular to the fault orientation. In many cases a combination of sections of different orientation has been used for tracking a single fault, especially within complicated structures.

The newly generated fault attribute volume showing fault information as high contrasted lines, beneath horizon interpretations (by RAG Austria), surface projections and others were used as guidance for identifying faults (see Chapter 3).
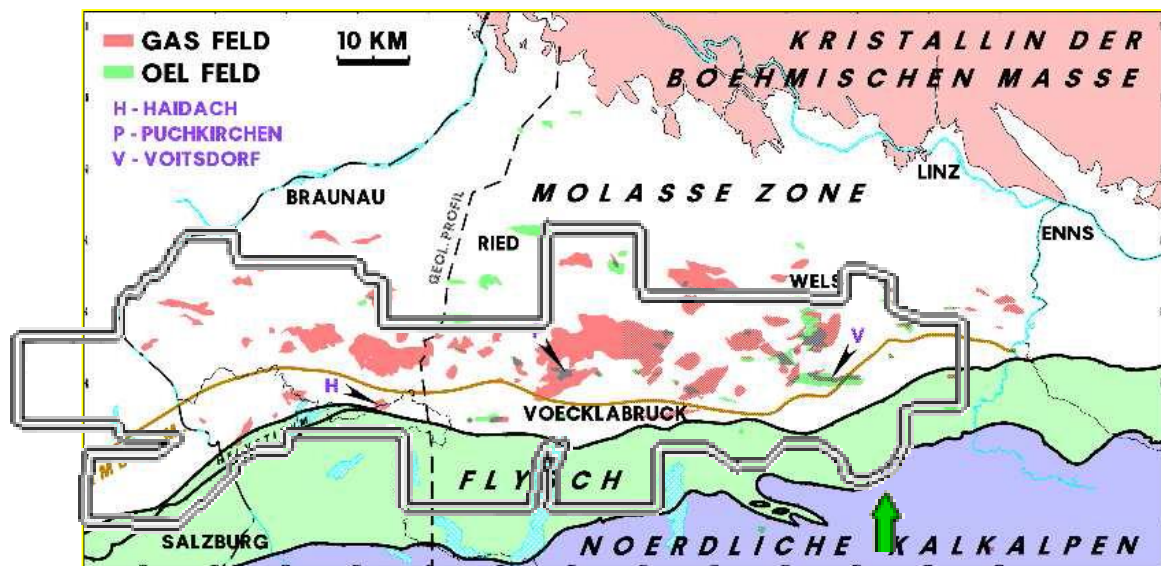


**Figure 34: Geological overview and approximate location of seismic volume (about 3000 km²). The Molasse Zone inside of the seismic volumes outline is the relevant area for fault mapping of the autochthonous Molasse and its Mesozoic basement (modified from Nachtmann, 2003).**

**Surfaces**

All surfaces are depicted with a mini map that shows the outline of the whole volumes area and the location of the seismic cross sections as yellow lines, which is the same as shown on the surface (Figure 36). Additionally there is always an arrow giving the orientation of the depicted segment, where green color indicates a top view and red a view from below. In the upper left the projected units and colors according to their range can be found.

**Cross Sections**

Figures depicting cross sections have nearly the same structure as those depicting surfaces. They include a minimap indicating the location of the intersection, information of the section's orientation, the horizontal scale at the bottom center (constantly 2 kilometers for whole length), the color code of the shown seismic or attribute (attribute, intensity), and the Z-Scale, which is fixed at 1:5 (Figure 35).

# 5.1 Lithostratigraphic Framework and Mapped Horizons

The horizon interpretations have been done and provided by RAG Austria. Figures in the following paragraphs display horizons in specific colors and include from top to the bottom:

| Color | Horizon Name | Lithostratigraphy | Age (Ma) |
|---|---|---|---|
| Yellow | BASIS HALL | Base Hall Formation | 20.8 [1] |
| Light orange | TOP RBDRM | RupelBänDeRMergel; Rupelian Banded Marl | 26 [1] |
| Orange | TOP EO | Eocene | 33.9 [1] |
| Green | TOP CE | Cenomanian | 94.2 [1] |
| Light blue | TOP JURA | Jurassic | 145.5 [1] |
| Blue | TOP MSST | MalmianSandSTone | |
| Red | XBM ( _Swell) | Crystalline Bohemian Massif | $310 - 800$ [2] |

**[1] (PILLER et al., 2004); [2] (MALZER et al., 1993)**

**Reflectors**

The different reflectors and thus the interpreted horizons vary in quality and density. In general the deeper horizons are of less quality. Especially the Malmian Sandstone and the crystalline of the Bohemian Massif are often hard to clearly identify and track (Figure 35).
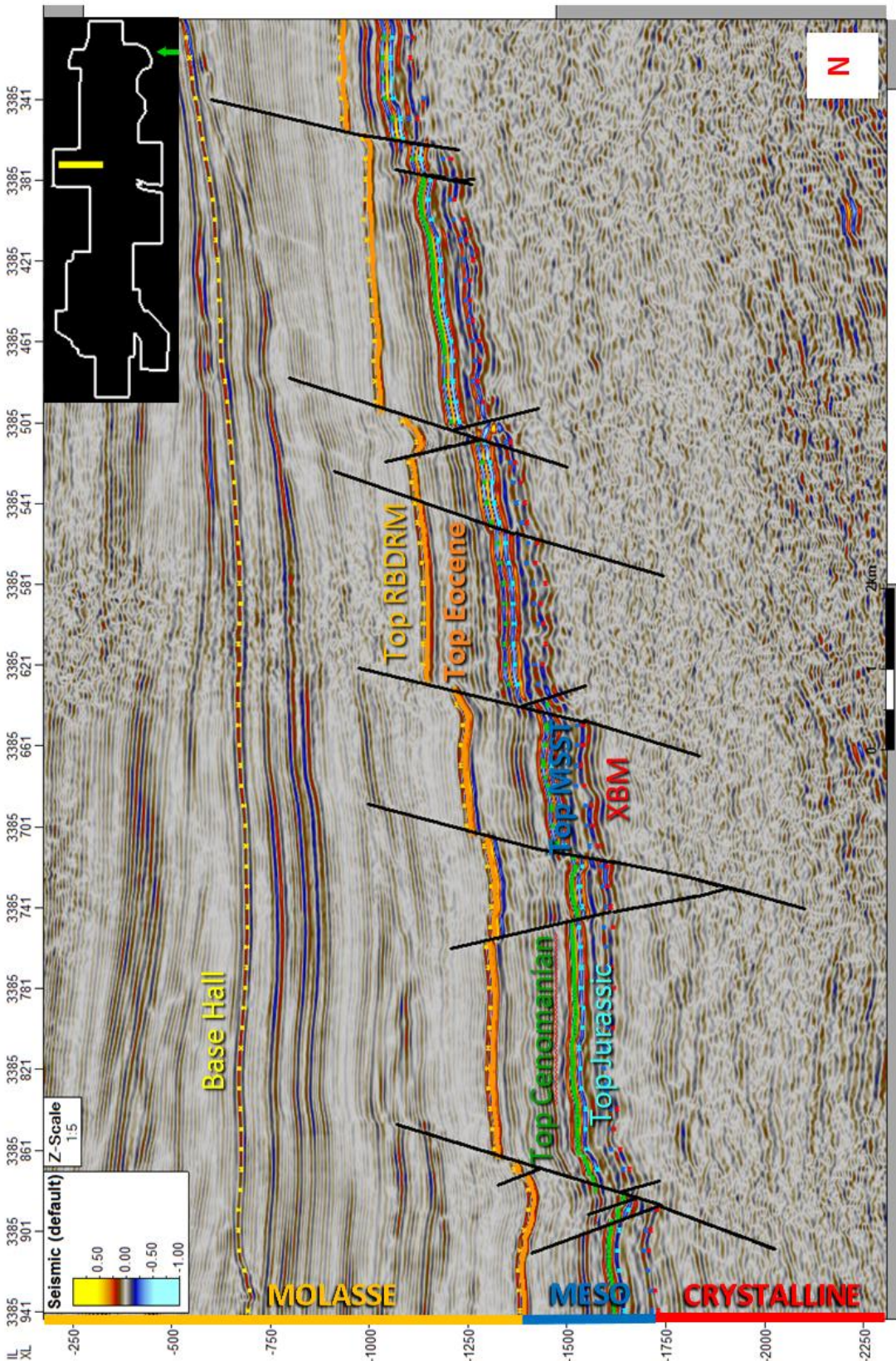
**Figure 35: Inline (PrSTM) showing the major lithostratigraphic successions on top of the crystalline basement in the central part of Upper Austria's Molasse Basin, as well as the Autochthone Mesozoic units and the successions of the Molasse foreland basin. Mapped horizons: BASIS HALL (Base Hall Formation), TOP RBDRM (Rupel Bändermergel; Rupelian Banded Marl), TOP EO (Eocene), TOP CE (Cenomanian), TOP JURA (Jurassic), TOP MSST (Malmian sand stone), XBM (Crystalline Bohemian Massif). Horizons mapped by RAG Austria.**

# 5.2 Cretaceous to Oligocene Reactivated Fault Systems

## 5.2.1 Central part of the seismic area

Map views of pre-Eocene surfaces, like the Top Jurassic (Figure 36), show prominent NNW-SSE striking faults together with approximately E-W striking structures that are discussed more detailed in chapter 5.3 (Kiscellian to Eggenburgian fault systems).
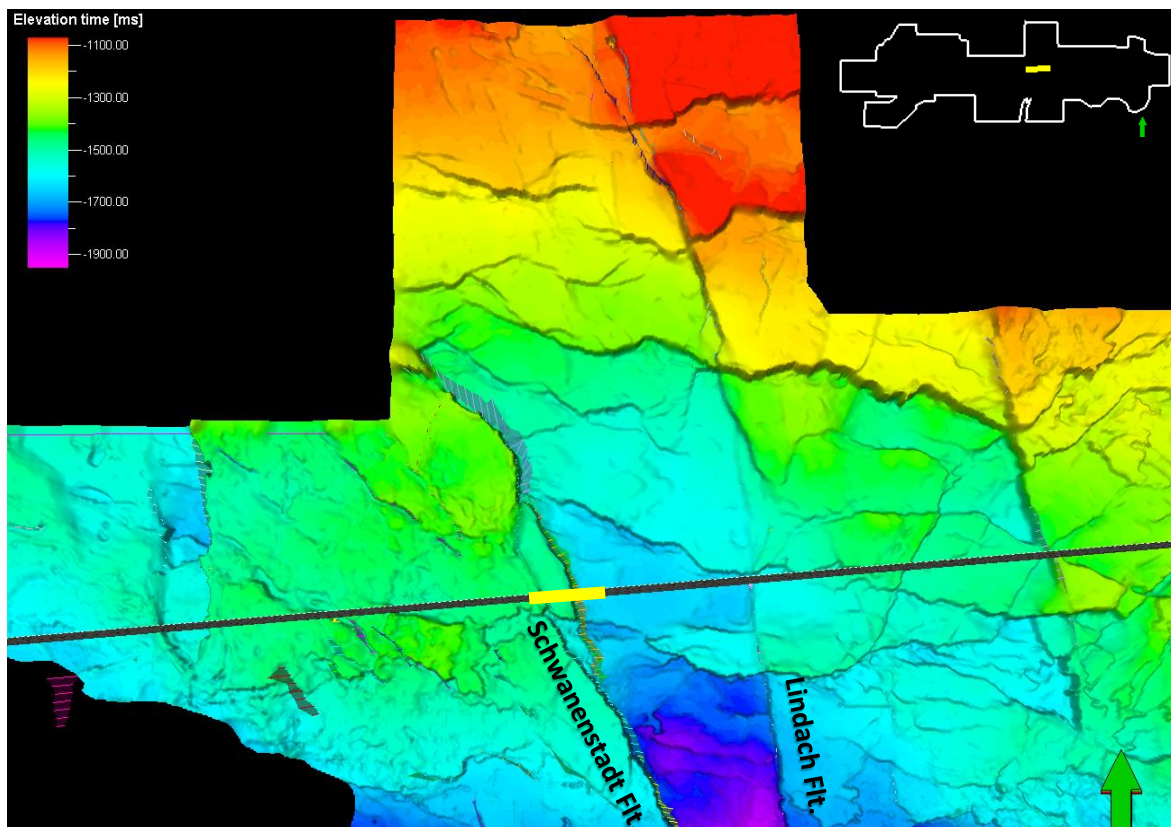


**Figure 36: Shaded relief of the Top Jurassic horizon (PrSTM; elevation in ms TWT, see upper left) with position of the intersection shown in Figure 38, Figure 39 (yellow line) and location in the volume (minimap: upper right).**

The following intersections show large differences in the thickness of Cretaceous sediments across faults (thickness differences of 130 to 0 ms; Figure 38, Figure 39). This can also be observed in the calculated thickness map for the Cretaceous sediments (Figure 37), which shows that the thickness differences are caused by the three main NNW-striking faults (Schwanenstadt Fault, Lindach Fault and the easternmost unnamed fault), also shown in the cross sections (Figure 38 to Figure 40).

The Schwanenstadt Fault consists of several splay faults with convex up shapes that converge to depth. The faults are interpreted to root in a single master fault (Figure 38, Figure 39). Adjacent to the easternmost fault of this structure, the reflector edges are dragged up. Hence, the observed fault pattern leads to the interpretation of a positive flower structure (palm structure) and, therefore, strike-slip faulting.

The thickness of the Upper Cretaceous increases from about 30 ms west of the Schwanenstadt Fault to about 220 ms east of it. The seismic does not indicate Cretaceous growth strata at this fault. Upper Cretaceous growth strata, however, exist further to the east at the Lindach Fault, which strikes sub-parallel to the Schwanenstadt Fault and terminates upward within the Upper Cretaceous sediments (Figure 40). The Cretaceous reflectors are offset up to 30 ms by this fault.

The data suggest that most of the vertical displacement at the NNW-striking faults occurred between the Top Cenomanian and the Top Eocene.

The Top Eocene horizon above the Cretaceous succession is not offset by the splay faults (Figure 39). The Eocene sediments up to the horizon Top RBDRM cover all faults with constant thickness, indicating that no fault activity occurred during that time period.

The Top Eocene and younger reflectors right above the faults of the Schwanenstadt flower structure show a positive relief of about 50 ms (Figure 38, Figure 39). Onlaps of Oligocene growth strata on the western bulge allow assuming an Oligocene age for the formation of the bulge.
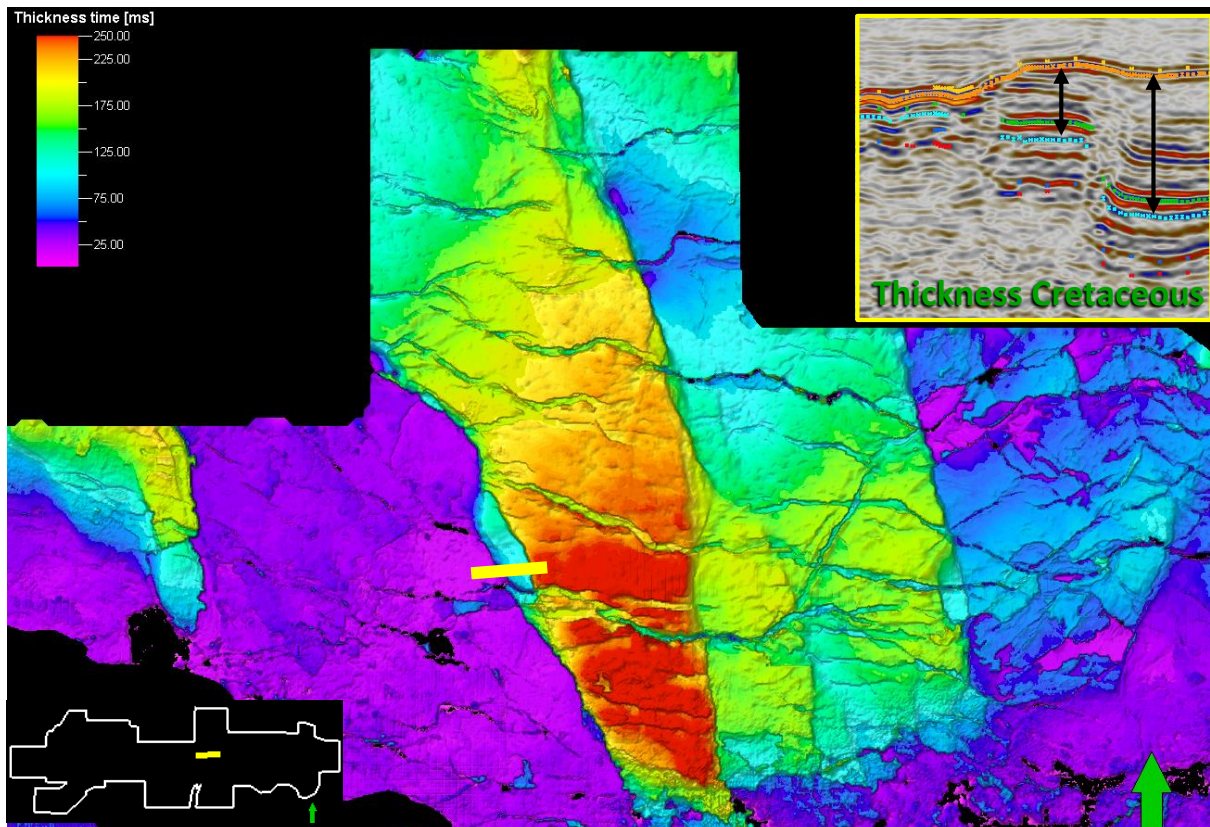


**Figure 37: Calculated TWT thickness of the Cretaceous by subtracting Top Jura from Top Eocene surface. Red: Cretaceous thickness >250 ms; Violet: 0 ms (no Cretaceous sediments). See minimap (lower left) for location.**
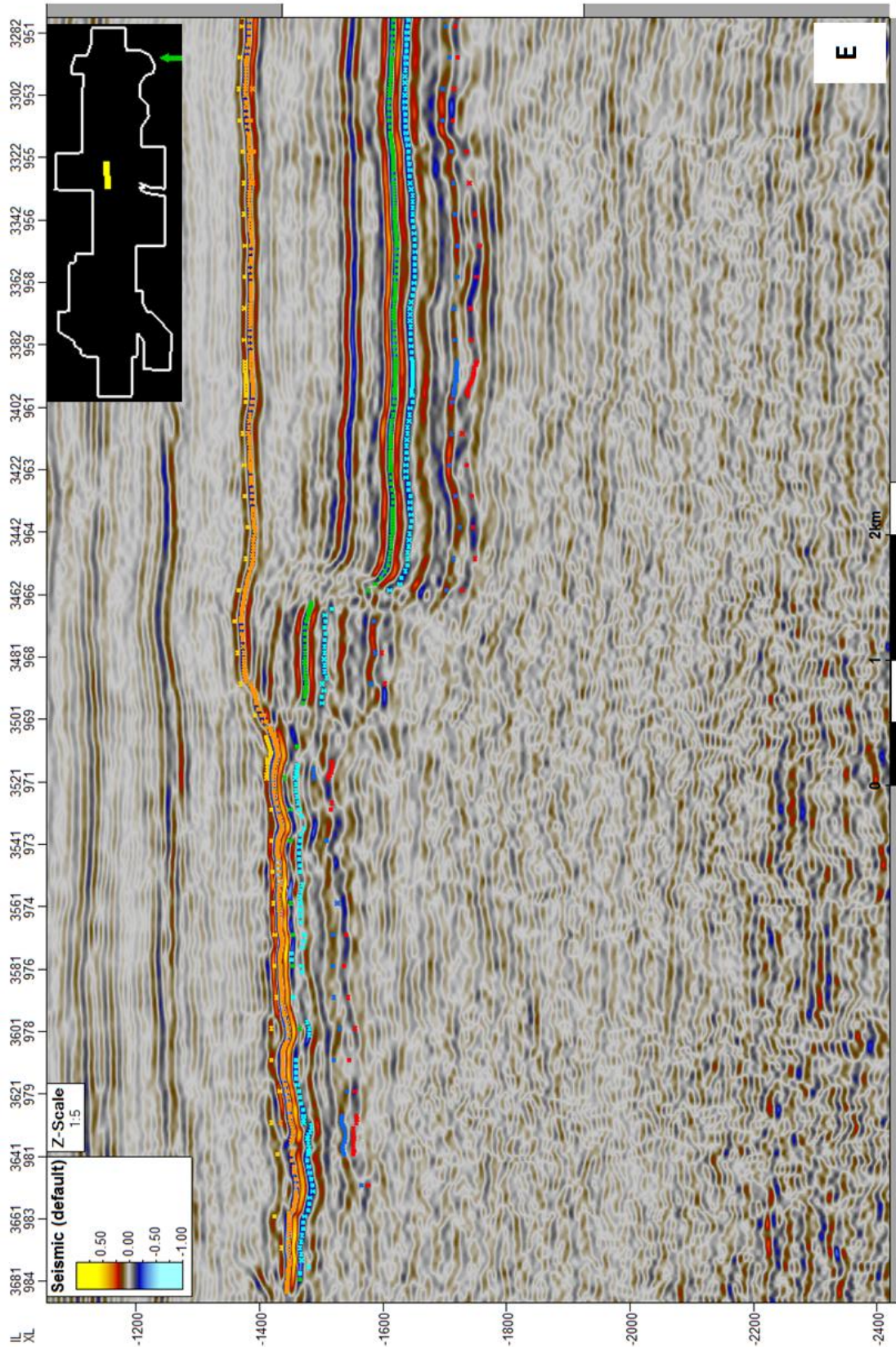
**Figure 38: Uninterpreted Random Line (PrSTM) with mapped stratigraphic horizons. See minimap (upper right) for location. The structural interpretation of the section is shown in Figure 39.**
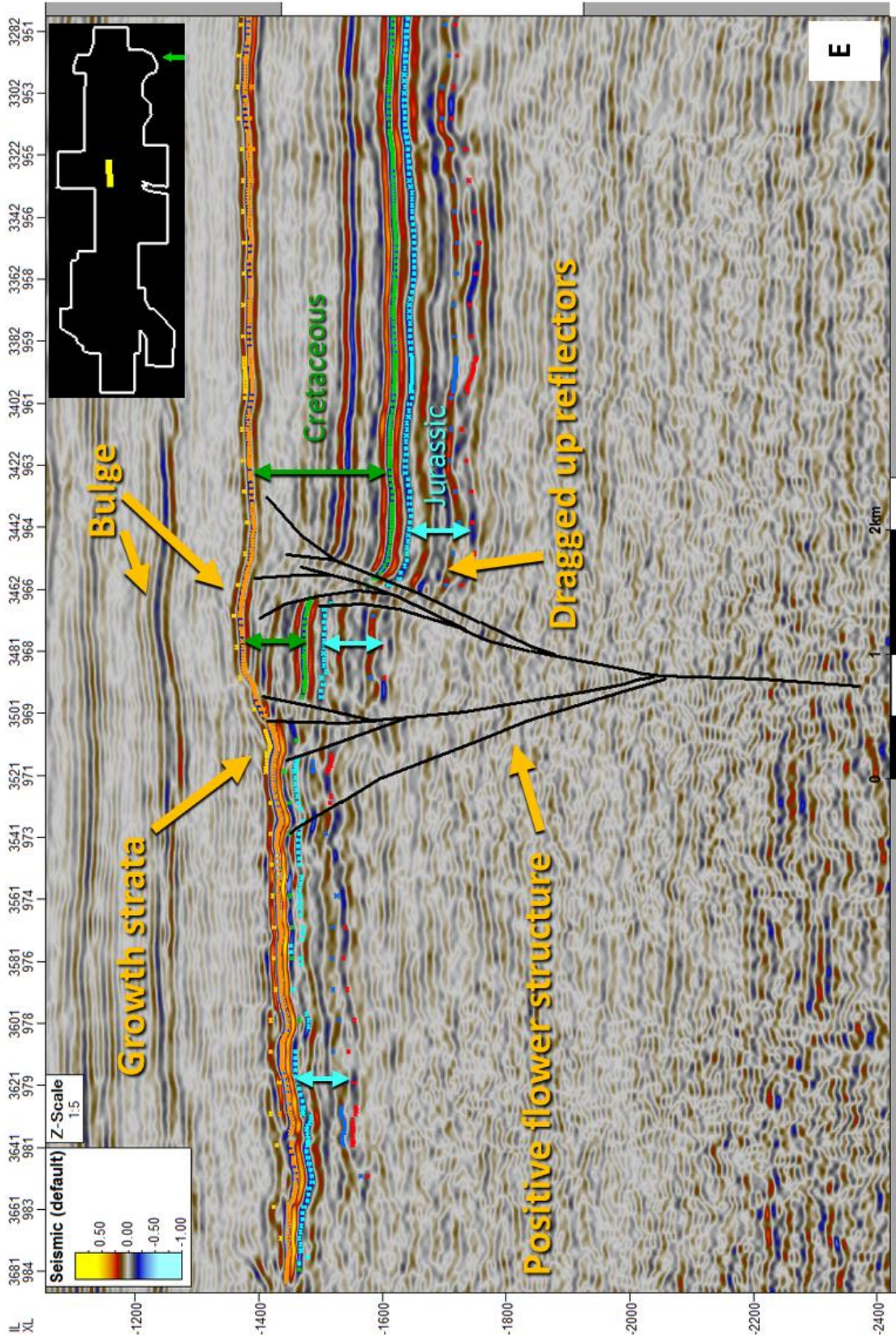
37

**Figure 39: Interpreted Random Line (TWT, PrSTM) across the Schwanenstadt fault showing a bulge of the horizons Top Eocene and Top RBDRM above a positive flower structure. Growth strata of Oligocene age are onlapping onto the structure. The mapped faults are interpreted to converge into a single major fault at depth. The fault is thought to be an Paleozoic strike-slip fault that became reactivated twice, between Top Eocene and the Cretaceous strata below, and the Oligocene. See minimap (upper right) for location.**
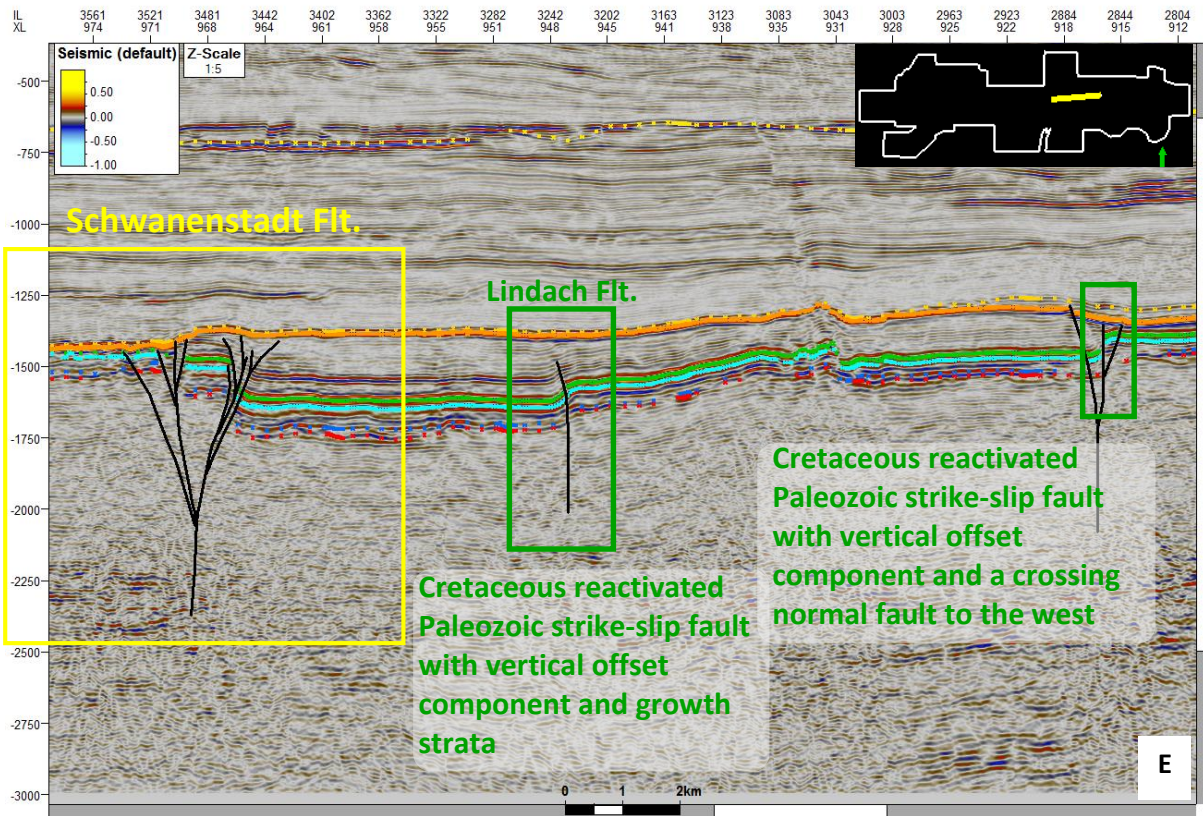
**Figure 40: Interpreted Random Line (TWT, PrSTM) with horizons showing the interpreted positive flower structure of the Schwanenstadt Fault, as well as the Lindach Fault and another NNW-striking fault offsetting Cretaceous sediments. See text for discussion. See minimap (upper right) for location.**

The bulge above the flower structure shows characteristic postsedimentary stratal geometries, which are shown in Figure 41. The axial surfaces of the deformed Oligocene sedimentary succession overlying the bulge and the Oligocene growth strata west of the positive flower structure dip away from the crest and therefore indicate that the deformed succession represents a drape sequence rather than growth strata. Fault activity leading to the uplift of the bulge therefore apparently stopped during the upper Kiscellian.
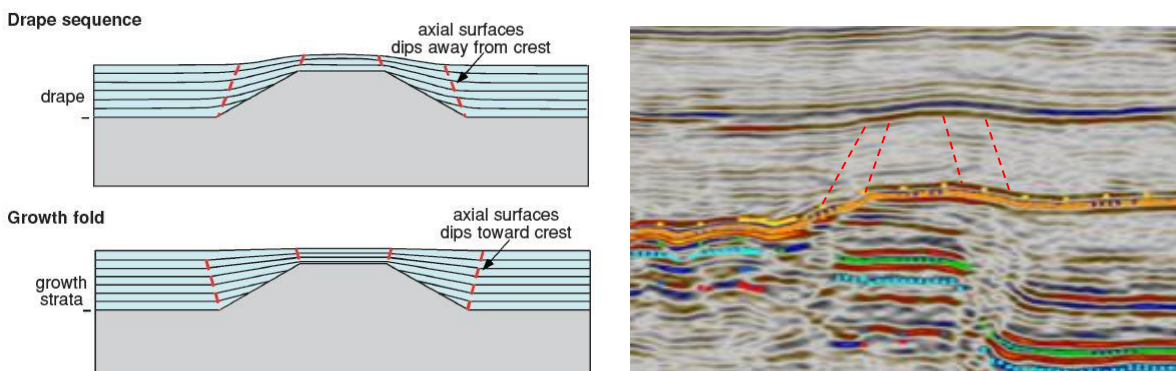


**Figure 41: Left: Sketch showing the characteristic features of syntectonic growth strata and postsedimentary drape sequences over an uplifted rigid structure (from Shaw et al., 2005); Right: Implication on the Oligocene succession on the top of the positive flower structure shown in Figure 39 and Figure 40. The axial surfaces are dipping away from the crest and therefore indicate a drape sequence.**

Focusing on the positive flower structure again one can imagine three steps in its tectonic evolution. The first step is faulting, which subsides the fault blocks inside and east to the flower structure, compared to the western block, between Top Eocene and the Cretaceous strata below. Then the sediments in the center experienced an uplift and after a phase of erosion that was followed by a tectonically inactive timespan, the Eocene to Oligocene sediments were deposited. According to the constant thickness of the mapped Paleocene horizons, the last step is an Oligocene transpressional regime leading to the formation of the bulge and growth strata west of it.

Due to the geometric pattern of the area in the 3D model it is also possible to interpret the faults crossing the Lindach strike-slip fault as Riedel shear sets (Figure 42), whereas the major faults are represented by the NNW -SSE directions (Figure 43). In fact that would indicate dextral strike-slip faults according to the orientations of the Riedel shears. Expanding this model on the whole path of the bended fault leads to further confirmation of the theory (Figure 43). Moreover, it is very probable that some of these faults acted as structural weaknesses and were therefore reactivated as normal faults later on.

So the idea is the prevailing of transpressional deformation during the origination of the strike-slip system, distorting the angles of the Riedel shear sets.
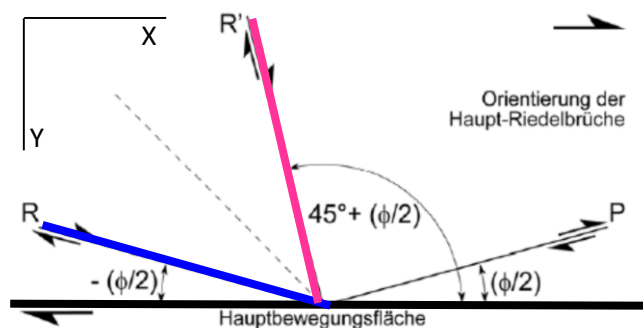


**Figure 42: Riedel shear set; R=Riedel shear, R'=Anti-Riedel shear, P-Shear (modified after Burg, 2007).**
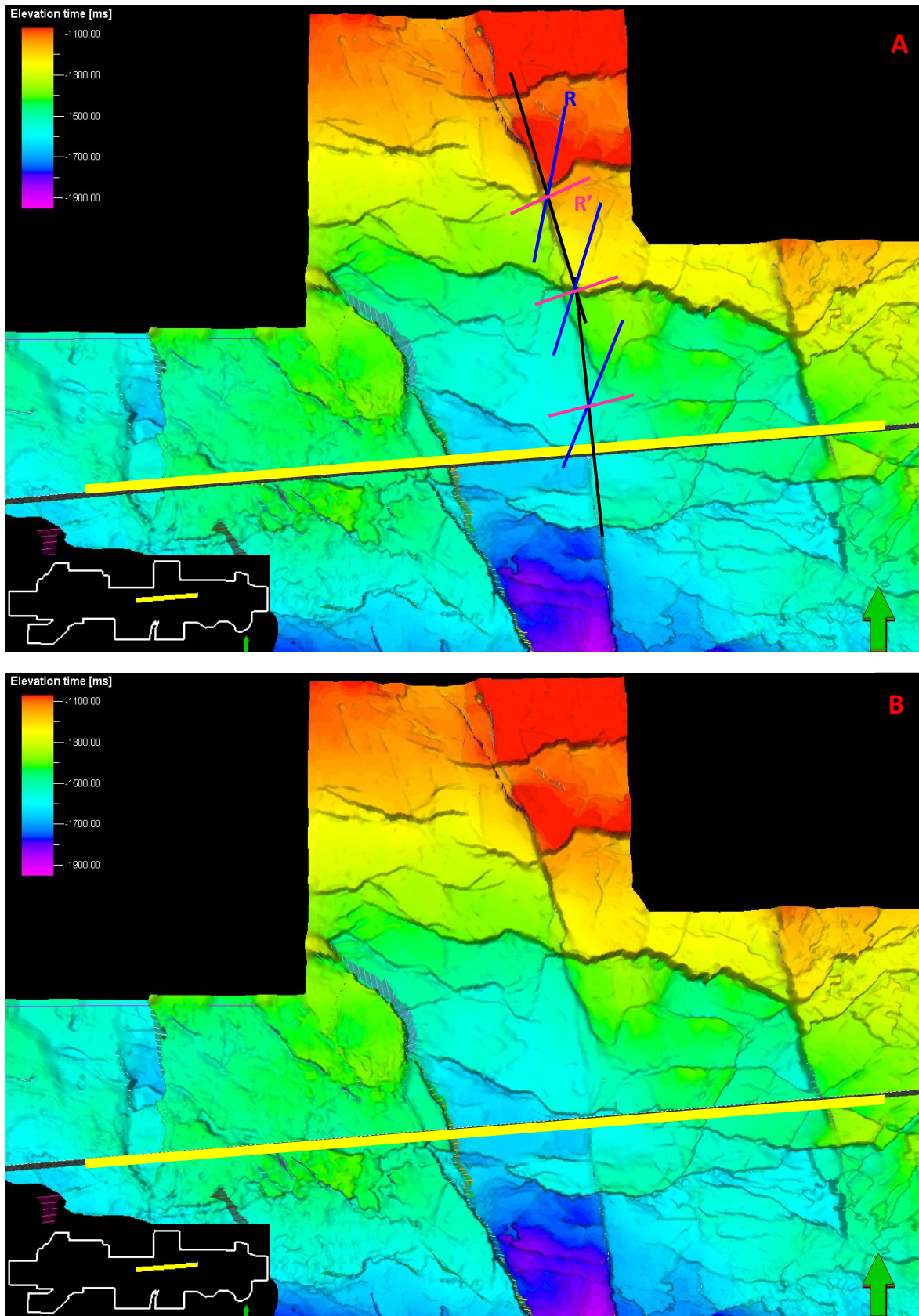
**Figure 43: Top Jurassic (PrSTM) with approximate position of the intersections and Riedel directions (see part A). The black, blue and pink lines are just the same as in Figure 42, applied on the flexure of the fault by spinning. See minimap (lower left) for location.**

## 5.2.2 Western part of the seismic area

The west represents an area with a complex pattern of mainly NW-SE striking faults with abundant fault bends, which are connected to a network (Figure 44).
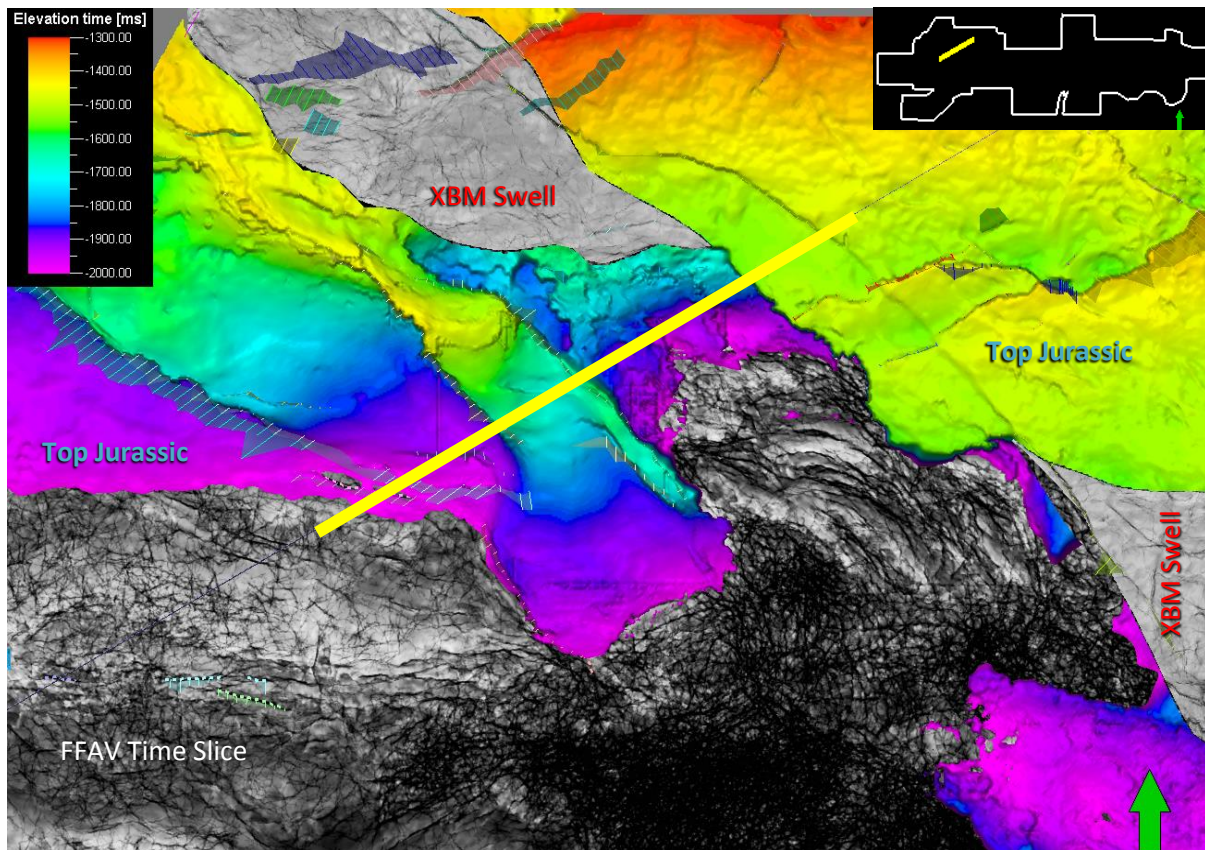


**Figure 44: Top Jurassic surface (TWT), Top XBM Swell surface (attributed with FFAV), time slice (FFAV) and location of the intersection, showing NW-SE striking bended faults. See minimap (upper right) for location.**

The intersections (Figure 45, Figure 46) show a similar pattern as discussed in the central part before. A difference in Cretaceous sediment thickness can be identified, ranging from about 355 ms in the southwest to 130 ms between Crosslines 785 and 824 of the section, and nearly no Cretaceous sediments in the northeast.

The three kilometer wide set of splay faults between the Crosslines 844 and 765 (XL in Figure 45, Figure 46) offsets the reflectors up to the Oligocene and forms approximately a V-shape below a bulge, with upward drag of adjacent reflectors to the southwest.

Other faults with minimal vertical offsets were mapped in the area to the northeast of the bulge and show upward terminations in Oligocene sediments. The strike-slip fault furthest to the northeast proceeds over a lateral distance of at least 15 km (Figure 44) and offsets the Top Eocene, but terminates within the thin stratigraphic section below Top RBDRM. The youngest deformation age of these faults can be determined quite accurately between 26 and 33.9 Ma (Oligocene, Kiscellian).
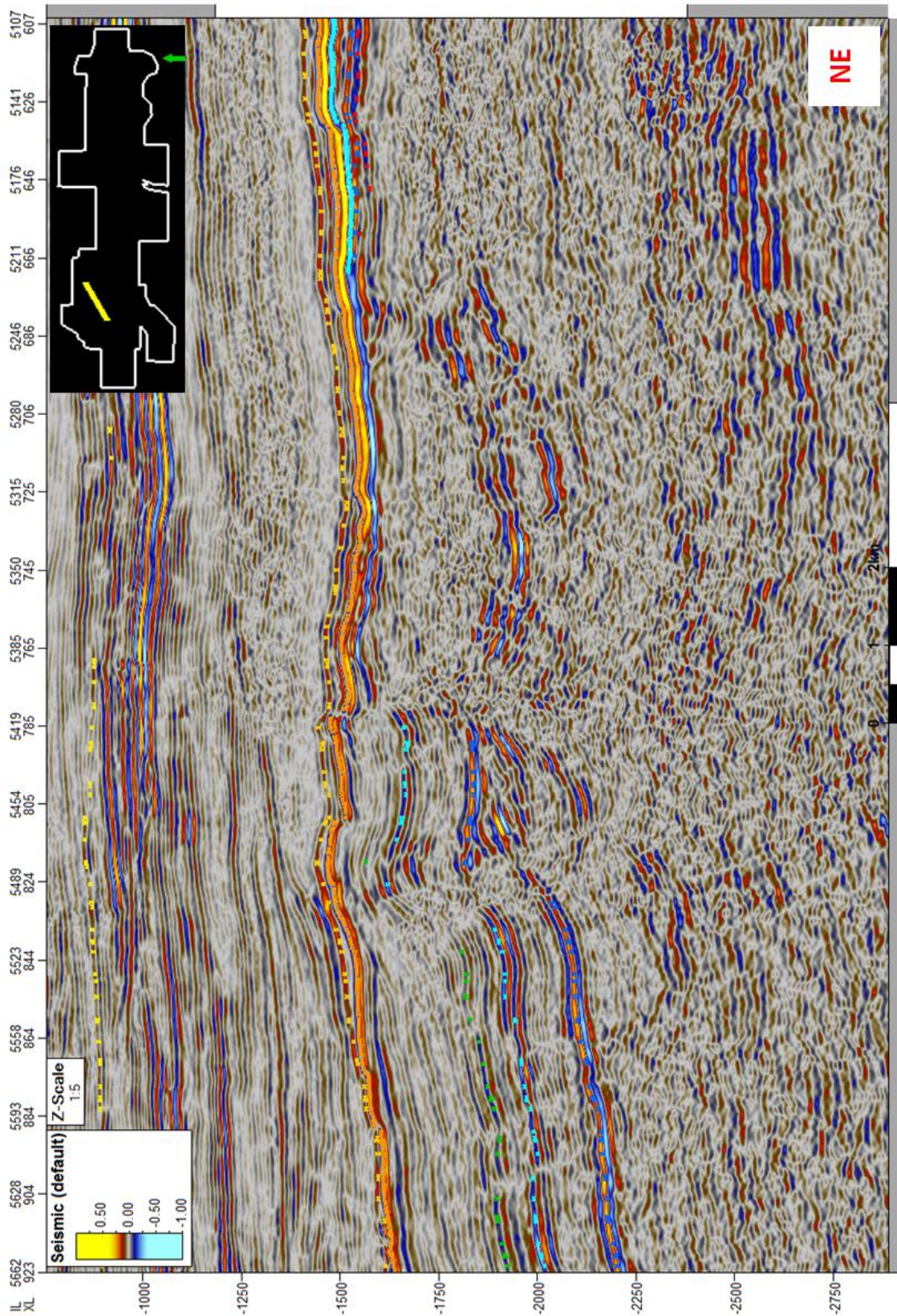
**Figure 45: Uninterpreted Random Line (PrSTM, TWT) with interpreted horizons. See minimap (upper right) for location. The structural interpretation of the section is shown in Figure 46.**
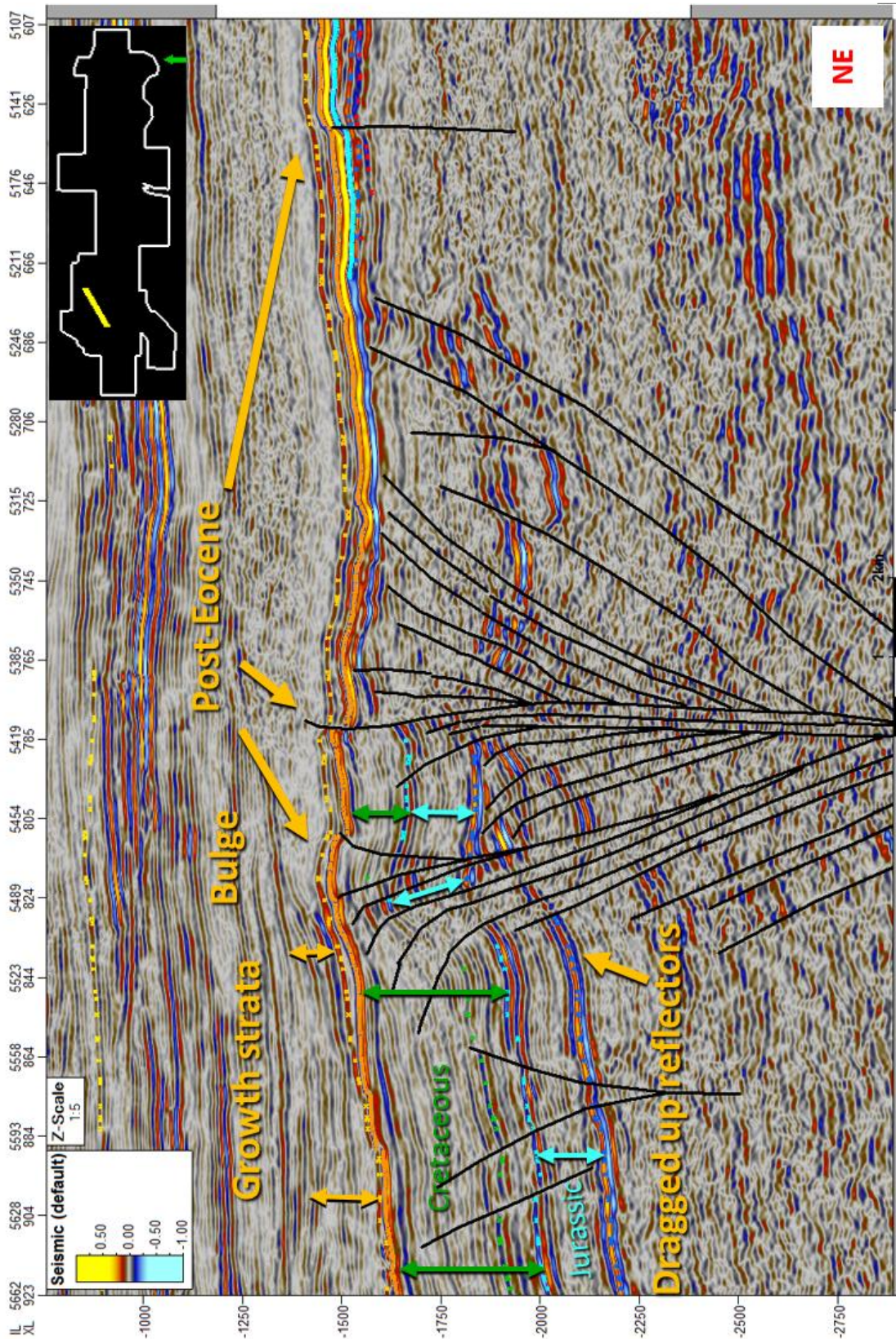
43

**Figure 46: Interpreted random Line (PrSTM, TWT) with interpreted horizons showing growth strata and a bulge above a positive flower structure indicative for dextral strike-slip deformation. Most faults of the flower structure terminate below the horizon Top Eocene. Only two faults of the flower structure and one fault northeast of the flower offset the Top Eocene. The flower structure is similar to the one shown in Figure 39, because a reactivation between Top Eocene and the Cretaceous strata below, and in the Kiscellian (Oligocene) occurred. See minimap (upper right) for location.**

Additionally, duplexes fitting to dextral transpressive strike-slip systems as well as restraining and releasing bends can be identified from the 3D topography of the surface and the calculated thickness for Cretaceous sediments (Figure 47, Figure 48 and Figure 49).
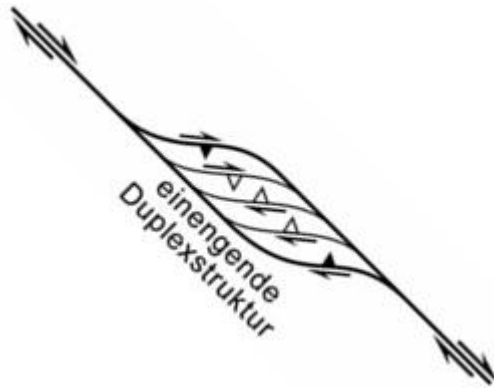


**Figure 48: Dextral transpressional strike-slip duplex (Burg, 2006; after Woodcock & Fischer, 1986).**
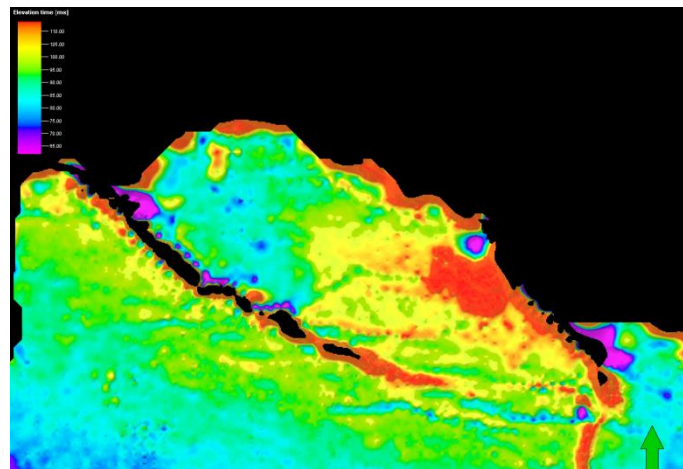


**Figure 47: Thickness of the Cretaceous sediments in TWT (115 ms: red; 60 ms: pink) illustrating a duplex pattern as depicted in Figure 49 (western structure).**
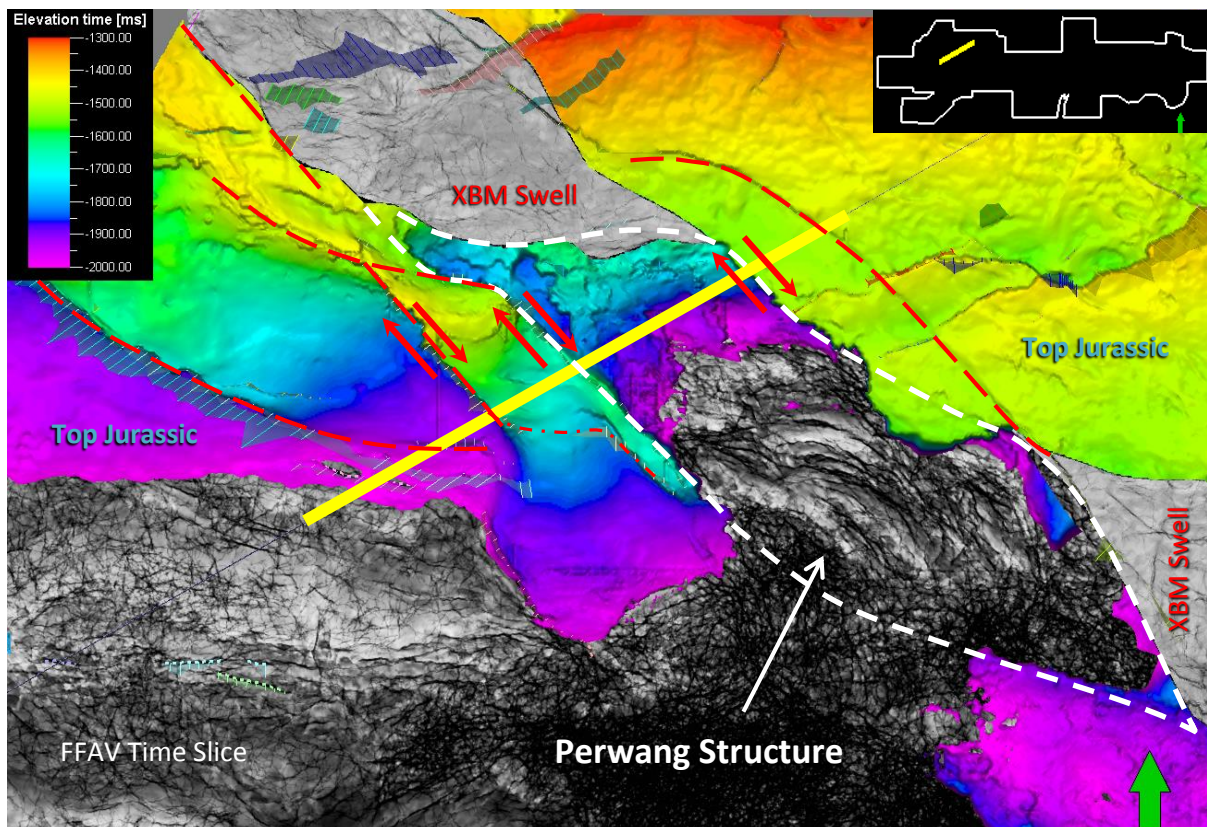


**Figure 49: Combined image of Top Jurassic surface (TWT), Top XBM Swell surface (attributed with FFAV) and time slice (FFAV) showing NW-SE striking dextral strike-slip duplexes and faults originating in the Bohemian Massif that were reactivated between the Upper Cretaceous and Oligocene. Yellow line indicates the location of cross section shown in Figure 45 and Figure 46.**

The Oligocene strata above the bulge indicate syntectonic growth strata and therefore prove an approximate age for tectonic activity in the Oligocene (Figure 50).
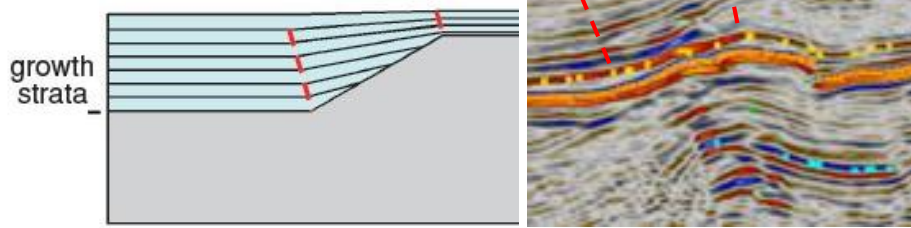
**Figure 50: Left: Sketch showing the characteristic features of syntectonic growth strata (from Shaw et al., 2005); Right: Implication on distorted outcrop of the top of the positive flower structure (Figure 45; TWT).**

The positive flower structure below the bulge of the Top Eocene is connected to differing Upper Cretaceous thicknesses. The absence of growth strata indicates a tectonic activity after the sedimentation of the Cretaceous strata, but earlier than the sedimentation of the Top Eocene and Top RBDRM, because the thickness between these two horizons remains constant. However, there must have been a second phase of activity, proved by the topography of the horizon Top Eocene forming a bulge above the flower and several faults that terminate above the Eocene, like the Oligocene dextral strike-slip fault in the center (Figure 46). The northeastern part of the positive flower structure is supposed to be connected with the so called Perwang Structure, because the FFAV Time Slice also shows conspicuous contours. The Perwang Structure is supposed to consist of Triassic to Carboniferous deposits overlying the crystalline basement (WAGNER, 1998; H. Sperl, pers. comm.)

## 5.2.3 Regional Interpretation

When considering the northwest bending of the strike-slip faults discussed in the central part of the seismic (Schwanenstadt Fault and Lindach Fault; Figure 51) and assuming that this bending proceeds outside of the seismic volume, then the orientation of the faults dealt with in this chapter would correspond to the Paleozoic dextral NW-SE striking strike-slip system in the crystalline of the Bohemian Massif, mentioned in the Regional Overview chapter.
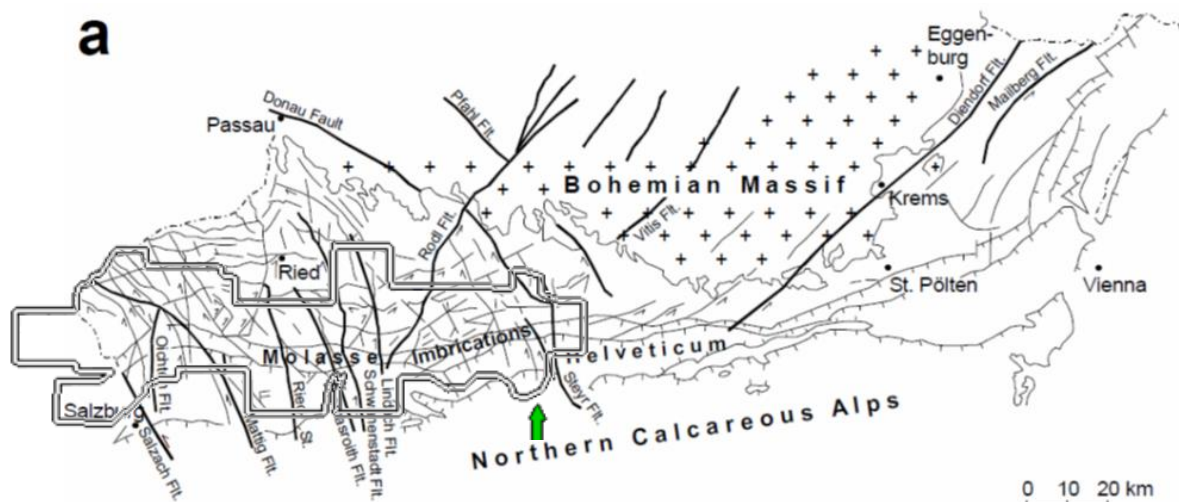


**Figure 51: Fault systems in the Bohemian Massif and the subcrop of the Molasse Basin of Upper Austria plus the outline of the seismic volume (modified after Schulz, 2002; Wagner, 1998)). Further bending of the faults leads to the assumption that the Schwanenstadt and Lindach Fault are part of the Bohemian Massif's NW-SE striking fault system.**

The varying thickness of the Cretaceous deposits and growth strata within them, gives information of a Cretaceous event, which led to the vertical offset and the formation of a basement low with the largest Cretaceous thickness. This event is supposed to have reactivated the pre-existing NW-SE striking dextral Paleozoic faults in the Bohemian Massif. For at least two of the faults, the Mattig and Lindach Fault, seismic interpretation indicates dextral offset. The growth strata west of the Lindach Fault are a strong indication of Upper Cretaceous fault activity leading to differential vertical displacement. The western block subsided relative to the eastern one.

The trigger of Cretaceous deformation could be the subduction of the Penninic Ocean in the south and the transmission to north directed compressional stress on the Helvetic Shelf (Figure 52).
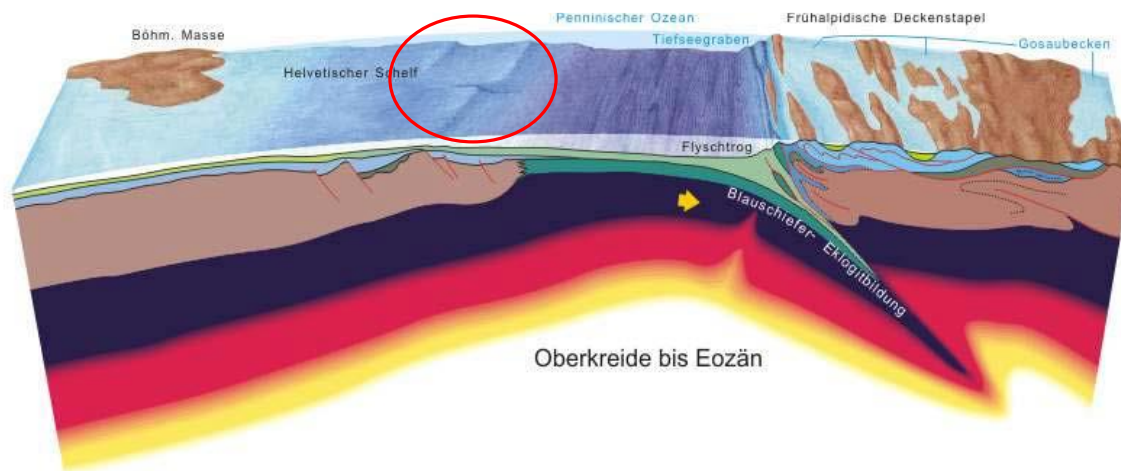
**Figure 52: Model for the subduction of the Penninic Ocean in the south of the Bohemian Massif, which is thought to be the reason for an Upper Cretaceous strike-slip fault reactivation (red ellipse) of pre-existing Paleozoic fault systems (modified after Schuster et al., 2013).**

The Cretaceous sediments inside the positive flower structures show a lower thickness than the blocks beside, without indicating any growth strata. Data therefore suggests post-sedimentary fault activity accomplishing the observed difference in Cretaceous sediment thickness.  Regarding this and the constant thickness of sediments between Top Eocene and Top RBDRM, which indicates a period of tectonic stagnation, the fault reactivation causing the uplift of the flower structure and therefore erosion of the Cretaceous sediments in the uplifted blocks must have occurred between the deposition of the youngest Cretaceous strata and the deposition of the Eocene sediments. The youngest known Cretaceous sediments form the Molasse Basin of Upper Austria are of Campanian age, and the Eocene sedimentation is restricted to the Upper Eocene (Priabonian; WAGNER, 1998). Faulting therefore could have also occurred in the Eocene, at the time when the Alps collided with the Helvetic Shelf. The onset of this collision is dated by the youngest overthrust sediments of the Ultrahelvetic Units, which are of Middle Eocene age (47 Ma; DECKER & PERESSON, 1996).

The positive flower structures of the Cretaceous faults can be found right below bulges of the horizon Top Eocene and the Top RBDRM, indicating fault reactivation during the Kiscellian. Oligocene faulting is further indicated by syntectonic growth strata. The reasons for the renewed fault reactivation may lie in the continued thrusting of the Alpine orogenic wedge over the Helvetic Shelf in the Oligocene, like described in the Regional Overview chapter.

# 5.3 Kiscellian to Eggenburgian Fault Systems

## 5.3.1 Central part of the seismic area

The following chapter discusses the ESE-WSW to E-W striking faults in the central part of the seismic volume. The striking direction is subparallel to the allochthonous Molasse overthrust.
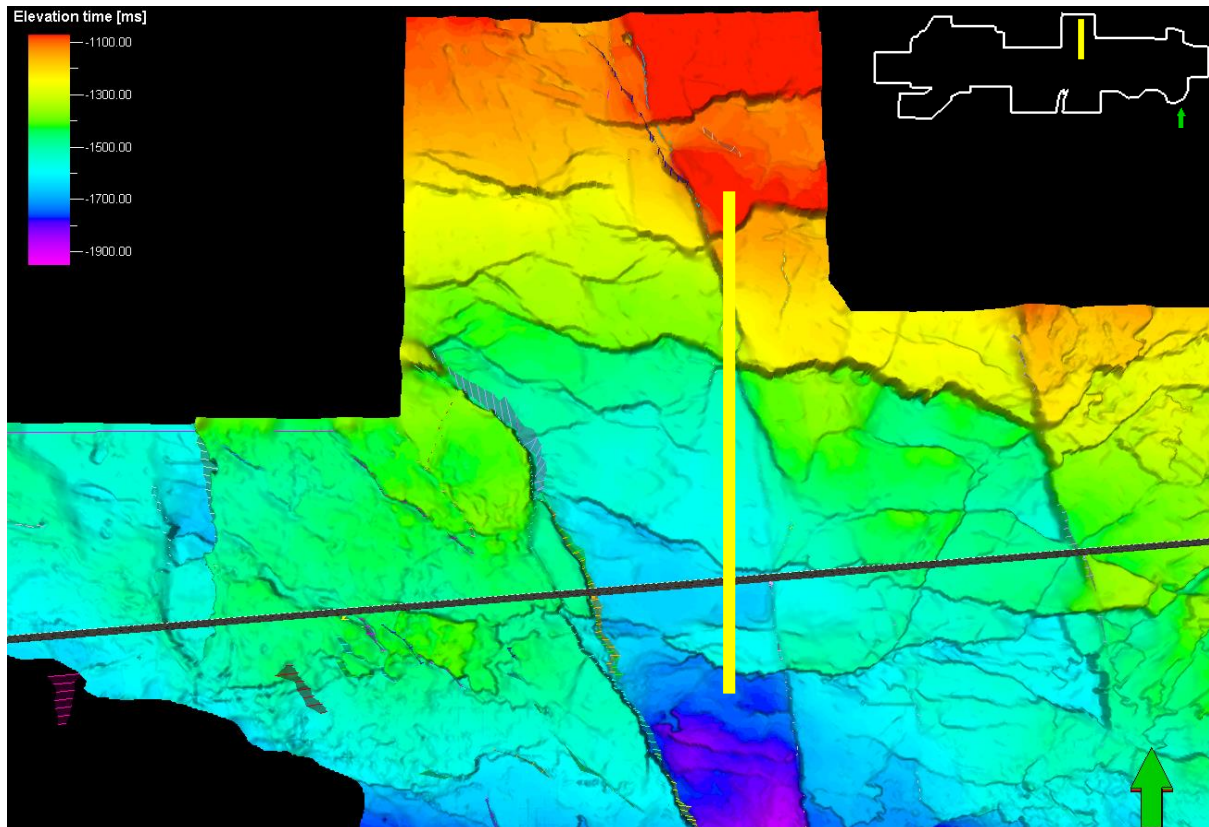


**Figure 53: Shaded relief of the Top Jurassic horizon (PrSTM; elevation in ms TWT, see upper left) with position of the intersection shown in Figure 54, Figure 55 (yellow line) and location in the volume (minimap: upper right).**

The faults are dipping either south or north, whereas the south dipping ones are constantly longer than the others. All horizons below Base Hall are offset by those faults (Figure 54, Figure 55). Moreover, the N-S directional Inlines depict the typical pattern of a foreland basin, namely the growing thickness towards the approaching orogenic wedge with a basement dipping under the wedge.

The upper fault terminations of the south dipping faults approximately follow a stratigraphic boundary, which is supposed to be the border between the Upper and Lower Puchkirchen Formation and the transition from Oligocene to Miocene (23 Ma, Egerian; Figure 33). For this reason and to allow a more detailed interpretation, two additional horizons were drawn (light blue and dark blue dotted line) between Base Hall and Top RBDRM. The light blue horizon is thought to be the Oligocene/Miocene border. According to the terminations, younger faults can be found farther to the south because there is a small offset ranging up to the Lower Miocene (Egerian).

Another observation is that the dark blue horizon, which probably illustrates the Base of the Lower Puchkirchen Formation, and the Top Eocene have equal offsets so the first activity of the faults must be younger than Kiscellian, thus Egerian (Upper Oligocene; Figure 33). Sediment thicknesses between the two newly inferred light blue and dark blue horizon vary across faults indicating the existence of Egerian growth strata.

Furthermore there is an upward drag of reflectors adjacent to faults, indicating normal faulting. Additionally synforms between north and south dipping reflectors adjacent to normal faults can be observed, especially when focusing on Top Eocene and the horizon above.

The 3D surface view shows some other conspicuous features, namely ramps between the faults. These are common in connection with normal faults, revealing that faults are not arranged in en-echelon-patterns and indicating pure normal faulting without a lateral shear component. Thus the so called relay ramps constitute another prove for normal faulting (Figure 56, Figure 57, Figure 58).

The comparison of Figure 56 and Figure 57 additionally shows the difference between the original seismic and the Final Fault Attribute Volume (FFAV). The FFAV time slice is particularly advantageous for locating faults as it also highlights very low contrast fault zones, which can hardly be seen in the original volume. The problem is that it seems to be too sensible for other features in the data and therefore only good as help for interpretation and used carefully.
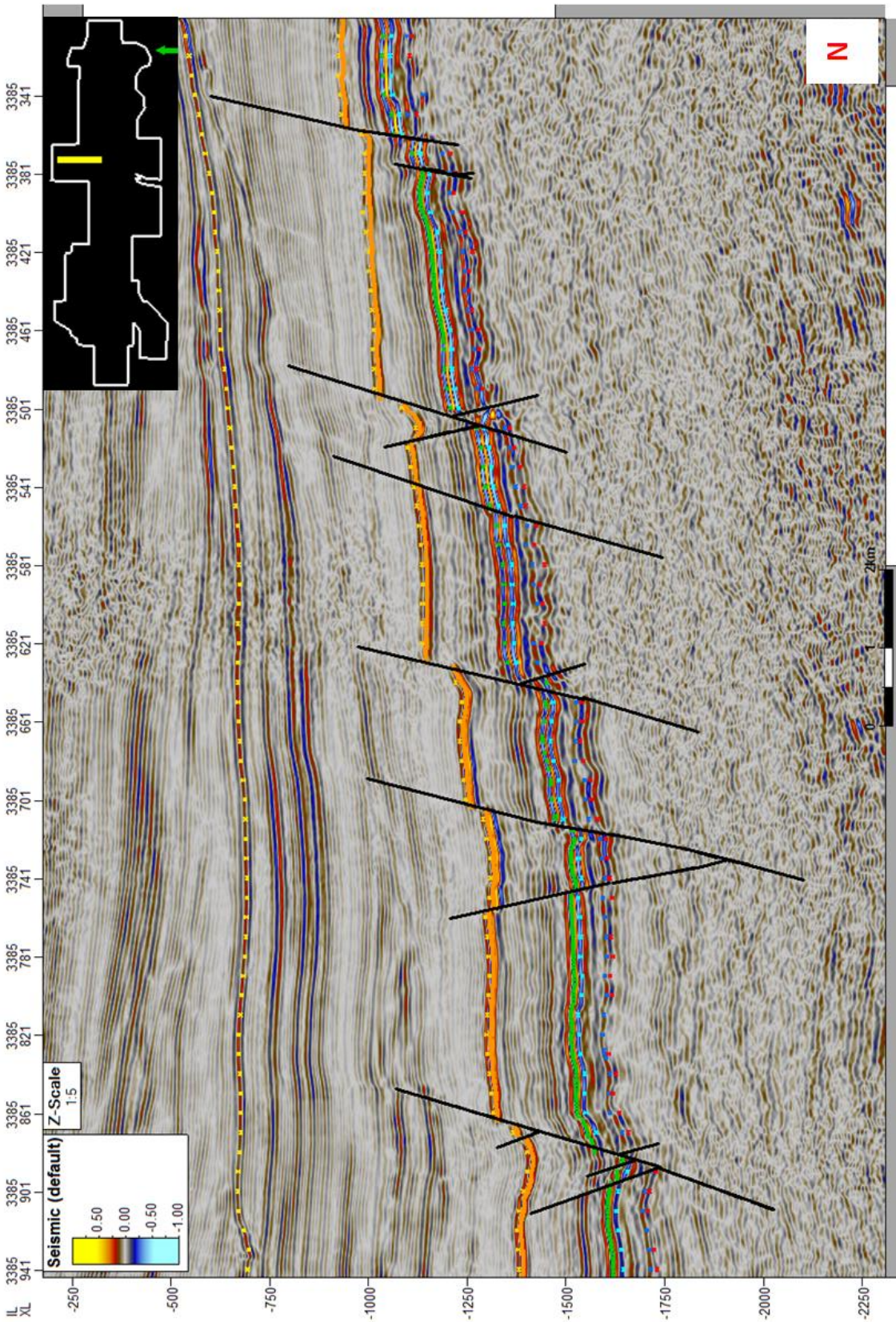
**Figure 54: Uninterpreted Inline 3385 (PrSTM, depth in TWT) with horizons. See minimap in the upper right for location.**
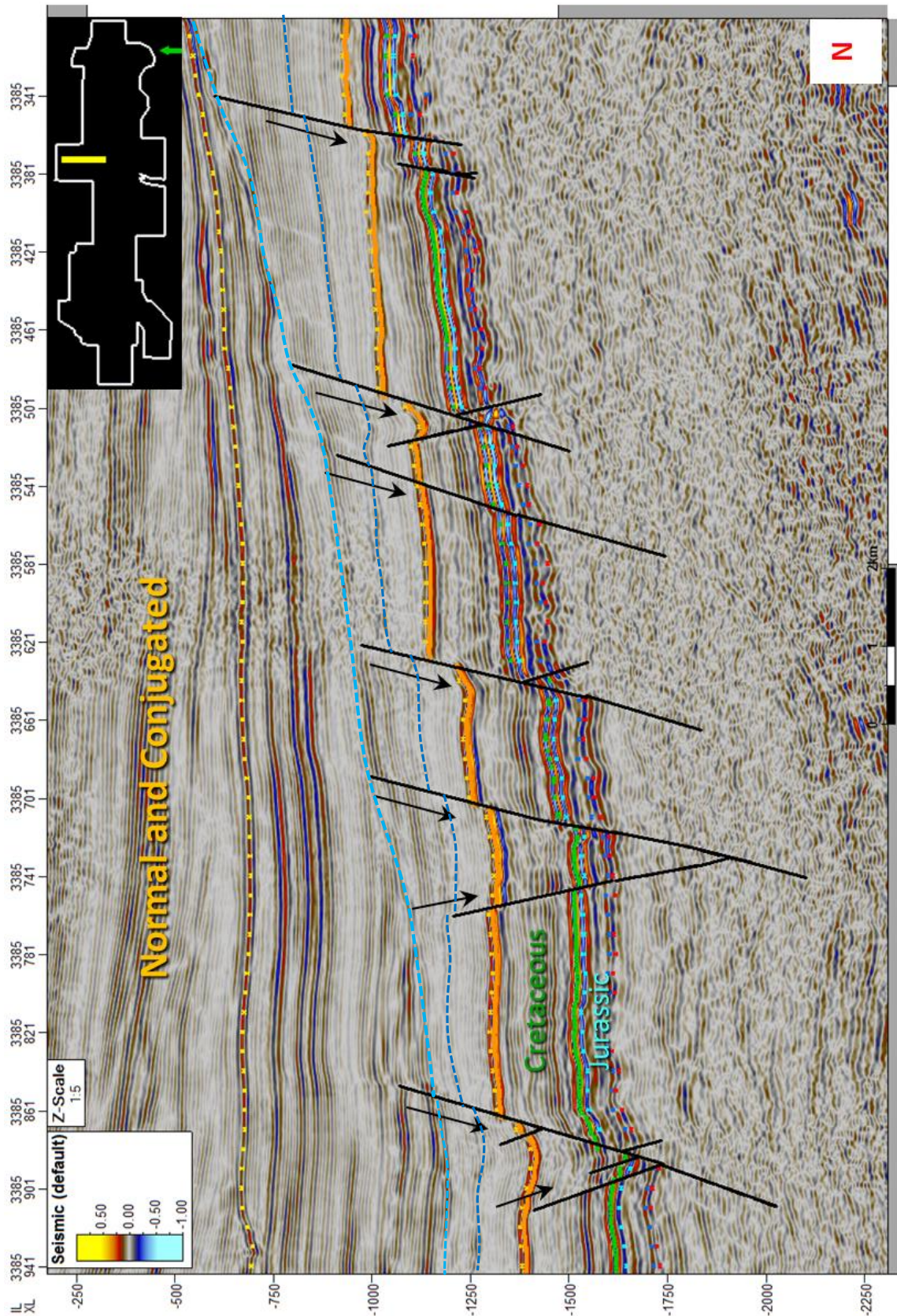
**Figure 55: Inline 3385 (PrSTM in TWT depth) showing a set of conjugated south-dipping and north-dipping normal faults in a typical succession for foreland basins. Two additional horizons were drawn (light blue and dark blue) between Base Hall and Top RBDRM to enable more accurate interpretation. The light blue horizon is thought to approximate the Oligocene/Miocene boundary; dark blue shows a horizon at or close to the base of the Lower Puchkirchen Formation. The latter horizon and the Top Eocene show equal offsets so the first activity of the faults must be younger than Kiscellian, thus Upper Oligocene (Egerian). The youngest faults terminate in Lower Miocene (Egerian) strata.**
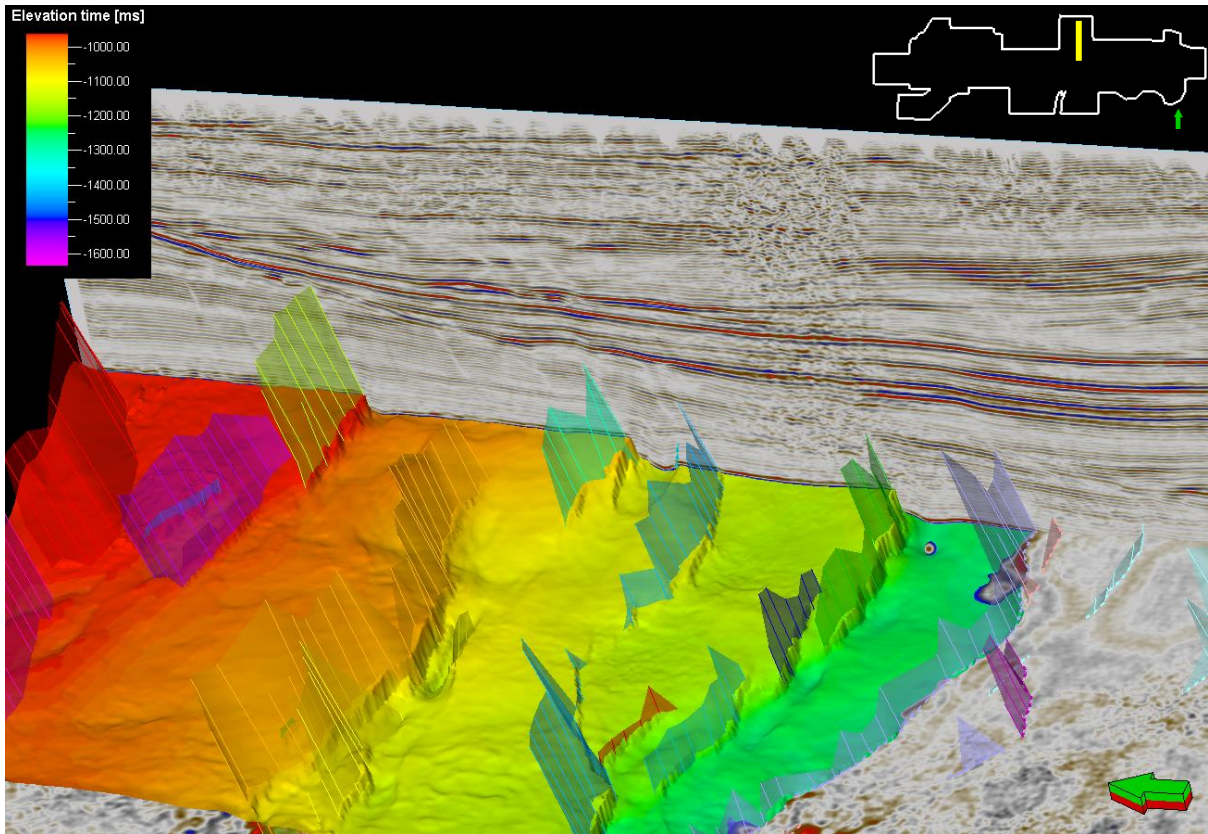
**Figure 56: Top Eocene surface (TWT) and manually tracked faults combined with a N-S-striking intersection and a time slice (PrSTM) of the original seismic. Fault patterns show relay ramps between normal faults and lows of the Top Eocene between conjugated faults.**
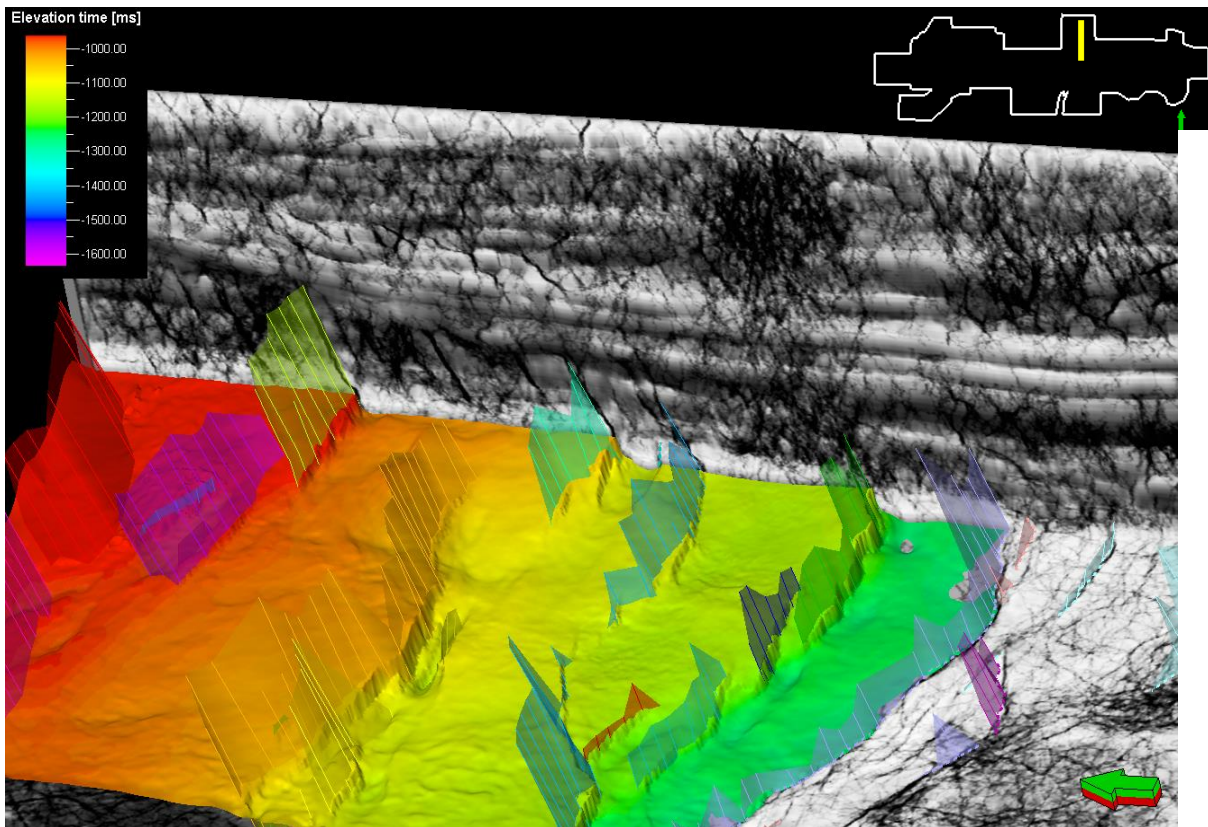


**Figure 57: Top Eocene surface (TWT) and manually tracked faults combined with a N-S-striking intersection and time slice of the FFAV (same slices as shown in Figure 56) illustrating the properties of the FFAV (given more contrast for this**

**image). High-contrast features are very abundant in the FFAV. However, the features need to be used with prudence because of other features being tracked sometimes.**
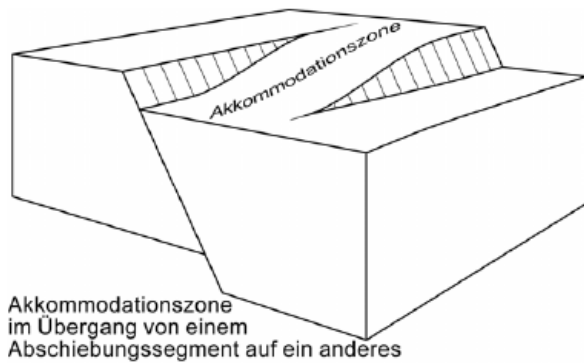


**Figure 58: Relay ramps between two normal faults (Burg, 2007)**

## 5.3.2 East to the central part of the seismic area (youngest faults mapped)

Further to the east NE-SW striking, southeast and northwest dipping, curved, sub-parallel faults are prevailing (Figure 59). They tend to change their striking direction to WSW-ESE. The fault in the middle left of Figure 59 (a) coming from the west branches into a little SSE-dipping fault splay, and a main fault striking in northeast direction.
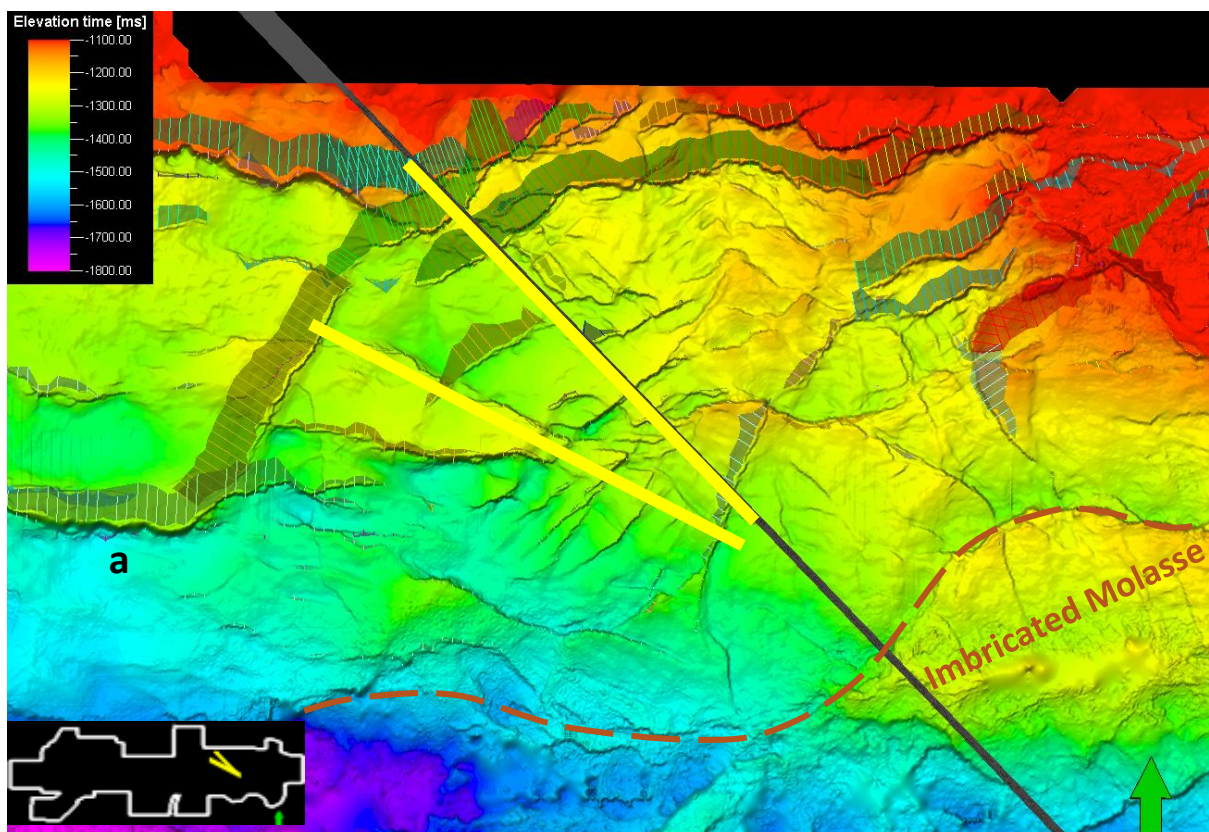


**Figure 59: Shaded relief of the Top Eocene surface (TWT) with mapped fault surfaces. Also shown are the positions of the intersections shown in Figure 60, Figure 61, Figure 62 (yellow lines) and location in the volume (minimap lower left). The fault interpretation shows mainly NE-SW striking huge curved fault planes. The dashed line approximates the outline of the Imbricated Molasse, which trends nearly in the same direction as the faults.**

The intersections (Figure 60, Figure 61, Figure 62) show faults with similar ages like the ones described in the previous chapter. The Oligocene to Lower Miocene timing of the youngest fault slip is deduced from the upward termination of the faults in sediments of that age. Only few faults are terminating further up just below the horizon Base Hall and one fault even offsets this horizon, therefore giving a minimum age of Eggenburgian (Lower Miocene). These faults constitute the youngest faults tracked in the course of this thesis. Furthermore, the offset of the youngest fault decreases upwards and growth strata occur, thus indicating Egerian to Eggenburgian fault activity (Figure 61). Moreover, the faults seem to become younger from south to north.

The strike directions of the mapped Kiscellian to Eggenburgian normal faults are subparallel to the curved trend of the Imbricated Molasse, which displays a change of the Molasse overthrust's strike direction from E-W (east) to NE (center) and E-W again in the west (Figure 59). Faults striking subparallel to the thrust of the allochthonous Molasse are also observed in the central part of the study area (see previous subchapter and geological overview). Faults with dipping directions towards the thrust wedge are predominant. Additionally, fault-bounded blocks are tilted northwest down as effects of crustal down bending (Figure 61, blocks between X-line 868 and 954; compare BRADLEY & KIDD, 1991).
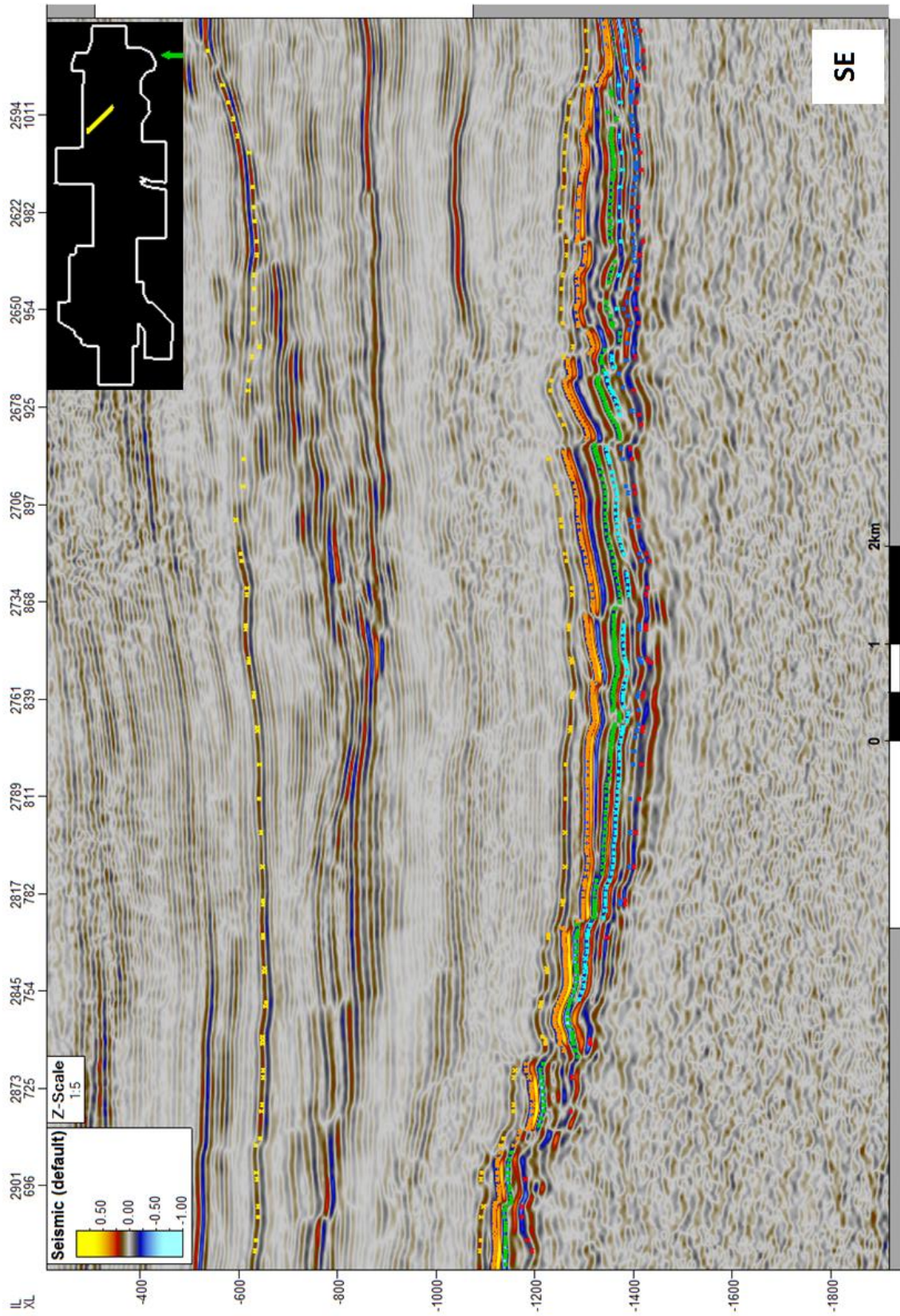
**Figure 60: Uninterpreted Random Line (PrSTM, TWT) with horizons and location in the area of interest.**
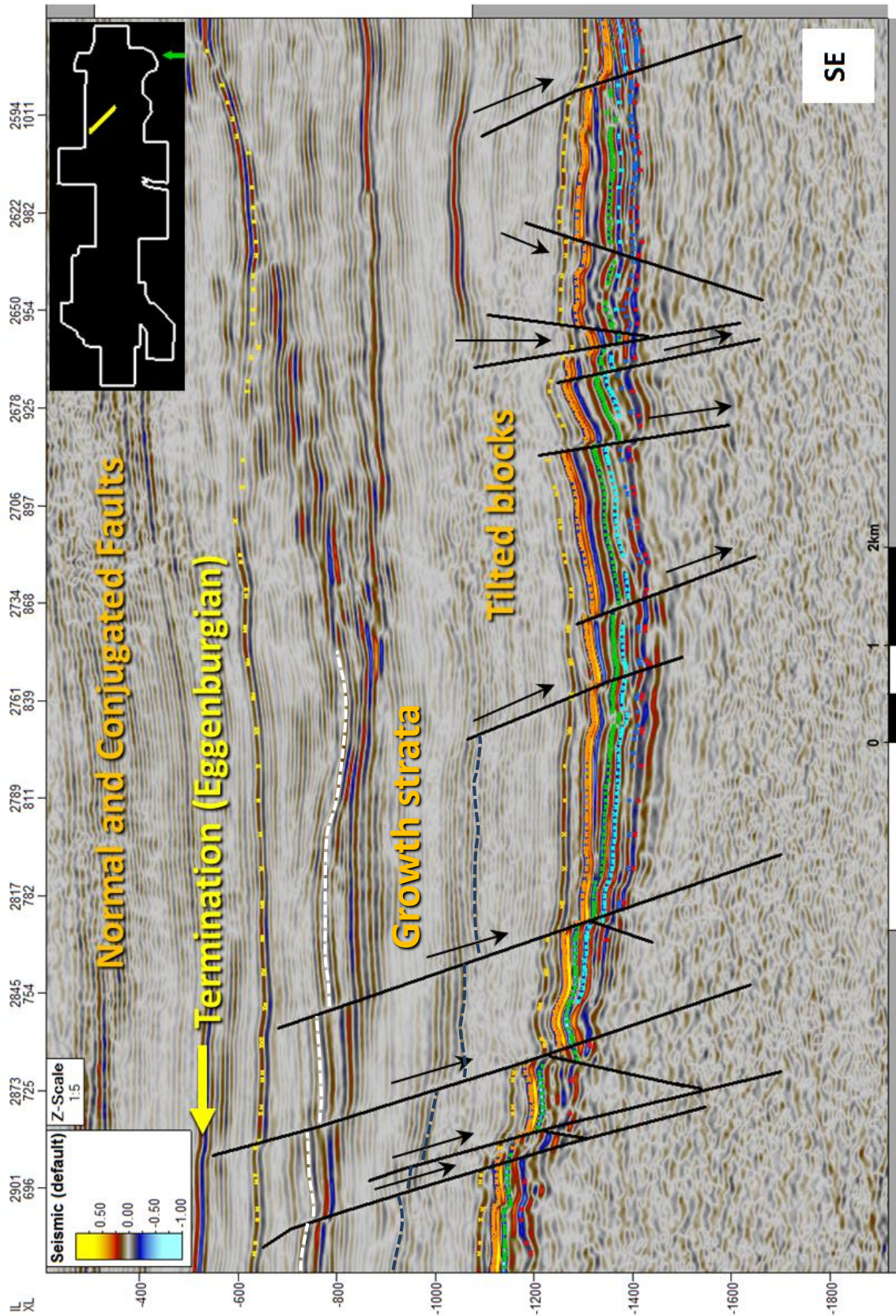
56

**Figure 61: Random Line (PrSTM, TWT) with horizons and location in the area of interest, showing south-dipping normal and conjugated north-dipping normal faults. The youngest faults observed (Eggenburgian) occur in the northwestern part of the section. Additionally, southeast up tilting of blocks occurs, which is a consequence of the crustal down-bending. The white and blue dotted lines are just drawn as marker and help for indicating growth strata and activity changes.**
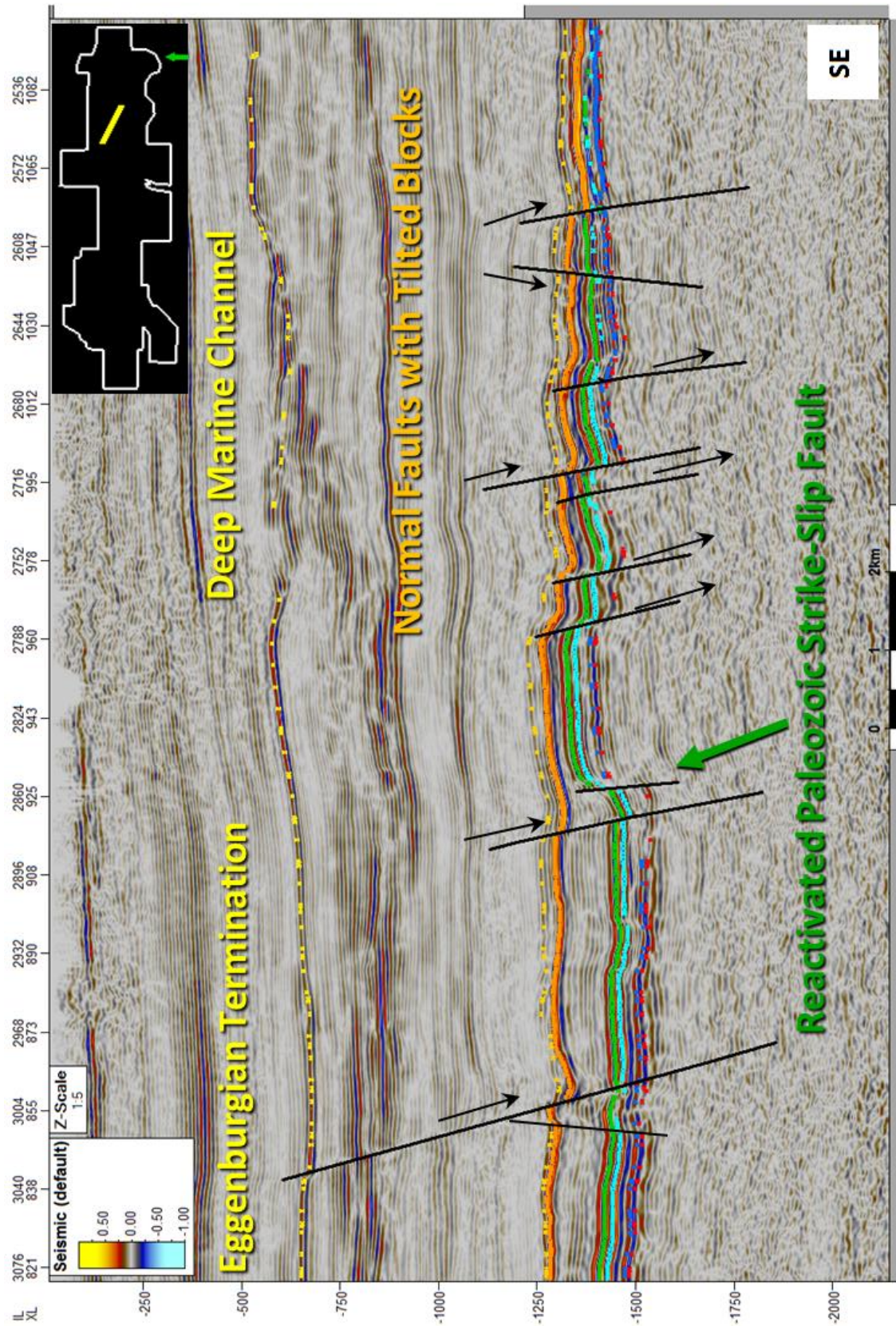
**Figure 62: Random Line (PrSTM, TWT) with horizons and location in the area of interest showing normal faults, block rotation between normal faults, one of the youngest faults observed in the volume (Eggenburgian) and a crossing strike-slip fault. The up to 5 km wide deep marine channel system on top of the horizon Base Hall is shown in Figure 63.**

A 3D view of the Base Hall reveals more interesting things, like the tops of the youngest fault planes terminating above Base Hall and a deep marine channel, which trends subparallel to both, the northeast striking normal fault and the Imbricated Molasse border (Figure 63). Comparison with the cross section shows that the 5 km wide channel is located just above a set of normal faults striking parallel to the channel's trend (Figure 62). This observation leads to the assumption that the pre-existing faults influenced the orientation of the channel.
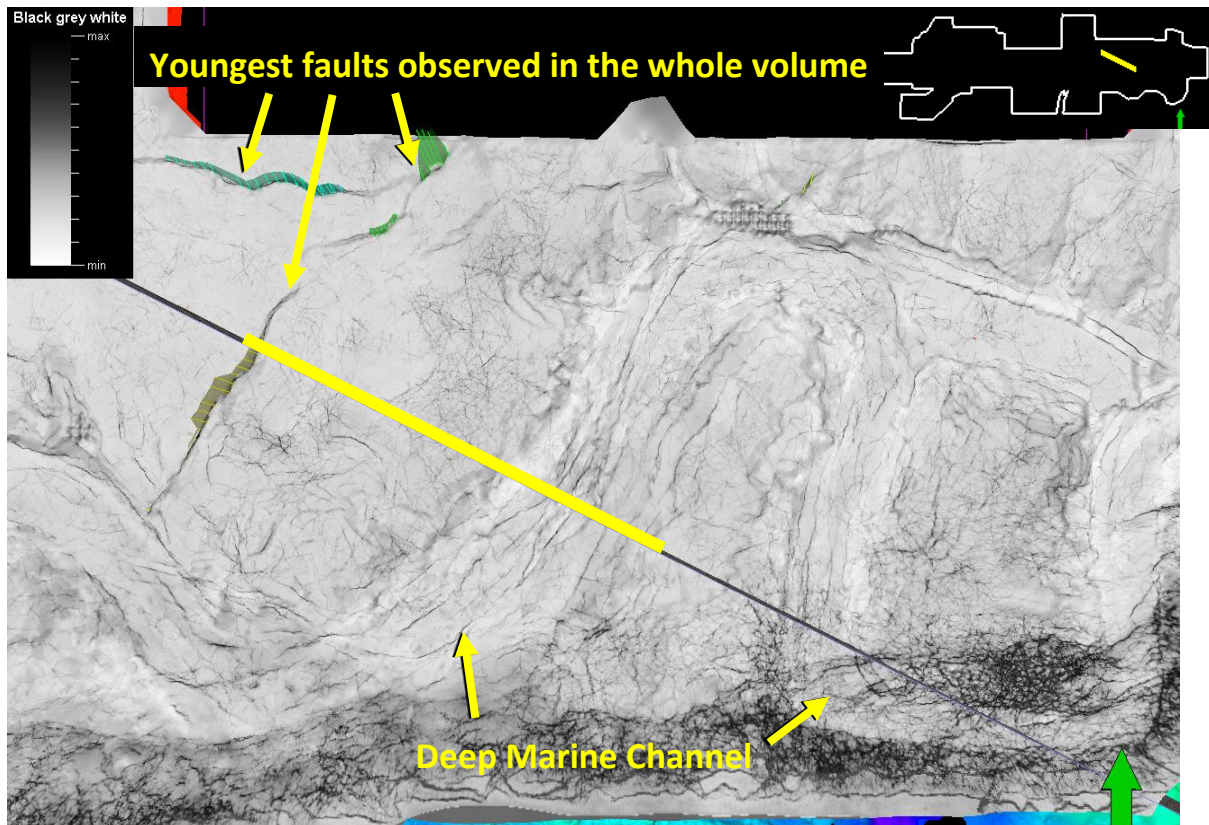


**Figure 63: Base Hall surface attributed with FFAV showing the youngest faults observed in the volume (Eggenburgian) and a huge up to 5 km wide deep marine channel system. Also shown are the position of the intersection in Figure 62 (yellow line) and location in the volume (minimap upper right). The figure shows side effects of the FFAV: structures tracked inside of the channel cannot be interpreted as faults as shown by the cross section in Figure 62. The high-contrast lines inside the channel are explained as sedimentary features.**

### 5.3.3 Easternmost part of the seismic area

The easternmost part of the study area is dominated by more or less E-W striking, mainly south dipping, as well as NE-SW to NNE-SSW and NW-SE striking faults (Figure 64).

The intersection shown in Figure 65 reveals E-W striking normal and conjugated normal faults transecting the foreland basin succession and terminating below the horizon Base Hall. The indicated fault ages fit very well to those observed in the other parts of the study area, where data proves Upper Oligocene to Lower Miocene fault activity. All other NE-SW to NNE-SSW and NW-SE striking faults are older than the E-W striking normal faults. The faults are reactivated Paleozoic strike-slip faults, which are discussed in the previous chapter.

The cross section is typical for foreland basins concerning the dipping of the basement reflectors towards the approaching thrust wedge and the upwards flattening of the basin sediments.
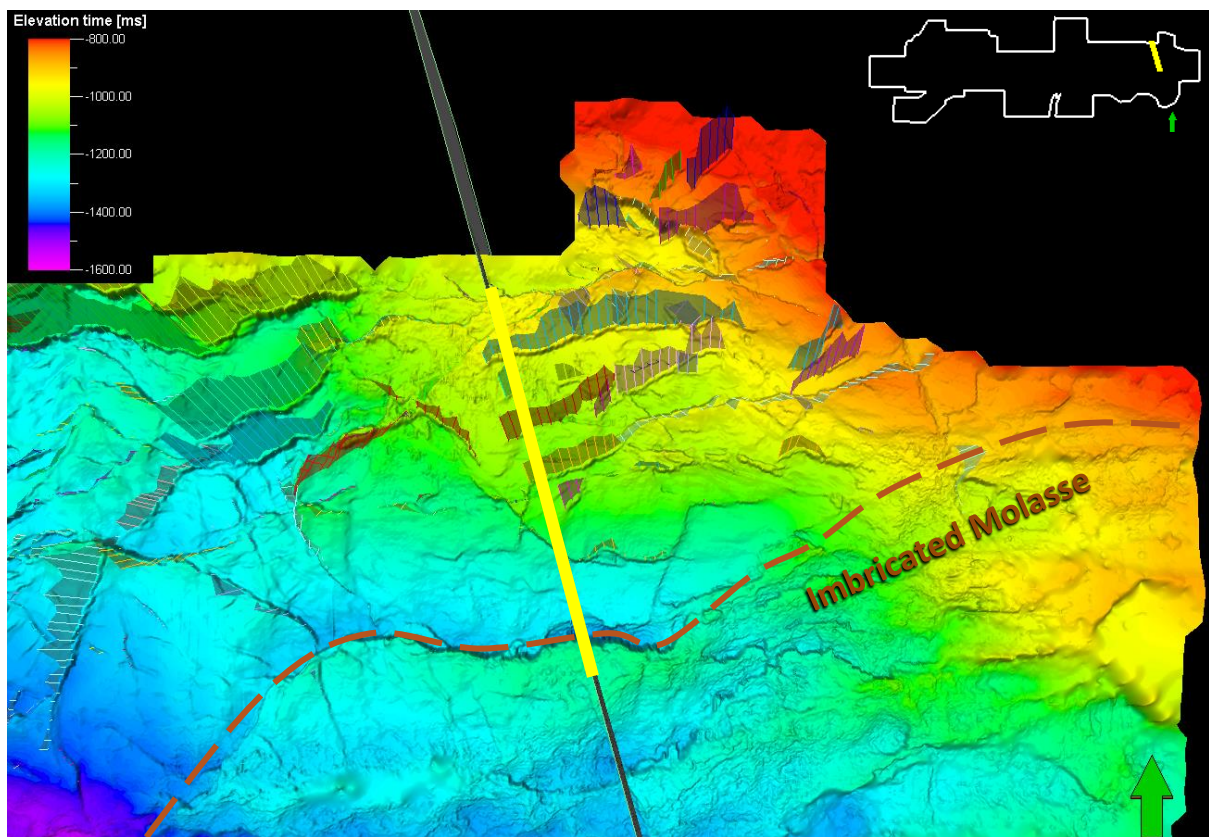


**Figure 64: Top Eocene surface (TWT) with position of the intersection (yellow line) and location in the volume, showing normal faults striking parallel to the thrust front (Imbricated Molasse) Front of the Imbricated Molasse sketched after Hinsch, 2013.**
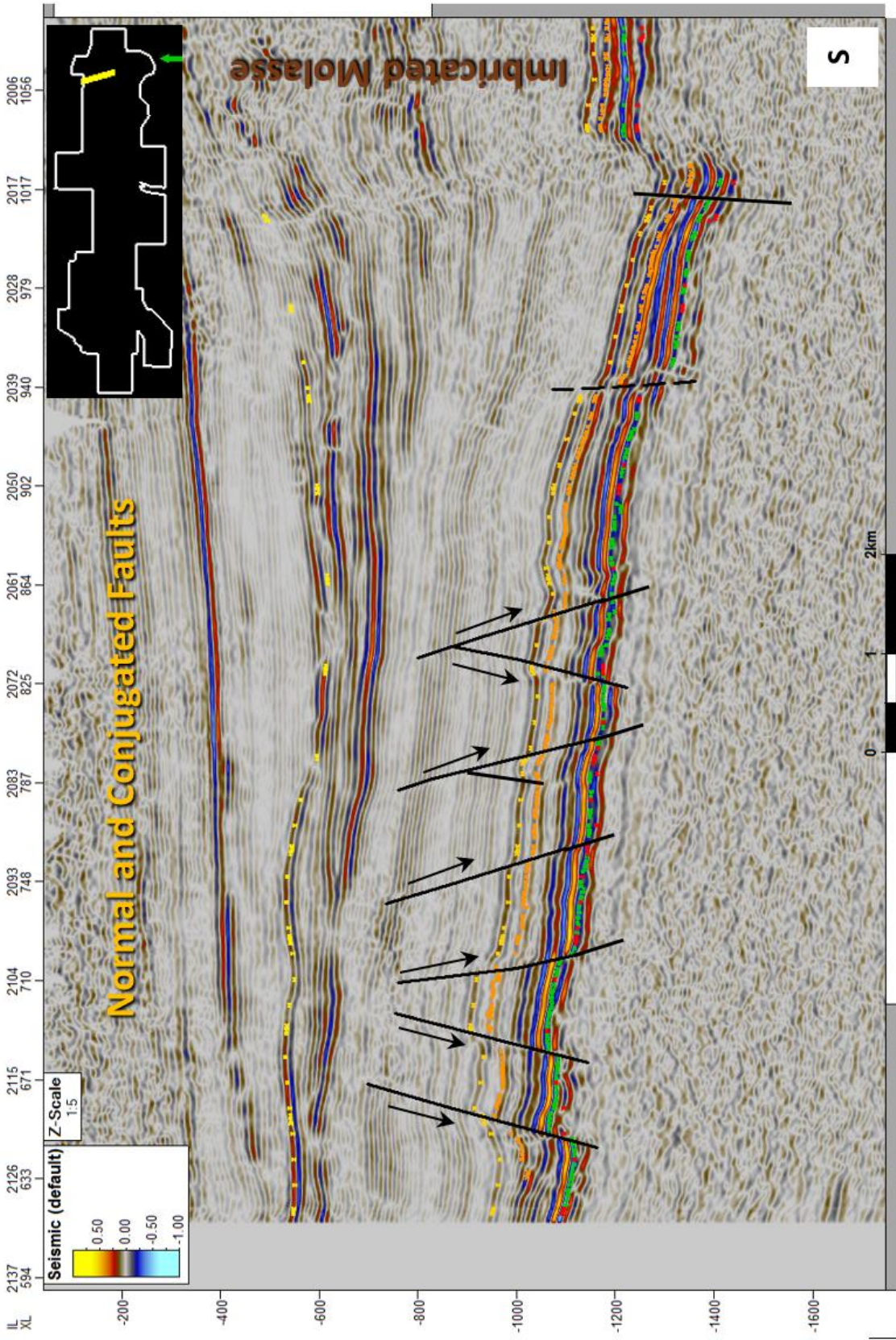
**Figure 65: Random Line (PrSTM in TWT depth) with horizons showing south-dipping normal and conjugated north-dipping normal faults as an effect of flexural bending and overthrusting in the south of the Molasse basin.**

## 5.3.4 Northwestern part of the seismic area

The most conspicuous faults in the northwestern part of the study area are NE-SW striking, northwest dipping normal faults (Figure 66).
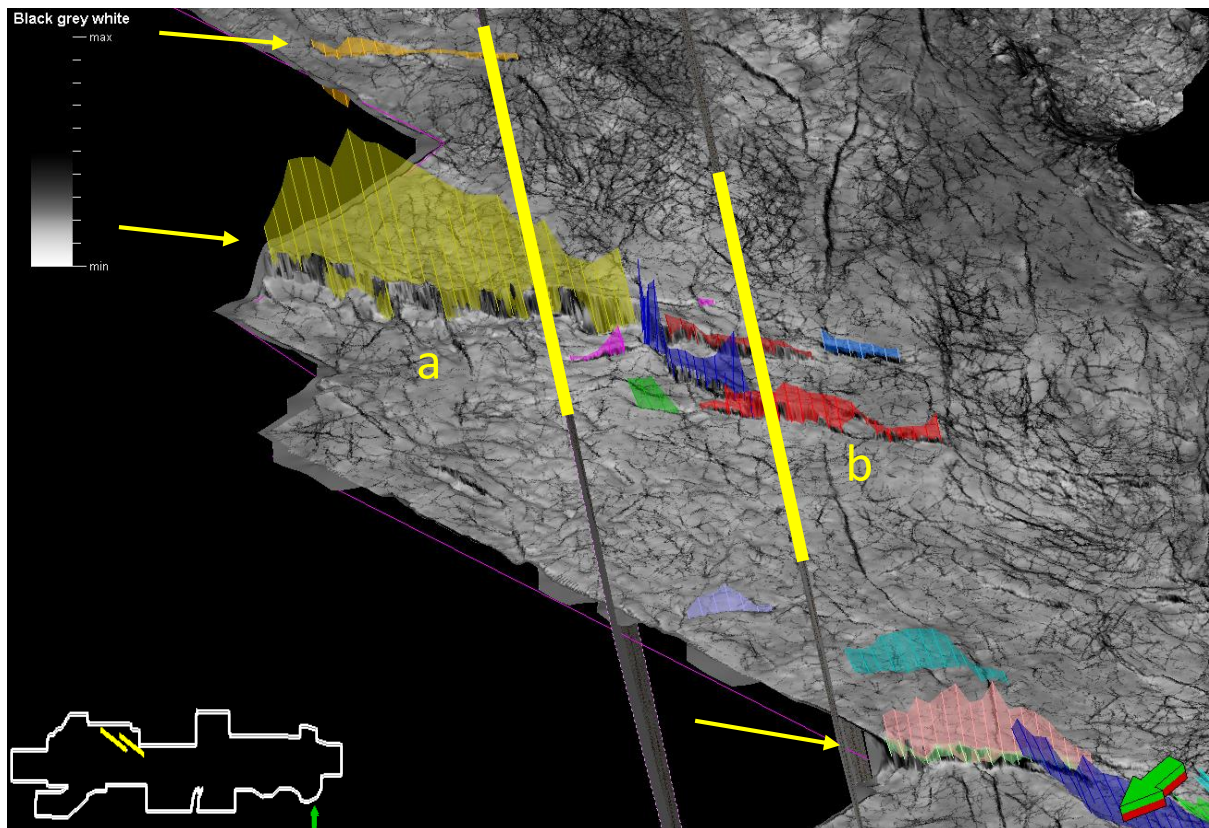


**Figure 66: Top Eocene surface attributed with FFAV and mapped fault surfaces showing northwest dipping normal faults. Also shown are the position of the intersections in Figure 67, Figure 68 (yellow lines) and the location of in the volume.**

The intersection in Figure 67 shows that the youngest faults have ages up to Lower Miocene as deduced from their upper terminations well below the horizon Base Hall. Most of the faults, however, are supposed to be of Oligocene age (Figure 67, Figure 68). The faults tend to get older from north to south when focusing on a single fault (Figure 66, from "a" to "b") as shown by the cross sections in Figure 67 and Figure 68. Moreover growth strata (Figure 67, Figure 68) can be recognized at several faults indicating synsedimentary faulting during the Oligocene.
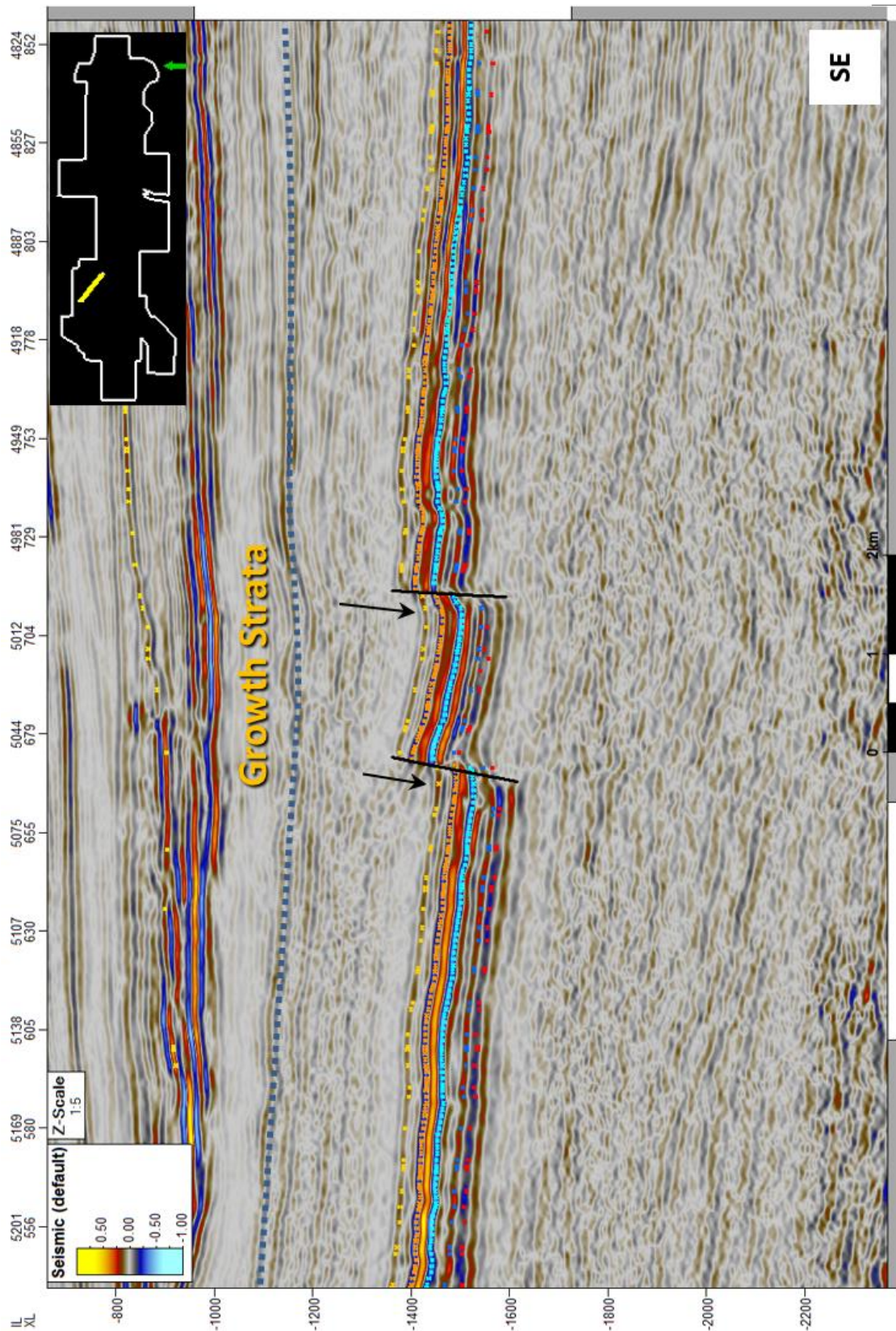
**Figure 67: Interpreted Random Line (PrSTM, depth in TWT) with horizons and location in the area of interest, showing growth strata of Oligocene age at northwest dipping normal faults, as well as block rotation. The blue horizon helps visualizing the growth effect.**
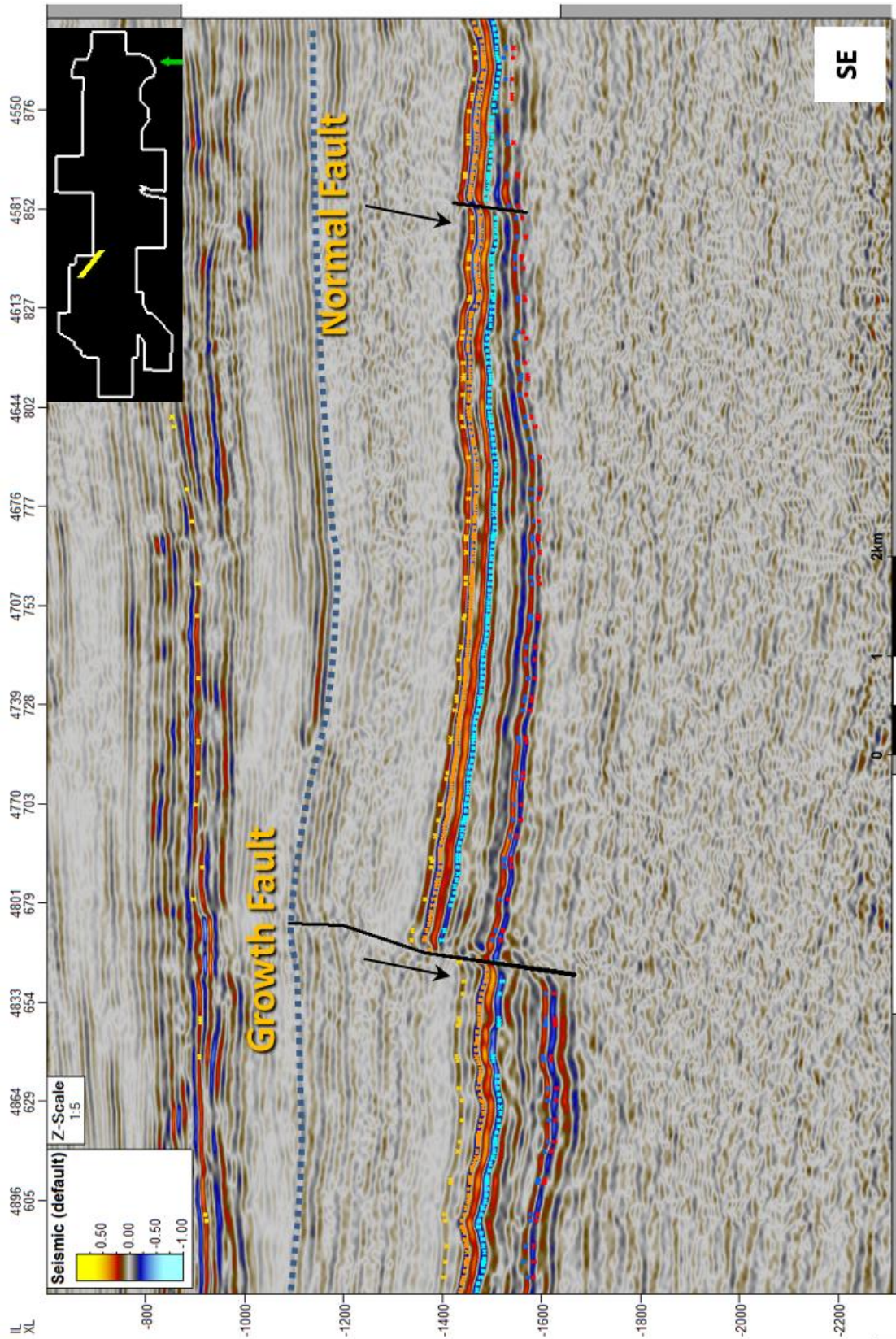
**Figure 68: Interpreted Random Line (PrSTM, TWT) with horizons and location in the area of interest, showing growth strata and northwest dipping normal faults, as well as a growth fault. The blue horizon aproximates the oldest post-tectonic strata.**

## 5.3.5  Regional Interpretation

The E-W striking faults in the central and eastern part of the seismic volume (5.3.1, 5.3.3), as well as the northeast striking faults in between (5.3.2), define normal and conjugated normal faults. The various faults are connected through relay ramps, observed on the 3D surfaces. The striking direction approximately coincides with the striking of the allochthonous Molasse overthrust. Also the predominant dipping is directed towards the thrust front, thus south to southeast. Additionally, the striking of the faults is supposed to follow weakness zones of pre-existing Paleozoic fault systems of the Bohemian Massif (Figure 51). The age of the normal and conjugated faults can be determined as Kiscellian to Eggenburgian, according to the upward terminations reaching above the Base Hall horizon.

The NE-SW striking normal faults observed in the northwestern part of the study (5.3.4) are also thought to follow the direction of the Paleozoic faults, which served as weakness zones and have been reactivated as normal faults in the Oligocene. These pre-existing faults dip towards northwest.

The reason for the south dipping planes being always longer than the north dipping ones is the presence of conjugated faults. In such conjugate faults the south dipping fault is always the continuous one (e.g. Figure 55; compare Figure 70). An explanation for this phenomenon would be a southward rotational component that comes with flexural bending (Figure 69).
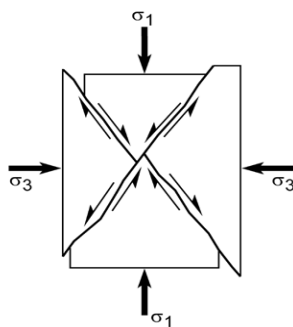


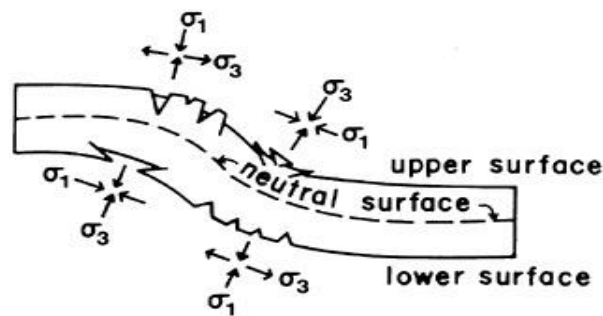Figure 70: Conjugated normal fault model (modified after Burg, 2007)

Figure 69:  Model for flexural bending with stress directions and fault systems (Yeats, 1986)

The geological evolution, the regional fault pattern, fault orientations and deformation ages support the assumption that fault formation is a consequence of **extensional deformation during flexural bending** of the crust. Flexure and subsidence of the European foreland is caused by the load of the northward moving Alpine thrust wedge.

An analogous model for the tectonic setting is illustrated in Figure 71, which shows the setting of the Taconic collisional foredeep. Similarities between the Taconic model and the Upper Austrian foredeep include the subparallel striking of normal faults to the thrust front, the presence of

conjugated normal faults with a dominance of faults dipping towards the thrust front, and abundant relay ramps.
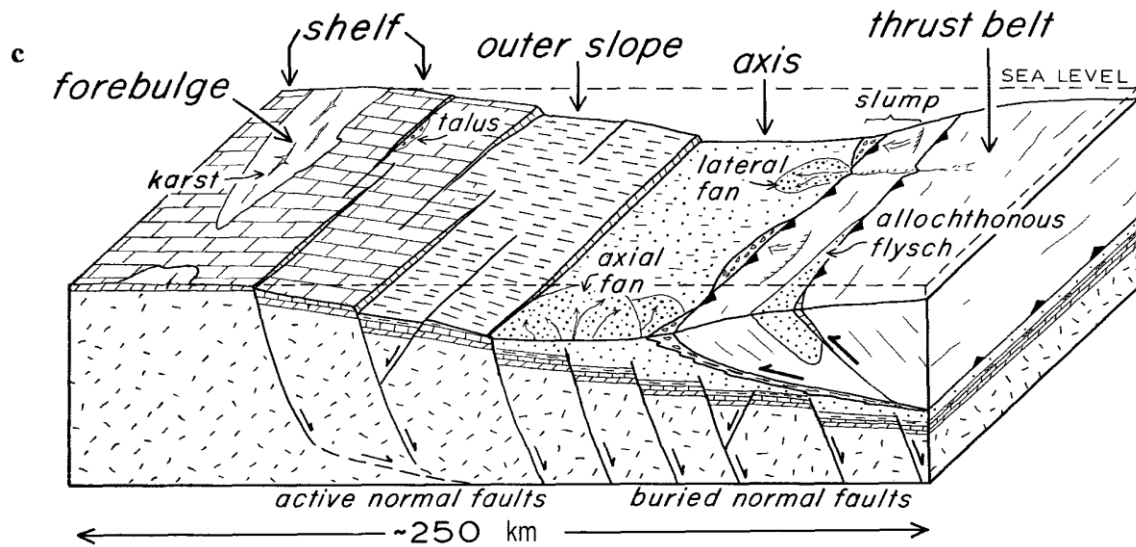


**Figure 71: Schematic block diagram of the Taconic collisional foredeep, showing the distribution of facies belts and structural regimes shortly before plate convergence ended (Bradley & Kidd, 1991). This model can be regarded as an analog to the Upper Austrian Molasse foreland basin. Many important features are comparable, like normal and conjugated normal faults striking subparallel to the thrust belt front, relay ramps, and the predominance of normal faults dipping towards the orogeny.**

As mentioned before, the youngest faults mapped in the seismic give an age of Lower Miocene, while some of them even offset the Base Hall surface (Base Eggenburgian). The time for **deactivation of normal faulting** in the foreland basin coincides with the stop of the northward advance of the Alpine thrust belt. This indicates that no additional flexural bending occurred after the Eggenburgian. Thrusting at the floor thrust of the allochthonous Molasse ceased in the Eggenburgian, as shown by the onlap of Eggenburgian strata onto the thrust wedge of the allochthonous Molasse (BRIX & HAMILTON, 1989; WAGNER, 1996; EGGER et al., 2007; HINSCH, 2013). That fits to the expectation that the north movement of the Alpine thrust wedge should have lasted until this time period and was the reason for the fault generation.

Continued thrust shortening of the Alpine thrust wedge occurred at out-of-sequence thrusts south of the Molasse basin (BEIDINGER & DECKER, 2014) and apparently did not cause additional bending in the foreland.

# 6 CONCLUSIONS

## 6.1 Seismic Attribute Extraction

The development of a special routine for extracting 3D seismic attributes aimed to display all fault structures as high contrast lines, enable a fast identification of faults, and facilitate tectonic overview. This was accomplished by creating a sequential combination of attributes for horizontal and vertical features in Petrel and combining these attributes with a formula (see chapter 3.4). The attributes that were used after several tests are:

| Horizontal Attribute Volume | Vertical Attribute Volume |
|:---:|:---:|
| Relative Acoustic Impedance | Variance |
| RMS Amplitude | Ant Tracking |
| Instantaneous Phase | |

All the parameters used for the extraction of the different attributes where tuned for easy and most detailed fault tracking possible. The large area of the seismic volume caused problems in treating the seismic by a workflow, which is uniformly applied to the whole volume because the quality of the reflectors varies horizontally and vertically. Attribute extraction targeted towards a compromise to produce the best possible results for the entire volume. Hence, the parameters could not be tuned to produce best possible results for small areas of the volume. The use of seismic attributes for extracting fault information revealed the following advantages and disadvantages:

**Pros:**
- Faults appear as high contrasted lines
- Fast identification and overview of fault structures
- Basis for automated fault extraction
- Good help for interpretation
- Nice for starting (especially with big volumes)

**Contras:**
- Other features are tracked sometimes
- Very well tuning for high accuracy necessary
- Automated fault extraction possible but problematic
- Needs to be handled with care and results need to be verified using the original seismic data

In conclusion it can be stated that the generation of a fault attribute volume is useful, if the time spent on applying and tuning all the algorithms can be predicted to be significantly shorter than the time used to track the faults manually. This assessment is depending on the knowledge of how to apply and tune the algorithms, geological information, size and quality of the 3D volume, and the quantity and quality of the faults.

Ultimately, the fault attribute volume can be a huge help and guidance, but for an accurate interpretation manual fault tracking seems to stay the best method.

The master's thesis by Stefan Sageder (2010), who also tried to automate the fault extraction, arrived more or less at the same conclusion: *"The final step following ant-tracking would be automatic fault extraction. This step was tested, but because the results were not satisfactory, automatic fault extraction was not applied. Nevertheless ant tracking volumes are of tremendous help in interpreting and identifying faults. The operation can be performed before one single fault or horizon is mapped and thus guides subsequent interpretation."*

## 6.2 Tectonic Evolution

The tectonic evolution of Upper Austria's Molasse units and their Mesozoic basement can be described with two major events, according to the outcome of this thesis.

The first tectonic event is related to the subduction of the Penninic Ocean and the thrust of the Alpine orogenic wedge towards and finally on the Helvetic Shelf. It is characterized by slip on both, approximately NNW-SSE to NW-SE striking and NE-SW striking faults (e.g., Mattig-, Schwanenstadt- and Lindach-Fault; Figure 72). Some of the NNW-striking faults show indications for dextral strike-slip faulting, like possible Riedel shear sets and positive flower structures. The faults were active in distinct periods between the Upper Cretaceous and the Oligocene. Upper Cretaceous fault ages are determined by growth strata and upward terminations of faults within Upper Cretaceous sediments. A period of Eocene activity is indicated by offset Upper Cretaceous sediments, the absence of Upper Cretaceous growth strata, the termination of faults below the horizon Top Eocene, and constant thickness of overlying strata. Faulting during the Eocene occurred concurrently with the thrust of the Alpine wedge on the Helvetic Shelf during this time (compare DECKER & PERESSON, 1996). Oligocene fault activity is shown by growth strata onlapping the bulge above the positive flower structure. The strike direction of the faults suggests that they originated as Paleozoic strike-slip faults in the Bohemian Massif, which became repeatedly reactivated during Upper Cretaceous to Oligocene convergence.

The second tectonic event started and ended with extensional deformation caused by flexural bending of the crust under the load of the Alpine thrust belt. Deformation resulted in the formation of Kiscellian (Oligocene) to Eggenburgian (Lower Miocene) normal and conjugated normal faults. Faults often appear to follow pre-existing fault zones originating in Paleozoic systems of the Bohemian Massif. The strike directions of the faults are subparallel to the strike of the thrust front. Accordingly, most of the faults strike E-W and dip towards the thrust front. Fault ages are determined by upward terminations of faults and growth strata. The youngest faults of Eggenburgian age are located at and near the Rodl Fault (Figure 72). The age of faulting, the fault pattern, and the comparison with other foreland basins (Figure 71) confirm that the faults formed as a consequence of the flexural bending during the northward movement of the Alpine thrust wedge over the Helvetic Shelf and the Molasse foreland basin.
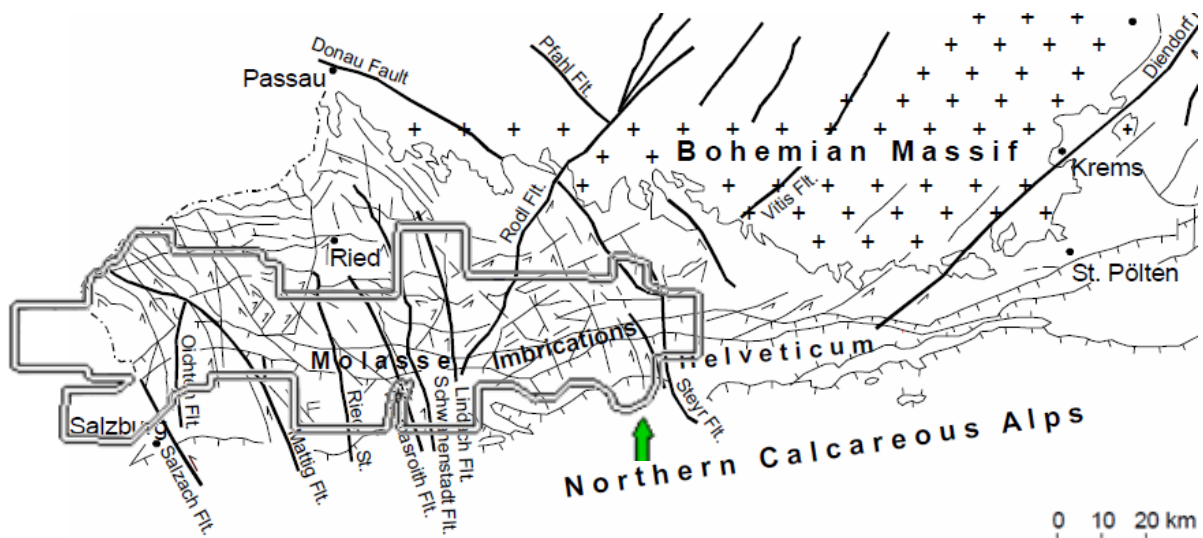


**Figure 72: Fault systems in the Bohemian Massif and the subcrop of the Molasse Basin of Upper Austria (modified after Schulz, 2002; Wagner, 1998))**

Both groups of faults, Upper Cretaceous to lower Oligocene strike-slip faults and Kiscellian to Eggenburgian normal faults, are related to the evolution of the Alpine foreland between the Upper Cretaceous and Lower Miocene times.

# 7  ACKNOWLEDGEMENTS

# 8   REFERENCES

Beidinger, A. & Decker, K. (2014): Quantifying Early Miocene in-sequence and out-of-sequence thrusting at the Alpine-Carpathian junction. - Tectonics, DOI 10.1002/2012TC003250.

Bieg, U. (2005): Paleoocenaographic modeling in global and regional scale - An example from the Burdigalian Seaway, Upper Marine Molasse (Early Miocene). - Diss. Univ. Tübingen, 108 S. (http://tobias-lib.uni-tuebingen.de/volltexte/2005/2132/pdf/thesis_bieg_2005.pdf) (Data retrieved in 2013).

Blakey, R. (2011): Paleogeographic and Tectonic History of Europe. - Colorado Plateau Geosystems, Arizona, USA. (http://cpgeosystems.com/) (Data retrieved in 2013).

Blanckenburg, F.v. & Davis, J.H. (1996): Feasibility of a double slab breakoff (Cretaceous and Tertiary) during the Alpine convergence. - Eclogae Geologicae Helvetiae, **89**, DOI 10.5169/seals-167896, Basel.

Blanckenburg, F.v., Kagami, H., Deutsch, A., Oberli, F., Meier, M., Wiedenbeck, M., Barth, S. & Fischer, H. (1998):  The origin of Alpine plutons along the Periadriatic Lineament. - Schweiz. Miner. Petrogr. Mitt., **78**, 55-66, Zürich.

Bradley, D.C., & Kidd, W.S.F. (1991): Flexural extension of upper continental crust in collisional foredeeps. - Geological Society of America Bulletin, **103**, 1416-1438.

Brandmayr, M., Dallmeyer, R.D., Handler, R. & Wallbrecher, E. (1995): Conjugate shear zones in the Southern Bohemian Massif (Austria): implications for Variscan and Alpine tectonothermal activity. - Tectonophysics, **248**/1–2, 97–116, Amsterdam.

Brix, F. & Hamilton, W. (1989): Geologische Ergebnisse von Tiefbohrungen im Flysch und Kalkalpin zwischen Wien und Salzburg. – In: Führer zur Exkursion der Österreichischen Geologischen Gesellschaft, **12**, edited by W. Hamilton, Geologische Bundesanstalt, Wien.

Burg, J.P. (2007): Verwerfungen. - Teaching material from the ETH Zürich (http://www.structuralgeology.ethz.ch/education/teaching_material/general) (Data retrieved: 2013)

Decker, K., Peresson, H. & Faupl, P. (1994): Die miozäne Tektonik der Östlichen Kalkalpen: Kinematik, Paläospannungen und Deformationsaufteilung während der "lateralen Extrusion" der Zentralalpen. - Jb. Geol. B.-A., **137**/1, 5-18, Wien.

Decker, K. & Peresson, H. (1996): Tertiary kinematics in the Alpine-Carpathian-Pannonian system: links between thrusting, transform faulting and crustal extension. – In: Oil and Gas in Alpidic Thrustbelts and Basins of Central and Eastern Europe, EAGE Spec. Publ., **5**, edited by G. Wessely and W. Liebl, pp. 69-77, Geological Society, London.

Egger,H. (1997): Das sinistrale Innsbruck-Salzburg-Amstetten-Blattverschiebungssystem: ein weiterer Beleg für die miozäne laterale Extrusion der Ostalpen. - Jb. Geol. B.-A., **140**/1, 47-50, Wien.

Egger, H., Heinrich, M., Lobitzer, H., Moshammer, B., Pavuza, R., Rupp, C., Schedl, A., Schubert, G., Schuster, R., Stummer, G., Husen, D.van, Wagner, L. & Wessely, G. (2007): Erläuterungen zu Blatt 67 Grünau im Almtal. - Geologische Karten der Republik Österreich im Blattschnitt 1:50.000, Geologische Bundesanstalt, Wien.

Faupl, P. (1975): Kristallinvorkommen und terrigene Sedimentgesteine in der Grestener Klippenzone (Lias – Neokom) von Ober- und Niederösterreich. – Jb. Geol. B.-A., **118**, 1-74, Wien.

Finger, F., Gerdes, A., Janousek, V., Rene, M. & Riegler, G. (2007): Resolving the Variscan evolution of the Moldanubian sector of the Bohemian Massif: the significance of the Bavarian and the Moravo–Moldanubian tectonometamorphic phases. - Journal of Geosciences, **52**: 9–28.

Freudenberger W. & Schwerd, K. (Eds.) (1996): Erläuterungen zur geologischen Karte von Bayern 1: 500.000. - Bayerisches Geol. Landesamt, 329 S., München.

Frisch, W., Kuhlemann, J., Dunkl, I., & Brügel, A. (1998): Palinspastic reconstruction and topographic evolution of the Eastern Alps during late Tertiary tectonic extrusion. - Tectonophysics, **297**, 1-15, Amsterdam.

Handy, M.R., Schmid, S.M., Bousquet, R., Kissling, E. & Bernoulli, D. (2010): Reconciling plate-tectonic reconstructions of Alpine Tethys with the geological-geophysical record of spreading and subduction in the Alps. - Earth-Science Reviews, **102**, 121-151, Amsterdam.

Hinsch, R. (2008): Continued internal and external research efforts of RAG: New insights for the geological evolution of the Molasse Basin of Austria. - Oil & Gas Europ. Mag., **3**, 138-143, Hamburg-Wien.

Hinsch, R. (2013): Laterally varying structure and kinematics of the Molasse fold and thrust belt of the Central Eastern Alps: Implications for exploration. - AAPG Bulletin 10/2013, DOI:10.1306/04081312129

Hinsch, R., Hubbard, S. & Kofler, N. (2007): Stratigraphic Trap Exploration in a Mature Basin: Examples for New Concepts from the Austrian Molasse Basin. - Oil & Gas Europ. Mag. **4**, 172-176, Hamburg-Wien.

Kröll, A., Meurers, B., Oberlercher, G., Seiberl, W., Slapansky, P., Wagner, L., Wessely, G. & Zych, D. (2006b): Erläuterungen zu den Karten über die Molassebasis Salzburg-Oberösterreich. - 24 S., Geol. B.-A., Wien.

Linner, M., Finger, F. & Reiter, E. (2011): Moldanubikum (Kristallin der Böhmischen Masse). – In: Rupp, Ch., Linner, M. & Mandl, G.W. (Red.) (2011): Geologische Karte von Oberösterreich 1:200 000: Erläuterungen. - 255 S., Geol. B.-A., Wien.

Linzer, H.-G., Frisch, W. & Ratschbacher, L. (1990): Kinematisches Modell der Nördlichen Kalkalpen (Vortragskurzfassung). - TSK III, 3. Symposium für Tektonik, Strukturgeologie und Kristallingeologie, Graz.

Linzer, H.-G., Ratschbacher, L. & Frisch, W. (1995): Transpressional collision structures in the upper crust: the fold-thrust belt of the Northern Calcareous Alps. - Tectonophysics, **242**, 41-61, Amsterdam (Elsevier).

Malzer, O., Rögl, F., Seifert, P., Wagner, L., Wessely, G. & Brix, F. (1993): Die Molassezone und deren Untergrund. - In: Brix, F. & Schultz, O. (Red.): Erdöl und Erdgas in Österreich. 2. Aufl. - Veröff. Naturhist. Museum Wien, N. F. **19**, 688 S., Wien - Horn, Naturhist. Mus. & F. Berger.

Mandl, G.W. (2011): Nördliche Kalkalpen. - In: Rupp, Ch., Linner, M. & Mandl, G.W. (Red.) (2011): Geologische Karte von Oberösterreich 1:200 000: Erläuterungen. - 255 S., Geol. B.-A., Wien.

Mattern, F. (2001): Permo-Silesian movements between Baltica and Western Europe: tectonics and "basin families". - Terra Nova, **13**, 368-375, 2001, Oxford.

Nachtmann, W. & Wagner L. (1987): Mesozoic and Early Tertiary evolution of the Alpine foreland in Upper Austria and Salzburg, Austria. – Tectonophysics, **137**, 61-76, Amsterdam.

Peresson, H. & Decker, K. (1997): The Tertiary dynamics of the northern Eastern Alps (Austria): changing paleostresses in a collisional plate boundary. - Tectonophysics, **272**, 125-157, Amsterdam.

Petrel Help (2012): Help file included in the program Petrel 2012.

Piller, W. E., Egger, H., Erhart, C., Gross, M., Harzhauser, M., Hubmann, B., Husen, D.van, Krenmayr, H.-G., Krystyn, L., Lein, R., Lukeneder, A., Mandl, G., Rögl, F., Roetzel, R., Rupp, C., Schnabel, W., Schönlaub, H. P., Summesberger, H., Wagreich, M. & Wessely, G. (2004): Die Stratigraphische Tabelle von Österreich 2004 (sedimentäre Schichtfolgen). – Österr. Akad. Wiss. u. Österr. Strat. Komm., Wien.

Reiser, H. (1987): Die Foraminiferen der bayerischen Oligozän-Molasse. Systematik, Stratigraphie und Paläobathymetrie. - Zitteliana, **16**, 3-131, München.

Rögl, F. (1999): Mediterranean and Paratethys. Facts and hypotheses of an Oligocene to Miocene paleogeography (short overview). – Geologica Carpathica, **50**/4, 339-349, Bratislava.

Rögl, F. & Rupp, Ch. (1996): Stratigraphie in der Molassezone Oberösterreichs. - In: Egger, H., Hofmann, Th. & Rupp, Ch. (Red.): Ein Querschnitt durch die Geologie Oberösterreichs. Wandertagung Österr. Geol. Ges. 1996. - Exkursionsführer, **16**, 66-72, Geol. B.-A., Wien.

Rupp, Ch. (2011): Autochthones Mesozoikum. - In: Rupp, Ch., Linner, M. & Mandl, G.W. (Red.) (2011): Geologische Karte von Oberösterreich 1:200 000: Erläuterungen. - 255 S., Geol. B.-A., Wien.

Rupp, Ch., Linner, M. & Mandl, G.W. (Red.) (2011): Geologische Karte von Oberösterreich 1:200 000: Erläuterungen. - 255 S., Geol. B.-A., Wien.

Sachsenhofer, R.F., Leitner, B., Linzer, H.G., Bechtel, A., Coric, S., Gratzer, R., Reischenbacher, D. & Soliman, A. (2010): Deposition, Erosion and Hydrocarbon Source Potential of the Oligocene Eggerding Formation (Molasse Basin, Austria). - Austrian Journal of Earth Sciences, **103**/1, 76 -99, Wien.

Sageder, S. (2010): Mesozoic and Cenozoic fault systems in the Molasse Basin: The example of the Trattnach area (Upper Austria). – Master's thesis, Univ. Leoben, 92.

Schulz, H.M., Sachsenhofer, R.F., Bechtel, A., Polesny, H. & Wagner, L. (2002): The origin of hydrocarbon source rocks in the Austrian Molasse Basin (Eocene-Oligocene transition). - Marine and Petroleum Geology, **19**/6, 683-709, Oxford (Elsevier).

Schuster, R., Mandl, G.W., Linner, M., Pestal, G., Rupp, Ch. & Husen, D.van (2011): Die geologische Entwicklungsgeschichte Oberösterreichs. - Ein Überblick. - In: Rupp, Ch., Linner, M. & Mandl, G.W. (Red.) (2011): Geologische Karte von Oberösterreich 1:200 000: Erläuterungen. - 255 S., Geol. B.-A., Wien.

Schuster, R., Daurer, A., Krenmayr, H.-G., Linner, M., Mandl, G.W., Pestal, G. & Reitner, J.M. (2013): Rocky Austria: Geologie von Österreich - kurz und bunt. – 3.Aufl., 80 S., Geol. B.-A., Wien.

Shaw, J. H., Connors, C. & Suppe, J. (eds.) (2005): Seismic Interpretation of Contractional Fault-Related Faults. - AAPG Seismic Atlas - Studies in Geology. Tulsa, Oklahoma, American Association of Petroleum Geologists.

Steininger, F. & Wessely, G. (2000): From the Tethyan Ocean to the Paratethys Sea: Oligocene to Neogene Stratigraphy, Paleogeography and Paleobiogeography of the circum-Mediterranean region and the Oligocene to Neogene Basin evolution in Austria. – Mitt. Geol. Ges. Wien, **92**, 95-116, Wien.

Wagner, L. R. (1996): Stratigraphy and hydrocarbons in the Upper Austrian Molasse Foredeep (active margin). - In: Wessely, G., Liebl, W. (Eds.), Oil and Gas in Alpidic Thrustbelts and Basins of Central and Eastern Europe. EAGE Special Publication, **5**, 217-235, London.

Wagner, L. R. (1998): Tectono-stratigraphy and hydrocarbons in the Molasse Foredeep of Salzburg, Upper and Lower Austria. - In: Mascle, A., Puigdefabregas, C., Lutherbacher, H.P. & Fernandez, M. (Eds.): Cenozoic Foreland Basins of Western Europe. - Geol. Soc. Spec. Publ., **134**, 339-369, London.

Wessely, G. (Red.) (2006): Geologie der österreichischen Bundesländer: Niederösterreich. – 416 S., Geol. B.-A., Wien.

Woodcock, N. H. & Fischer, M. (1986): Strike-Slip duplexes. – Journal of Structural Geology **8** (7), 725-735.

Yeats, R. S. (1986): Active Faults Related to Folding. - In: Active Tectonics: Impact on Society (1986), Nat. Acad. Press, Washington, D.C.

# 9  ATTACHMENTS

## 9.1 Table of Mapped Faults

| Faultsystem | Fault Interpretation # | Locations, Descriptions and Notes |
|---|---|---|
| **a1)** | **30** | **center; W-E striking; S dipping fault system** |
| | Fault Interpretation 1-30 | |
| **a2)** | **23** | **center; W-E striking; N dipping** |
| | Fault Interpretation 1-23 | |
| **a3)** | **44** | **center; N-S - NW-SE faults** |
| | Fault Interpretation 1-42, 2b, 4b | |
| **b1)** | **21** | **west; NE - SW striking** |
| | Fault Interpretation 1-20, 12b | |
| **b2)** | **15** | **west; NW - SE striking** |
| | Fault Interpretation 1-15 | |
| **d1)** | **11** | **western duplexes** |
| | Fault Interpretation 1-10, 1b | |
| **d2)** | **18** | **western duplexes; Interpretation on FFAV** |

| | | | |
|---|---:|---|---|
| | Fault Interpretation 1,3-9, 11-20 | | |
| **c)** | **32** | **westernmost (Bavaria)** | |
| c)seismic | 21 | Interpretation on original seismic | |
| | Fault Interpretation 1-4, 7-23 | | |
| c)FFAV | 11 | Interpretation on FFAV | |
| | Fault Interpretation 1-11 | | |
| **e)** | **38** | **NE-SW striking faults; center-east** | |
| | Fault Interpretation 1-37, 25b | | |
| **ae)** | **14** | **E-W striking; center-east** | |
| | Fault Interpretation 1-14 | | |
| **ae 1)** | **6** | **NW-SE striking; center-east** | |
| | Fault Interpretation 1-6 | | |
| **f)** | **31** | **Eastern part; NW-SE** | |
| | Fault Interpretation 1-31 | | |
| **f1)** | **55** | **Eastern part; ENE-WSW** | |
| | Fault Interpretation 1-55 | | |
| **f2)** | **9** | **Eastern part; NE-SW** | |
| | Fault Interpretation 1-9 | | |

## 9.2 Fault Surfaces
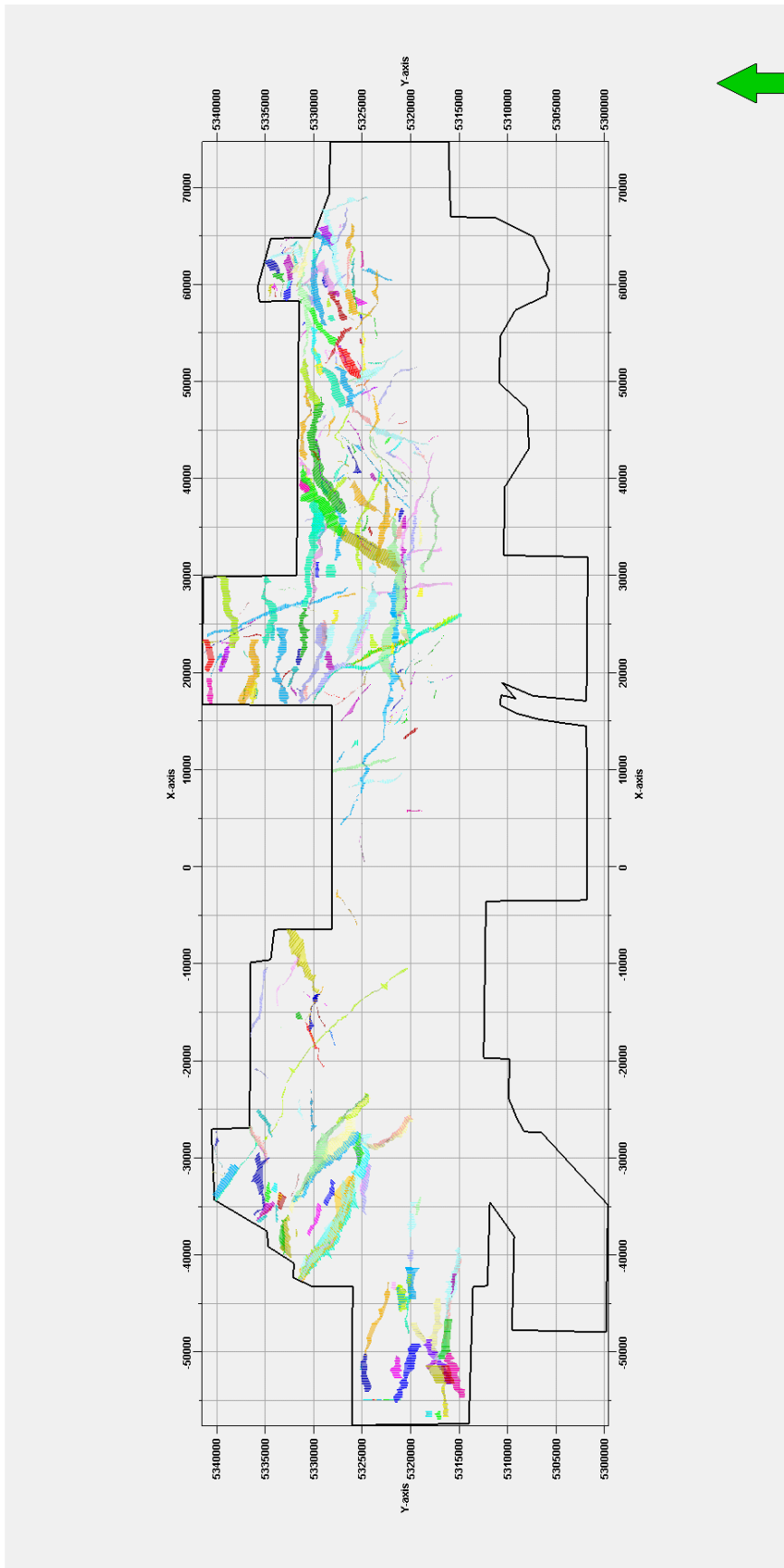


Figure 73: Fault Map with seismic boundary and mapped fault surfaces (colored)
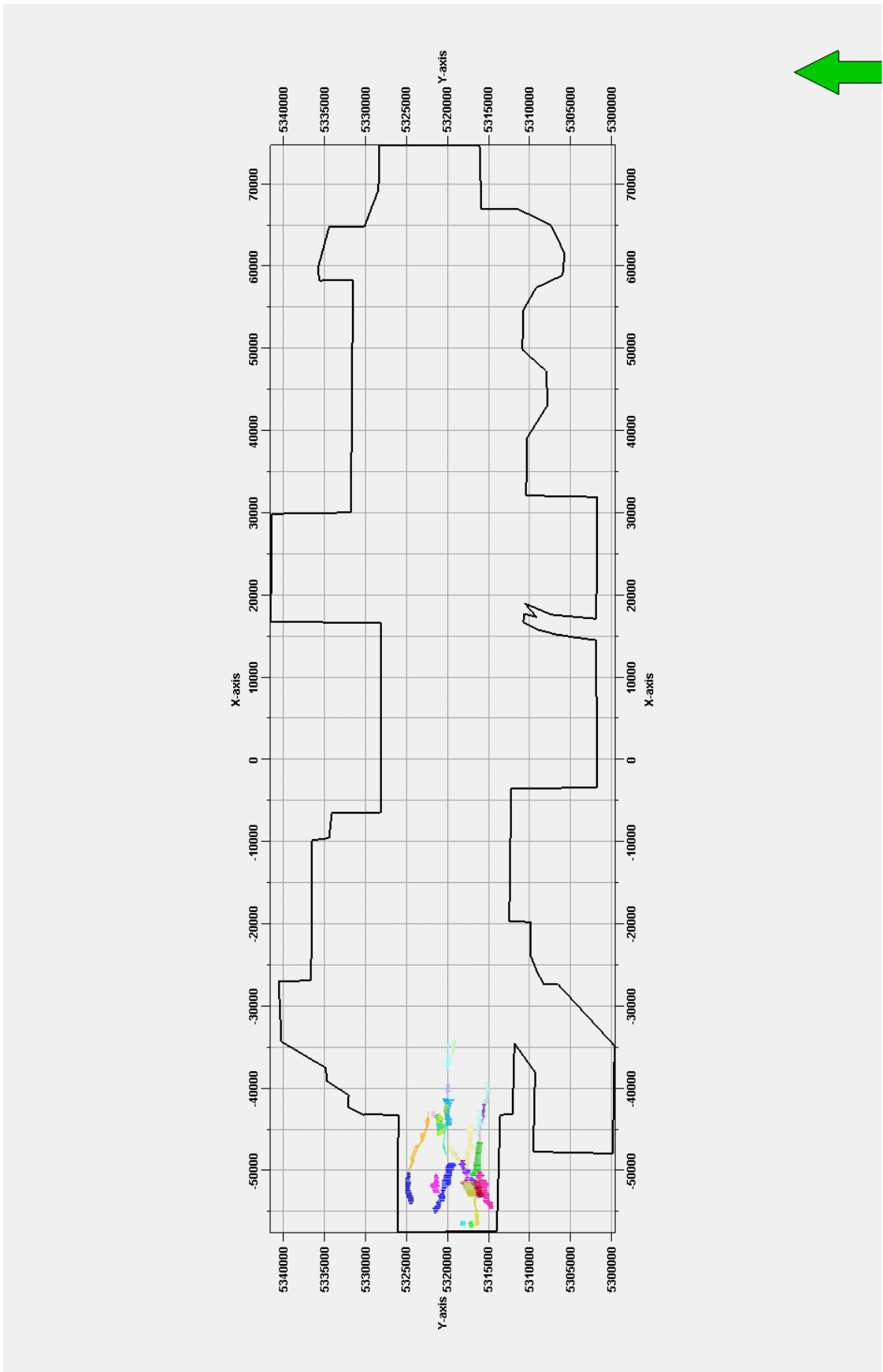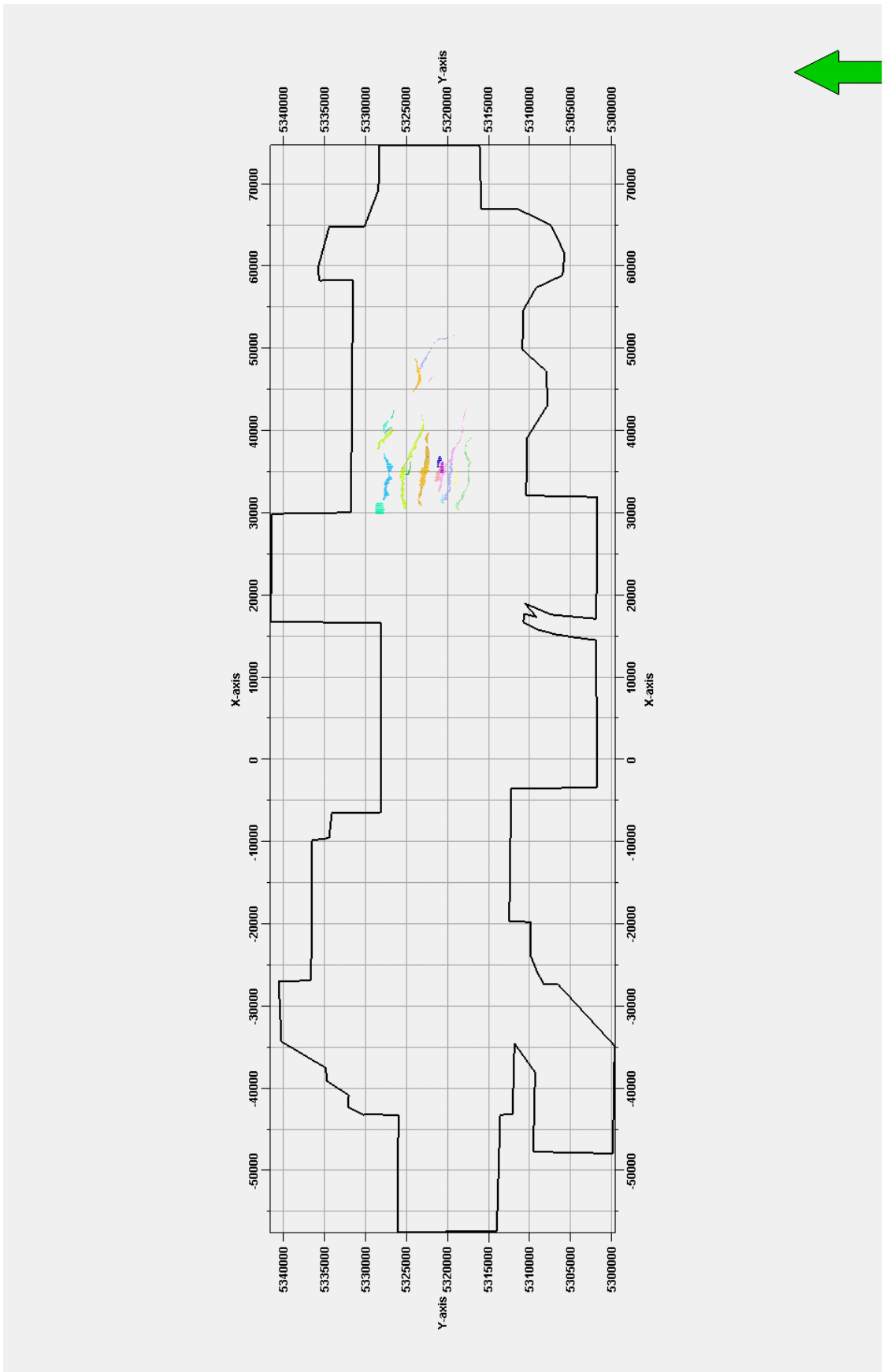
**Figure 74: Fault Map with seismic boundary and mapped fault surfaces (colored) in the subarea "c" (see table above)**
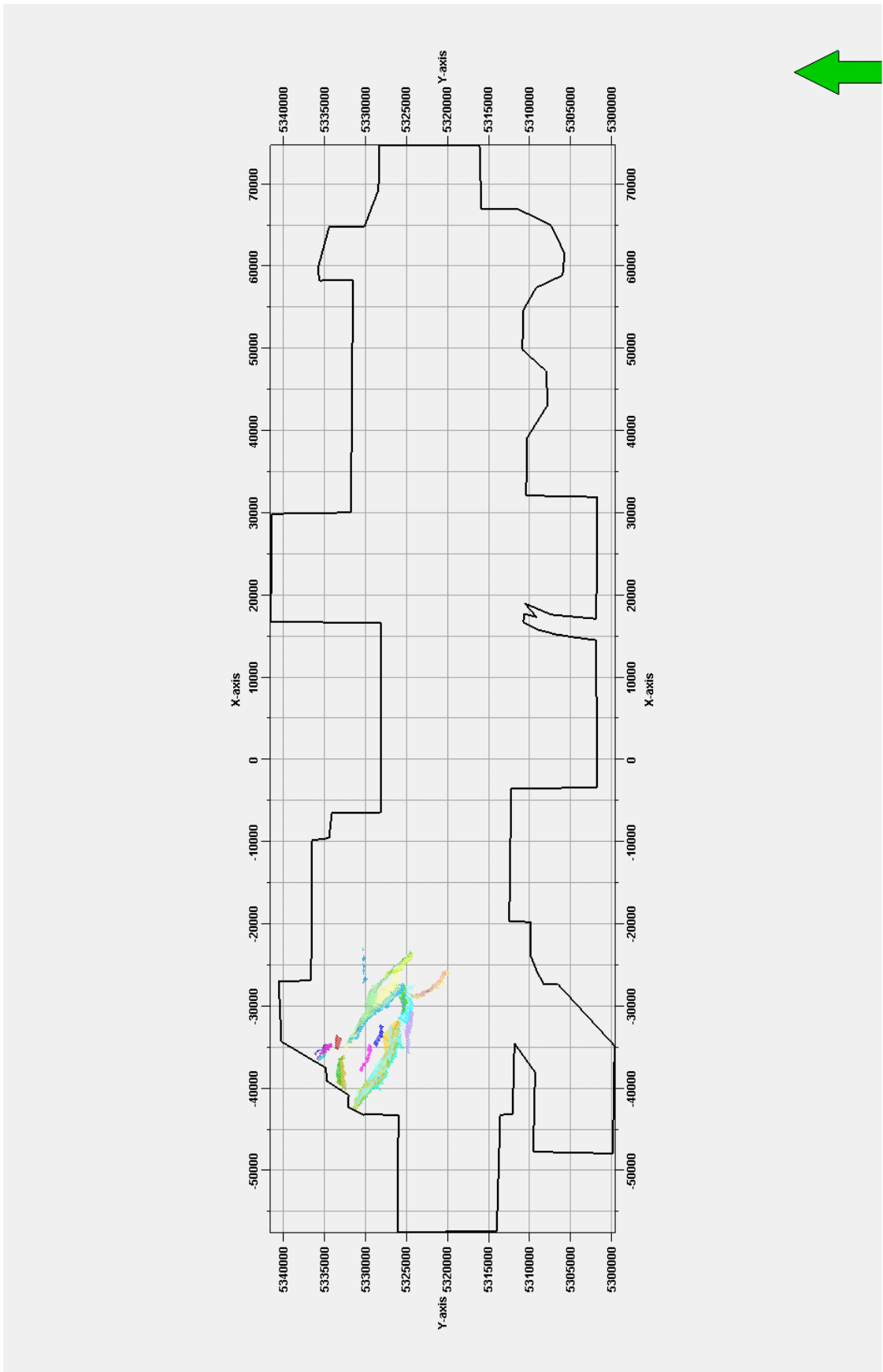
**Figure 75: Fault Map with seismic boundary and mapped fault surfaces (colored) in the subarea "d" (see table above)**
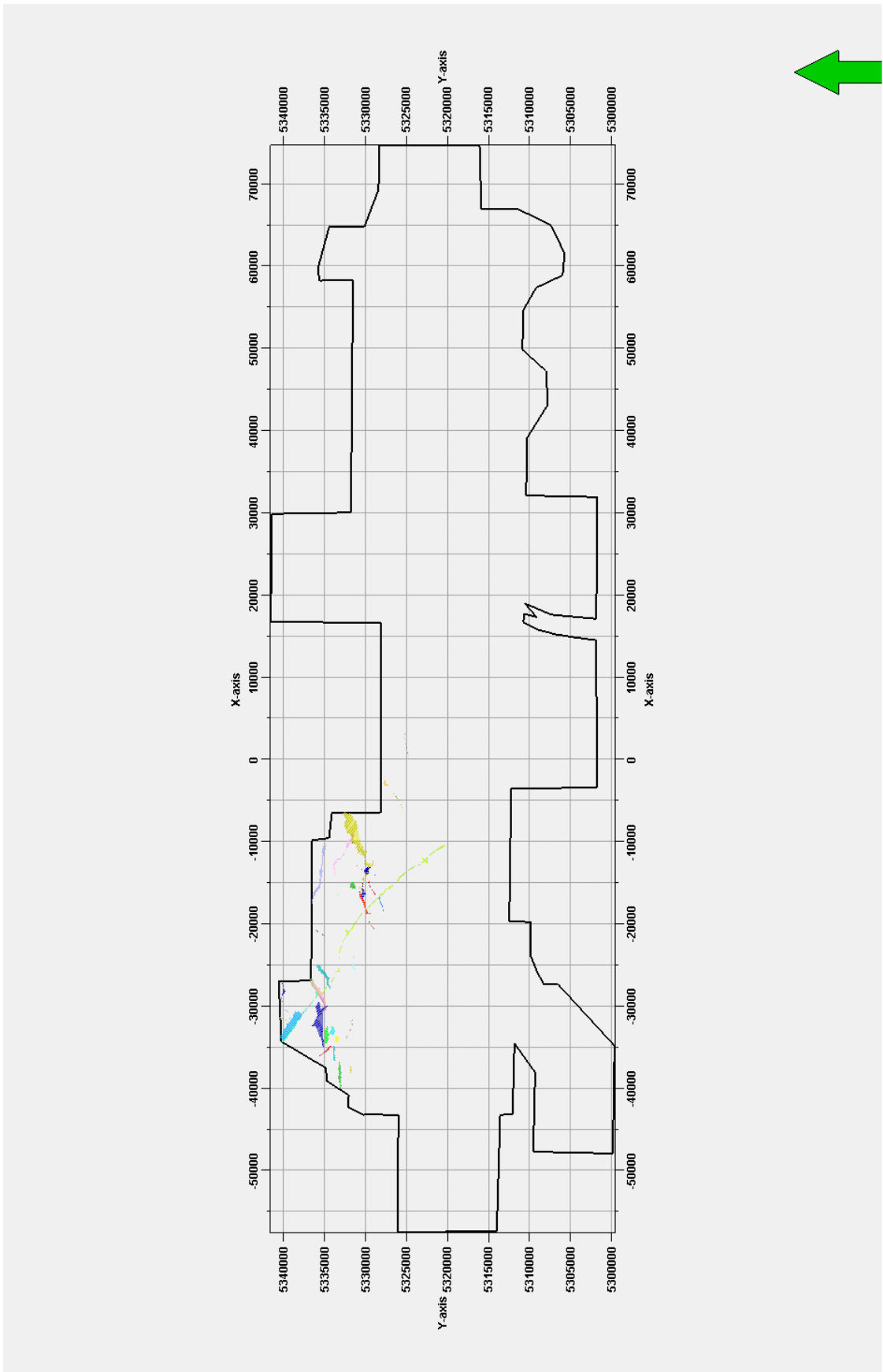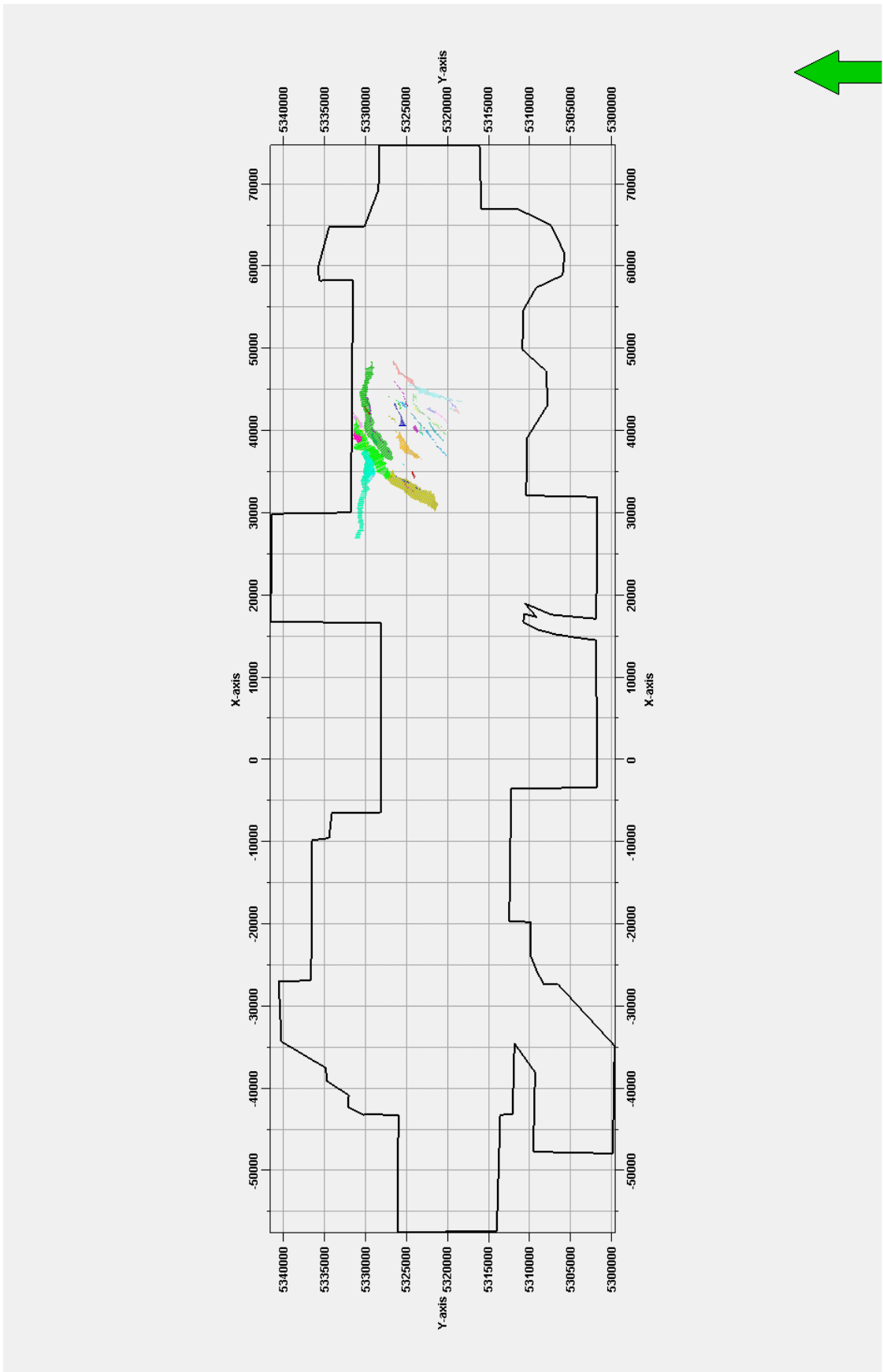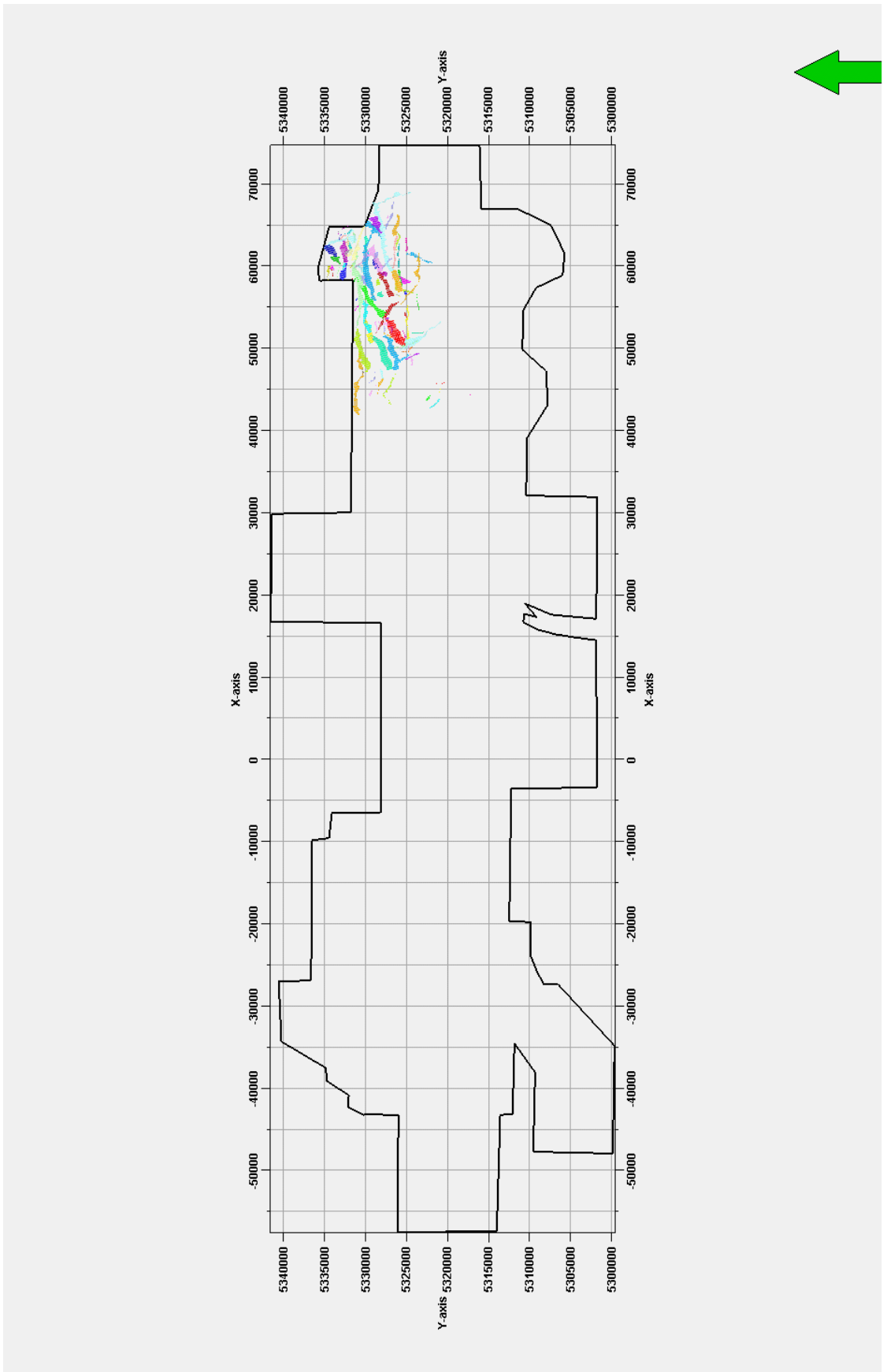
**Figure 76: Fault Map with seismic boundary and mapped fault surfaces (colored) in the subarea "b" (see table above)**
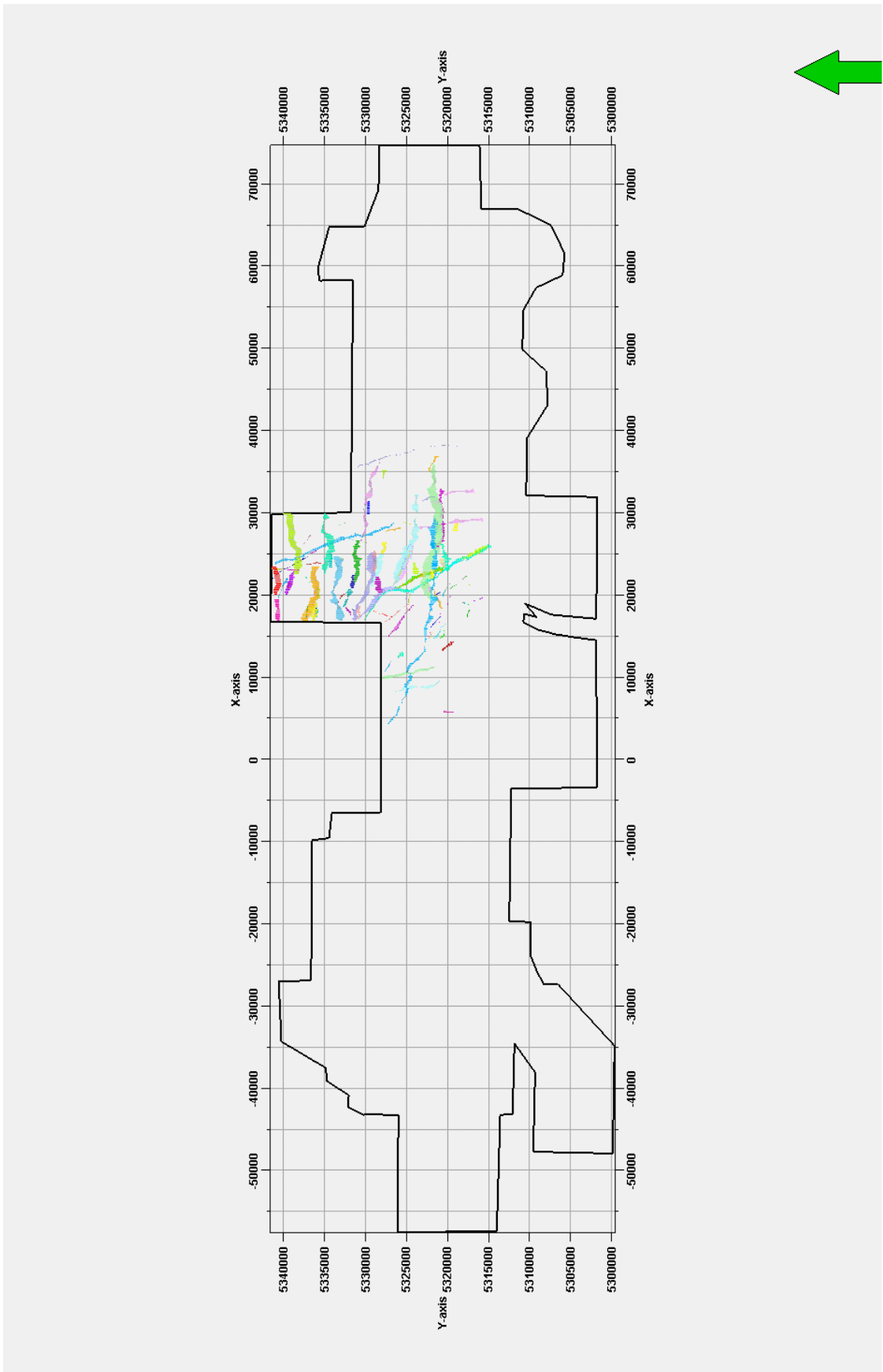
**Figure 77: Fault Map with seismic boundary and mapped fault surfaces (colored) in the subarea "a" (see table above)**

**Figure 78: Fault Map with seismic boundary and mapped fault surfaces (colored) in the subarea "ae" (see table above)**

**Figure 79: Fault Map with seismic boundary and mapped fault surfaces (colored) in the subarea "e" (see table above)**

**Figure 80: Fault Map with seismic boundary and mapped fault surfaces (colored) in the subarea "f" (see table above)**

## 9.3 Horizon Views (Comparison of Fault Surfaces with FFAV)
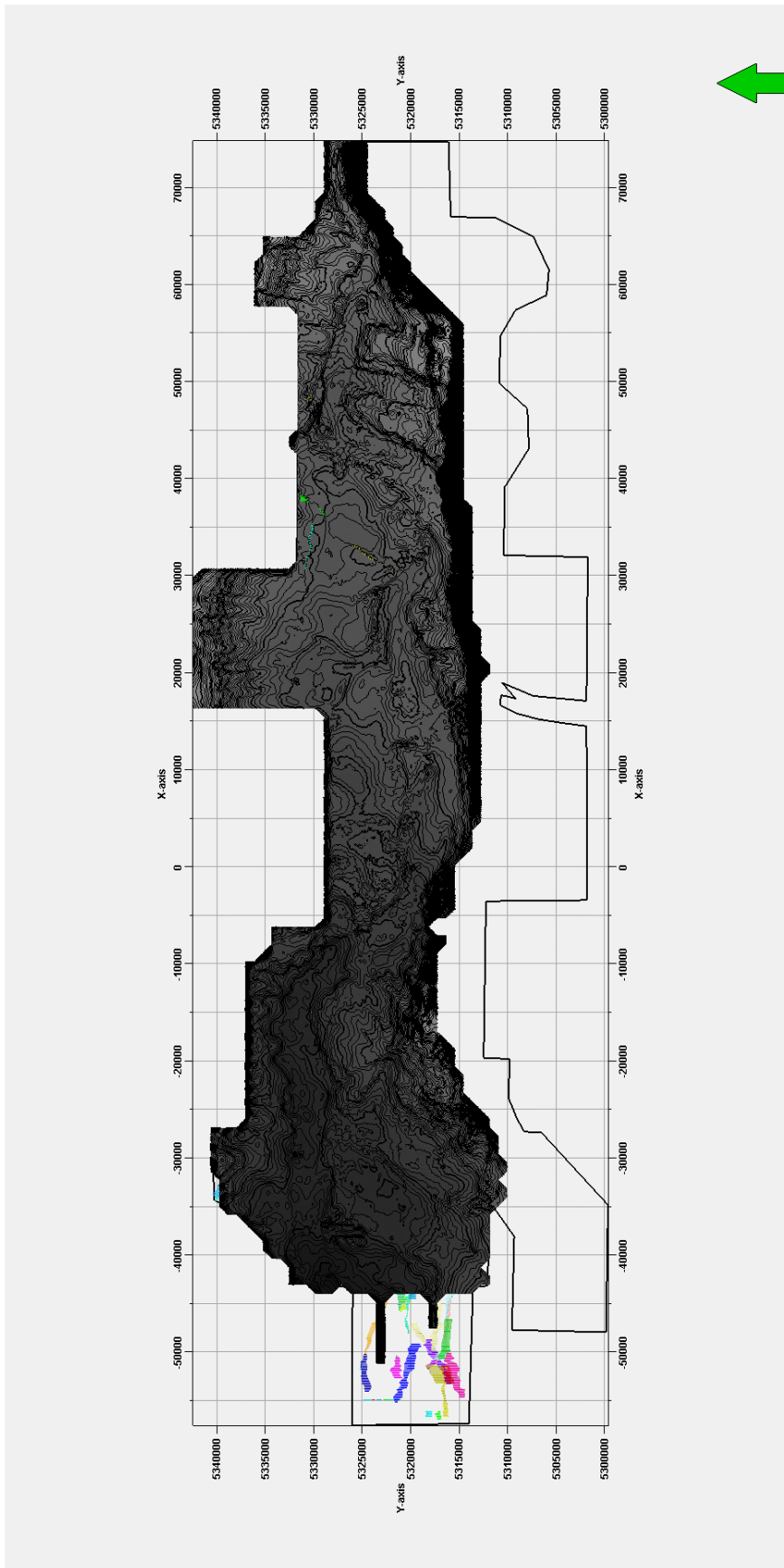


Figure 81: Fault Map with seismic boundary, mapped fault surfaces (colored) and Surface Hall with contours.
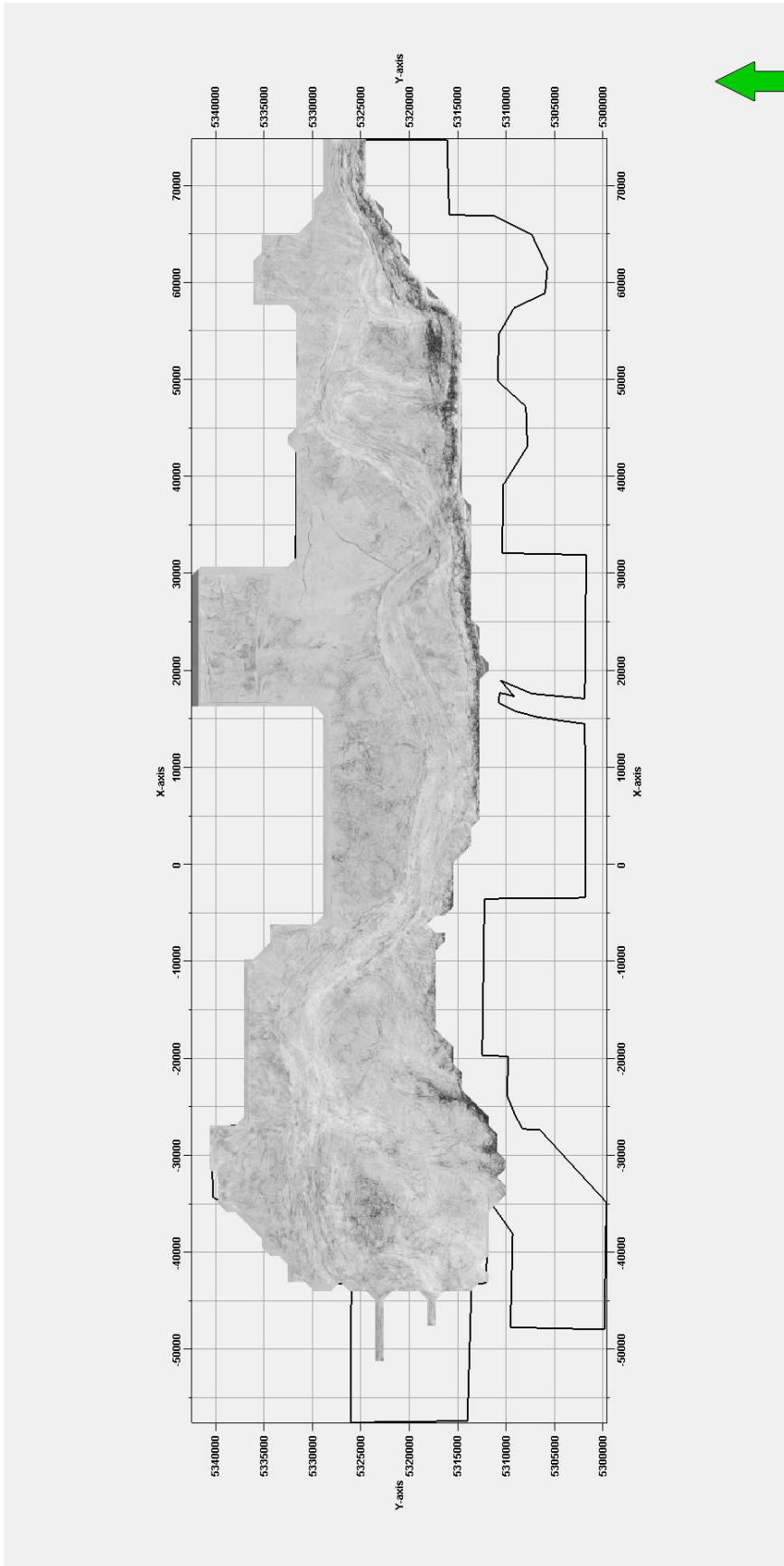
**Figure 82: Surface Hall attributed with the data of the Fault Attribute Volume. Dark areas indicate faults. Compare with manual interpreted faults of the previous figure.**
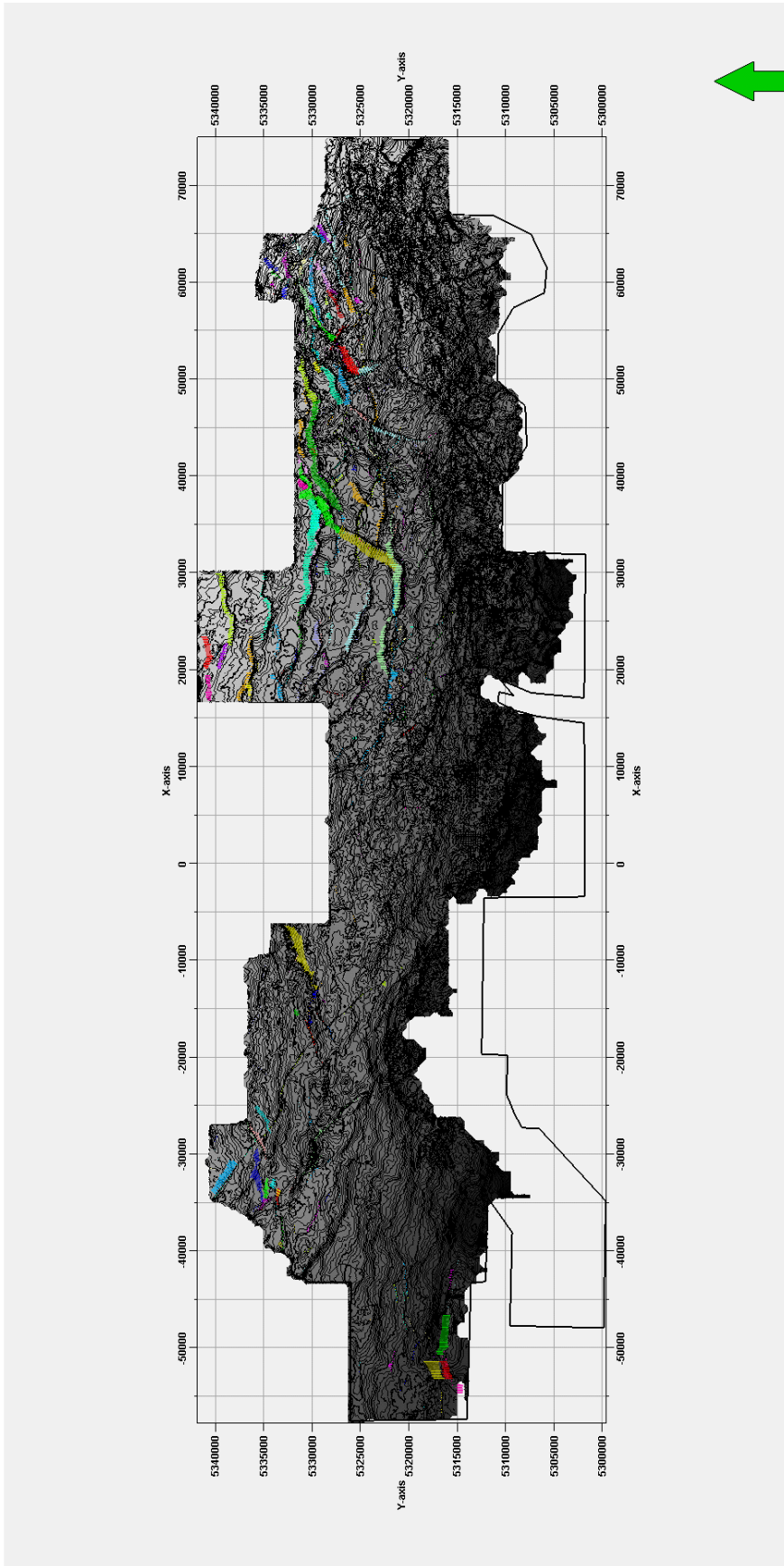
**Figure 83: Fault Map with seismic boundary, mapped fault surfaces (colored) and surface Eocene with contours.**
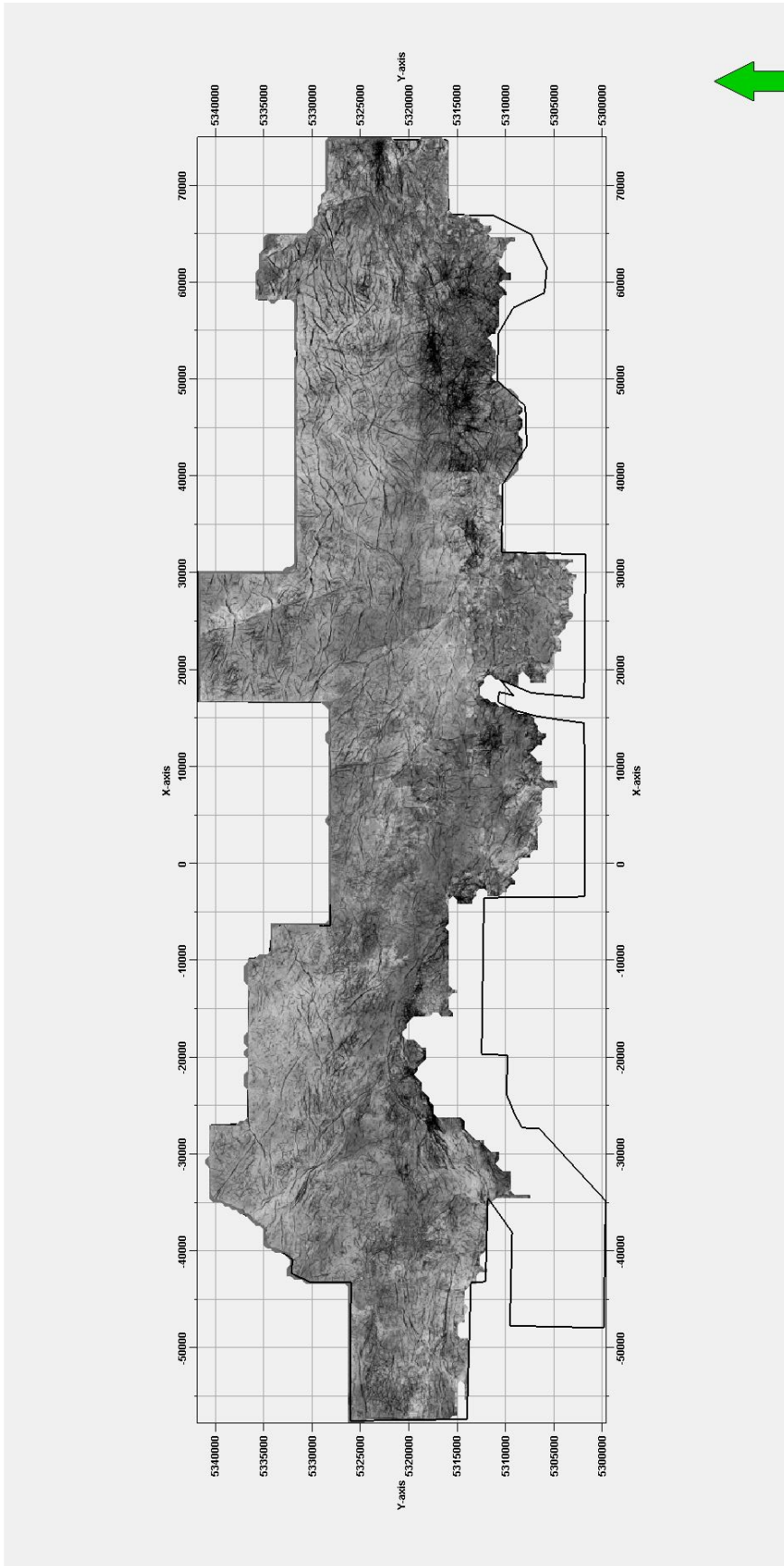
**Figure 84: Surface Eocene attributed with the data of the Fault Attribute Volume. Dark areas indicate faults. Compare with manual interpreted faults of the previous figure.**
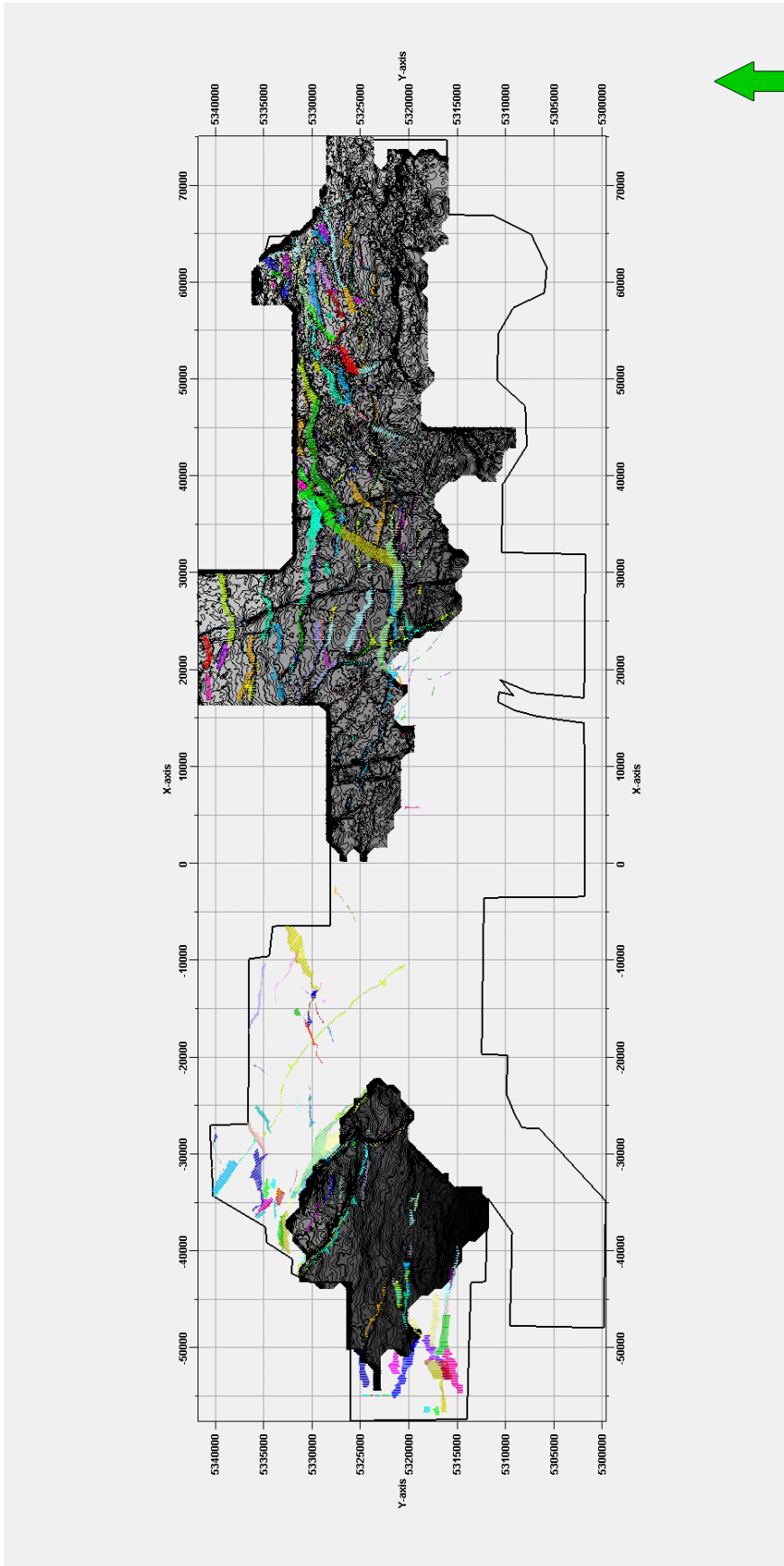
**Figure 85: Fault Map with seismic boundary, mapped fault surfaces (colored) and surface Cenomanian with contours.**
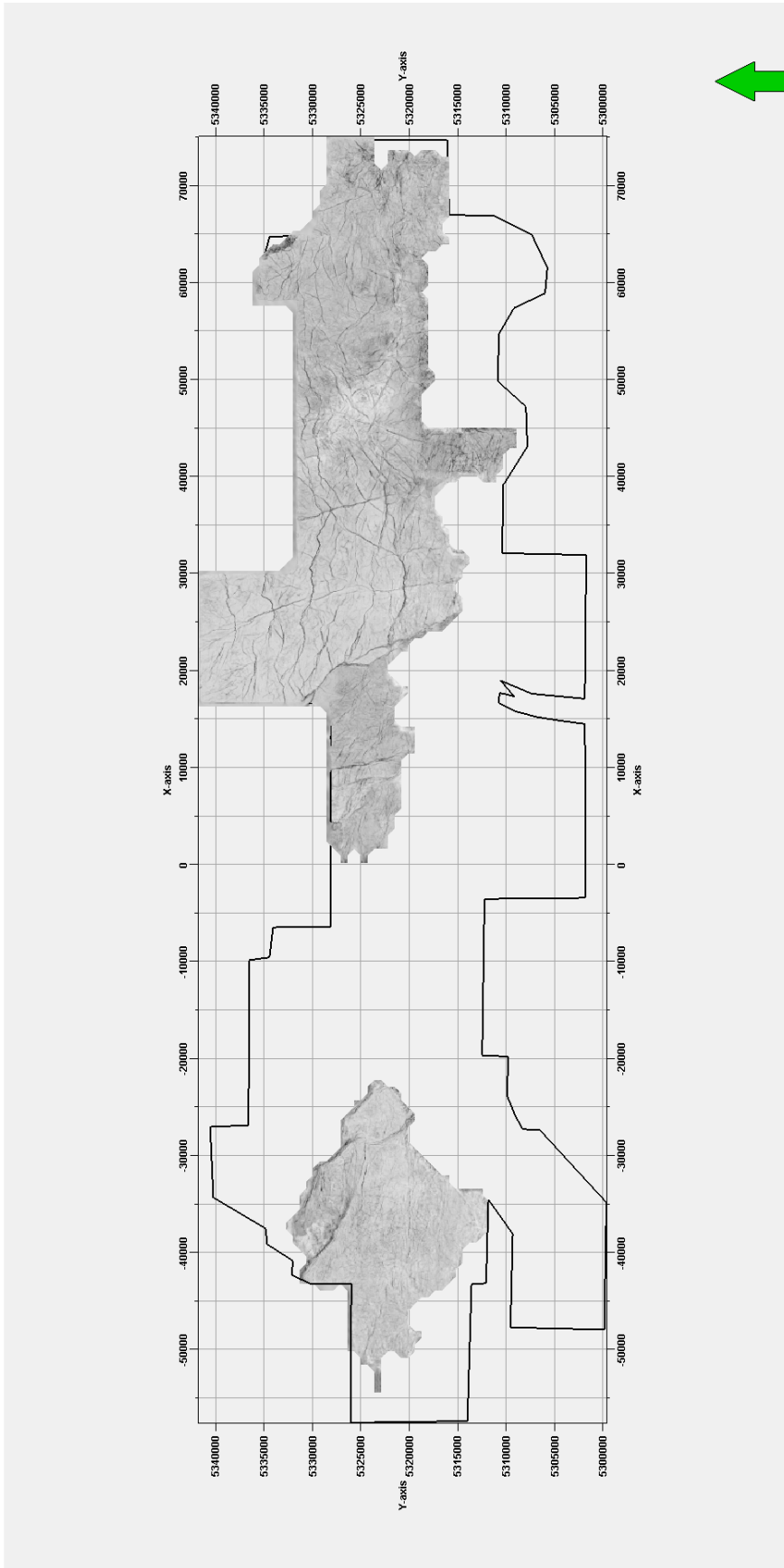
**Figure 86: Surface Cenomanian attributed with the data of the Fault Attribute Volume. Dark areas indicate faults. Compare with manual interpreted faults of the previous figure.**
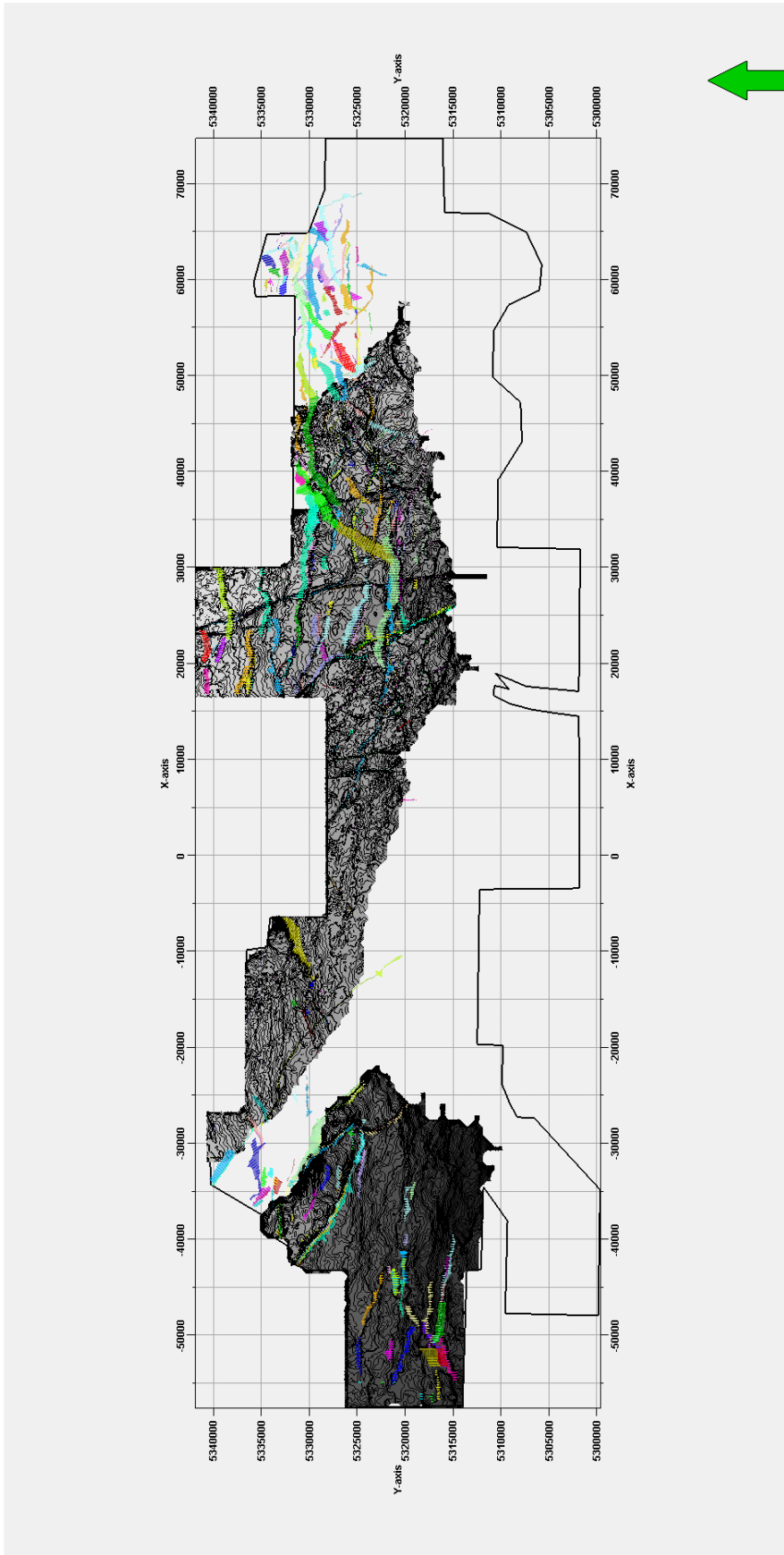
**Figure 87: Fault Map with seismic boundary, mapped fault surfaces (colored) and surface Jurassic with contours.**
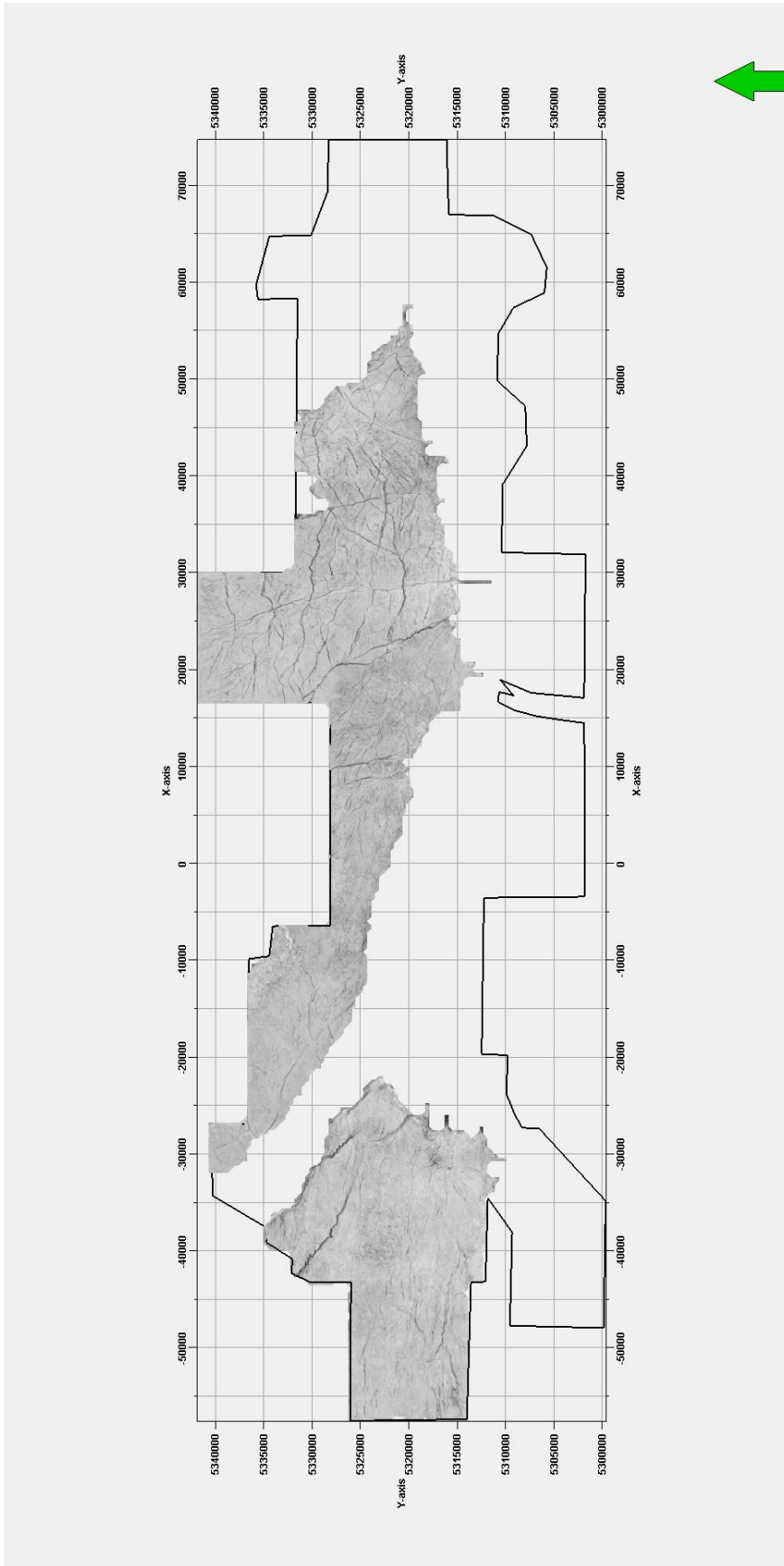
**Figure 88: Surface Jurassic attributed with the data of the Fault Attribute Volume. Dark areas indicate faults. Compare with manual interpreted faults of the previous figure.**
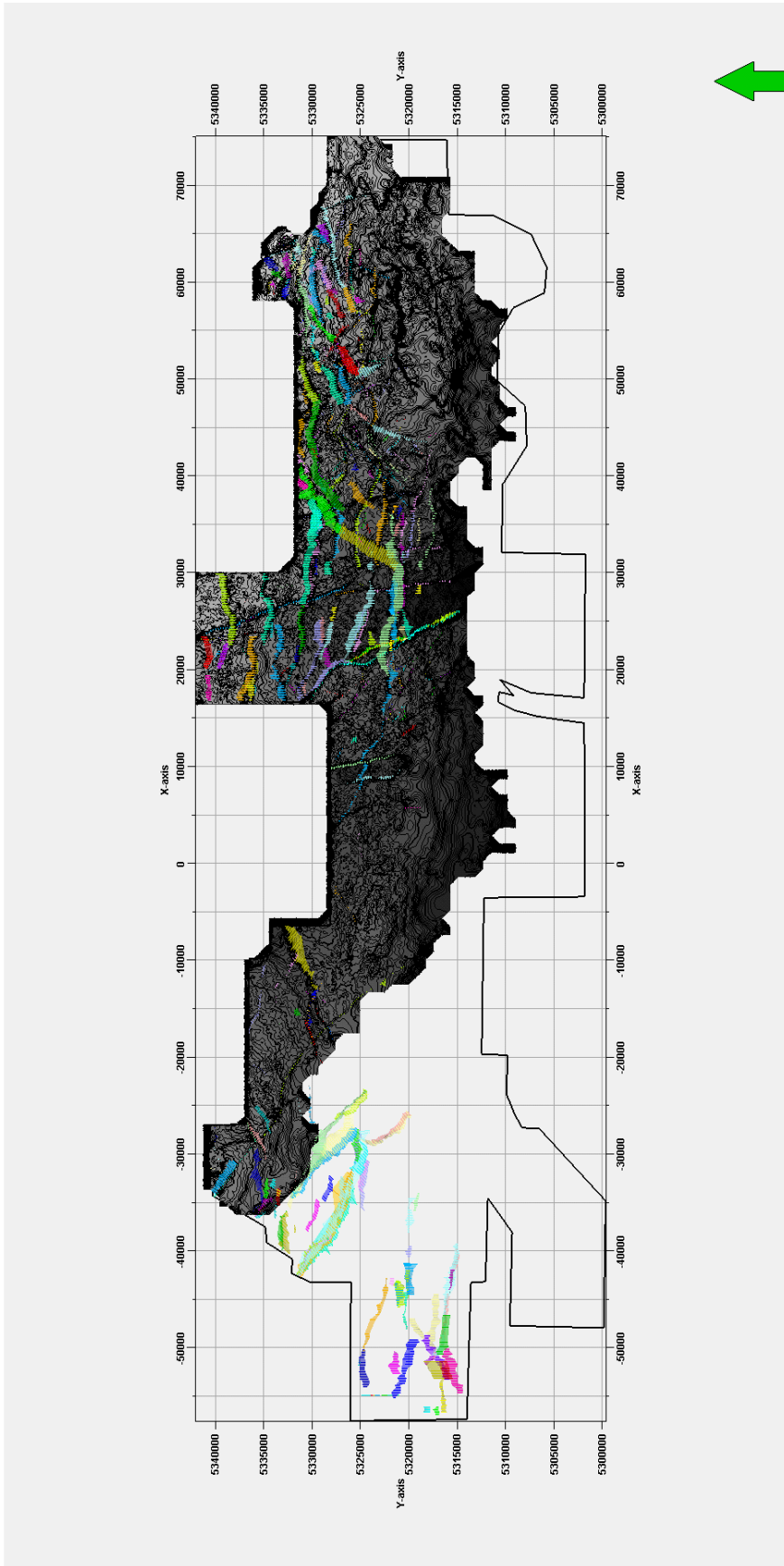
**Figure 89: Fault Map with seismic boundary, mapped fault surfaces (colored) and surface XBM with contours.**

# Manfred RETZL

Schererstraße 22/15/6
1210 Vienna
+43 664 / 531 22 20
manfred.retzl@gmail.com

## Personal Details

Born on July 21st, 1989 in Vienna
Austrian citizen

## Education

| | |
|---|---|
| 09/1995 - 07/1999 | Elementary school Pastorstraße, 1210 Vienna |
| 09/1999 - 07/2007 | Bundesrealgymnasium Franklinstraße 26, 1210 Vienna |
| 01/2008 - 07/2008 | Military service and paramedic education at the Van-Swieten-Kaserne |
| 10/2008 - 11/2012 | **Bachelor in earth sciences at the University of Vienna**<br>Bachelor's thesis: „Erstellung und Interpretation einer GIS-gestützten Karte der Basis und Mächtigkeit quartärer Sedimente im Wiener Becken" |
| 11/2012 - 03/2014 | **Master in earth sciences at the University of Vienna**<br>Specialization on geology;<br>Master's thesis: „The Tectonic Evolution of the Upper Austrian Molasse Foreland Basin and its Mesozoic Basement Based on 3D Seismic Fault Attributes" |

## Professional Experience

| | |
|---|---|
| 07/2010 - 08/2010 | **OMV** Exploration & Production GmbH<br>Internship, Trabrennstraße, 1020 Vienna |
| 07/2011 - 08/2011 | **OMV** Exploration & Production GmbH<br>Internship, Gänserndorf |
| 12/2012 – 07/2013 | **RAG Austria** Exploration & Production<br>Master's thesis, Schwarzenbergplatz, 1015 Vienna |

## Skills

| | |
|---|---|
| Languages | German (Native)<br>English (C1)<br>Latin<br>Italian (A1) |
| IT | Petrel 2012: Fundamentals and Geophysics Certificate<br>Basics in ArcGIS |